Comparison between manual and autonomous crack healing with regard to reinforcement corrosion

Renaat Callens

Supervisors: Prof. dr. Nele De Belie, Prof. dr. Kim Van Tittelboom
Counsellors: Ir. Bjorn Van Belleghem, Dr. ir.-arch. Philip Van den Heede

Master's dissertation submitted in order to obtain the academic degree of
Master of Science in Civil Engineering

Department of Structural Engineering
Chair: Prof. dr. ir. Luc Taerwe
Faculty of Engineering and Architecture
Academic year 2017-2018

GHENT
UNIVERSITY

Comparison between manual and autonomous crack healing with regard to reinforcement corrosion

Renaat Callens

Supervisors: Prof. dr. Nele De Belie, Prof. dr. Kim Van Tittelboom
Counsellors: Ir. Bjorn Van Belleghem, Dr. ir.-arch. Philip Van den Heede

Master's dissertation submitted in order to obtain the academic degree of
Master of Science in Civil Engineering

Department of Structural Engineering
Chair: Prof. dr. ir. Luc Taerwe
Faculty of Engineering and Architecture
Academic year 2017-2018

GHENT
UNIVERSITY

Toelating tot bruikleen

"De auteur geeft de toelating deze masterproef voor consultatie beschikbaar te stellen en delen van de masterproef te kopiëren voor persoonlijk gebruik. Elk ander gebruik valt onder de beperkingen van het auteursrecht in het bijzonder met betrekking tot de verplichting de bron uitdrukkelijk te vermelden bij het aanhalen van resultaten uit deze masterproef."

Permission for usage

"The author gives permission to make this master's dissertation available for consultation and to copy parts of this master dissertation for personal use. In the case of any other use, the limitations of the copyright have to be respected, in particular with regard to the obligation to state expressly the source when quoting results from this master's dissertation."

Ghent, June 2018

Renaat Callens

Acknowledgements

Now this master dissertation is almost completely written, I have only one thing left to do, namely writing an appropriate word of thanks. During my research I was able to count on the help and support of many people. Without their helping hand, this dissertation might never have come. That is why I now want to take the time to thank everyone explicitly.

First of all, I would like to thank my thesis supervisor Prof. dr. ir. Nele De Belie for giving me the opportunity to work on this subject. Secondly, I would like to express my gratitude to Prof. dr. ing. Kim Van Tittelboom, Dr. ir.-arch. Philip Van den Heede and Ir. Bjorn Van Belleghem for the guidance, the knowledge and the feedback throughout the year. Special thanks to Bjorn, since his door was always open whenever I ran into trouble or had a question about my research or writing.

I would also like to thank the technicians from the Magnel Laboratory, for helping me with the concrete casting and preparations of the experimental setup. I could always count on them when I needed help or advice in the lab and there was always time for a laugh in between.

Further, I would like to thank my good friend Pieterjan Pertz for supporting me with my thesis, but also for the distraction and entertainment besides it. Also special thanks to my classmates, with whom I worked with in the lab or the library throughout the year. Working on my thesis would have been much less fun without you guys and I will certainly miss the coffee breaks and the laughs during lunch (and diner).

Finally, I must express my very profound gratitude to my parents for giving me the opportunity to study Civil Engineering and for providing me with unfailing support and continuous encouragement throughout my years of study and through the process of researching and writing this thesis. This accomplishment would not have been possible without them. Thank you.

Renaat Callens

Abstract

Title:	Comparison between manual and autonomous crack healing with regard to reinforcement corrosion
Author:	Renaat Callens
Supervisor(s):	Prof. dr. ir. Nele De Belie, Prof. dr. ing. Kim Van Tittelboom
Counselor(s):	Ir. Bjorn Van Belleghem, Dr. ir-arch. Philip Van den Heede

Master's dissertation submitted in order to obtain the academic degree of Master of Science in Civil Engineering

Department of Structural Engineering
Chairman: Prof. dr. ir. Luc Taerwe
Faculty of Engineering and Architecture
Academic year: 2017-2018

Summary: In service, cracks are inevitably present in concrete Cracks in reinforced concrete are inevitable and form preferential ingress paths for aggressive substances such as chlorides. These chlorides can cause steel reinforcement corrosion and concrete degradation. This impairs the durability, ultimately leading to a reduction in service life of concrete structures. Therefore, repair of cracks is necessary in order to avoid major damage and/or extend the service life of concrete structures. However, maintenance and/or repair works impose high direct and indirect costs. The effectiveness of the healing agents in improving the corrosion resistance is thus of great importance. In this master dissertation, the influence of two healing agents (polyurethane (PU) and water repellent agent (WRA)) on the corrosion behaviour and transport properties of reinforced concrete was investigated, using different healing mechanisms: by applying manual healing (through injection or surface impregnation) or by incorporation of an autonomous healing mechanism (through encapsulation). This was done through three types of tests. First, a water absorption test was performed on mortar prisms in order to investigate the capillary water uptake through the (healed) cracks. Secondly, the chloride penetration in concrete cylinders was tested by an accelerated chloride diffusion test. The final part of the investigation consisted of corrosion monitoring, by means of electrochemical measurements, on cracked concrete beams which were cyclically exposed to a chloride solution with realistic concentration. It was found that the best overall healing performances were obtained with the water repellent agent, either by encapsulation, by manual injection or by surface impregnation after crack creation.

Keywords: autonomous healing, manual healing, chloride-induced corrosion, polyurethane, water repellent agent

Comparison between manual and autonomous crack healing with regard to reinforcement corrosion

Renaat Callens

Supervisor(s): Prof. dr. ir. Nele De Belie, Prof. dr. ing. Kim Van Tittelboom
Counsellor(s): Ir. Bjorn Van Belleghem, Dr. ir-arch. Philip Van den Heede

***Abstract*: Cracks in reinforced concrete create preferential ingress paths for aggressive substances such as chlorides to penetrate the concrete. As soon as a critical amount of chlorides has reached the location of the steel reinforcement, chloride-induced corrosion may occur. The effectiveness of the healing agents in improving the corrosion resistance is thus of great importance The resistance of manual and autonomous healed cracks using different healing mechanisms and healing agents was investigated and compared by conducting water absorption tests, chloride penetration tests and corrosion monitoring.**

***Keywords*: autonomous healing, manual healing, chloride-induced corrosion, polyurethane, water repellent agent**

I. Introduction

Cracks or micro-cracks are inevitably present in concrete. These cracks create preferential paths for the penetration of corrosion-inducing substances such as chlorides. As soon as a critical amount of chlorides has reached the location of the steel reinforcement, chloride-induced corrosion may occur, which is one of the main deterioration mechanisms of reinforced concrete structures. If left untreated, reinforcement corrosion accelerates the deterioration of reinforced concrete structures and may lead to several interrelated negative consequences, ultimately leading to a reduction in service life of these structures [1]. So, repair of cracks is necessary in order to avoid major damage and/or extend the service life of concrete structures.

However, maintenance and/or repair works impose high direct and indirect costs. The effectiveness of the healing agents in regaining the corrosion resistance is thus of great importance and consequently attracts considerable interest. In this master dissertation, the influence of two healing agents (polyurethane (PU) and water repellent agent (WRA)) on the transport properties and corrosion behaviour of concrete was investigated, using different healing mechanisms. This can be done either by applying manual healing (through injection or surface impregnation) or by incorporation of autonomous healing mechanisms (through encapsulation).

Three types of tests were conducted. First, a water absorption test was performed on mortar prisms in order to investigate the capillary water uptake through the (healed) cracks. Secondly, the chloride penetration in concrete cylinders was tested by an accelerated chloride diffusion test. The final part of the investigation consisted of corrosion monitoring, by means of electrochemical measurements, on cracked concrete beams subjected to cyclic exposure to a chloride solution with realistic concentration.

The aim of this master dissertation was to compare (different applications of) these types of healing. Moreover, a comparison will also be made between the different healing agents, mentioned above.

II. Materials and Methods

A. Materials

1) Mortar prisms

Ordinary Portland cement mortar with a W/C-ratio of 0.5 was used for the mortar prisms, used in the water absorption test. In order to obtain this, sand with a grain size of 0-2 mm, cement type CEM I 52.5 N and (tap) water were mixed with a respective mass ratio of 6:2:1.

Mortar prisms with dimensions of 160 mm x 160 mm x 40 mm were used. These were cast in wooden formworks and were reinforced with two bars with a diameter of 2 mm. In case of specimens with self-healing properties, two cylindrical borosilicate glass capsules (with an internal diameter of 3 mm and a length of 50 mm), filled with one of the healing agents, were sealed at both ends and glued on thin wires between the reinforcement bars in the centre of the prism. This can be seen on Figure II.1. Two different healing agents with a low viscosity were used: a one-component polyurethane, HA Flex SLV, and a water repellent agent, Sikagard 705 L.

Figure II.1 Mold preparation for a mortar prism with self-healing properties [3]

2) Concrete cylinders

In this research, a fly ash containing concrete mix with a water-to-binder (W/B) ratio of 0.41 was used. The concrete composition for both the concrete cylinders and the concrete beams (section 3)) is given in Table II-1.

For the chloride diffusion test, concrete cylinders with a diameter of 100 mm and a height of 75 mm were cast in cylindrical PVC molds, which were clamped on a wooden base.

Table II-1: Concrete composition

	Fly ash concrete	
Sand 0/4	696	kg/m³
Aggregates 2/8	502	kg/m³
Aggregates 8/16	654	kg/m³
Cement CEM I 52.5 N	317.6	kg/m³
Water	153	kg/m³
Fly ash	56	kg/m³
Superplasticizer	3	ml/kg binder

In order to create artificial cracks in the specimens (see section B.1), thin brass plates (60 mm x 50 mm, thickness 300 µm) were fixed 25 mm deep in the wooden base. This way, the thin plate (60 mm x 25 mm) was fixed in the specimens after casting and curing of the concrete. In case of specimens with self-healing properties, three holes with a diameter of 3.5 mm were drilled in the thin brass plates. Capsules filled with healing agent (PU or WRA) were then put through these holes and glued on nylon wires with PMMA to fix their position in the molds. The intermediate distance between the capsules was 20 mm and they were fixed at a depth of 12.5 mm (half of the crack depth). Figure II.2 shows a schematic representation of a concrete cylinder with an artificial self-healing crack after casting.

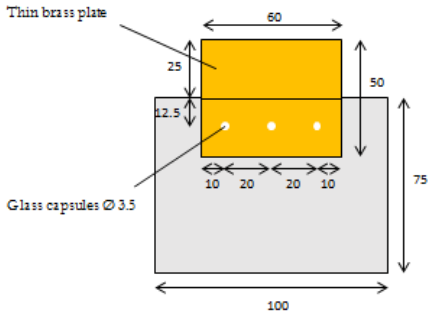

Figure II.2: Schematic representation of a concrete cylinder with artificial self-healing cracks after casting (dimensions in mm)

3) Concrete beams

For corrosion monitoring, concrete beams with dimensions of 120 mm x 120 mm x 500 mm were made. The experimental setup of these beams can be seen in Figure II.3. The steel reinforcement in the beams consists two reinforcement cages one at each side of the beam and a central rebar, which respectively serve as the cathode and anode in the corrosion process. Both reinforcement cages were made out of four longitudinal rebars (Ø 8 mm) which are welded to five stirrups (Ø 6 mm). The anodic rebar was partially coated with two layers of cement paste (W/C=0.4), in order to prevent crevice corrosion, and two layers of epoxy coating (SikaCor 277). In this way, only the central part of the rebar, with a length of 50 mm, was exposed to the concrete surrounding. Electrical connections by means of copper wires were made between both parts and the exterior and between both reinforcement cages. In order to avoid galvanic corrosion, all these copper wire connections were also coated with epoxy resin (SikaCor 277).

In addition to the reinforcement cages and the central rebar, four glass fibre reinforced polymer (GFRP) bars (Aslan™ 100), with a diameter of 6 mm and a length of 460 mm, were placed in the beams. These were needed as structural reinforcement, in order to prevent brittle failure of the beam during crack creation. Finally, an internal reference electrode was placed close to the anode.

In case of beams with self-healing properties, two layers of six capsules, filled with a healing agent (PU or WRA), were placed in the center of the beams. The position of these capsules is also indicated in Figure II.3. The capsules were glued on thin wires, attached to the molds, with an intermediate distance of 20 mm.

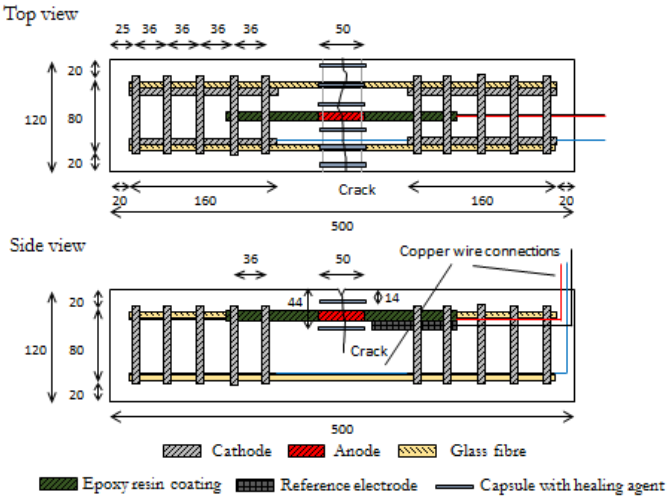

Figure II.3: Experimental setup for an autonomously healed concrete beam (dimensions in mm)

B. Methods

1) Crack creation

For all three types of specimens, a target crack width of 300 µm was chosen. The cracks in the mortar prisms were created by means of three-point bending, using a linear variable differential transformer (LVDT), attached at the bottom of the sample, in order to register and control the crack width during the bending test. Three point bending was also used for crack creation in the concrete beams. However, unlike for the mortar prisms, the concrete beams were kept in the three-point bending test frame in order to keep the crack open. Due to the presence of a triangular notch in the middle of the beam (see Figure II.3), it was intended to create the crack at this position, so the crack always crossed the anodic bar. For the concrete cylinders artificial cracks were created by carefully removing the thin brass plates 24 hours after casting of the concrete. This way, a crack was thus created with a length of 60 mm, a depth of 25 mm and a width of 300 µm.

2) Crack healing

Different healing mechanisms were tested in these experiments: autonomous healing, using embedded capsules filled with a healing agent, and manual healing, by injecting the crack or impregnating the crack surface with a healing agent. Below, an overview is given of the different test series. For each test series, at least three replicate specimens were made.

- Uncracked (UNCR),
- Cracked (CR),
- Cracked; encapsulation of PU (PU_CAPS),
- Cracked; encapsulation of WRA (WRA_CAPS)
- Cracked; manual injection with PU (PU_MAN)

- Cracked; manual injection with WRA (WRA_MAN)
- Cracked; surface impregnation with WRA before cracking (WRA_SURF_BEFORE)
- Cracked; surface impregnation with WRA after cracking (WRA_SURF_AFTER)

The latter two healing mechanisms were however not used for the chloride diffusion test. Instead, manual injection was performed after a few weeks of immersion in a NaCl solution (PU_MAN_AFTER and WRA_MAN_AFTER) (see section II.B.4).

3) Water uptake through capillary absorption

Prior to the water absorption test, all mortar prisms were partly covered with aluminium butyl tape (see Figure II.4) so only a region of 10 x 40 mm around the crack (or in the middle of the bottom surface in case of uncracked specimens) was exposed to water during the absorption test. After this preparation, the initial mass of all specimens was measured.

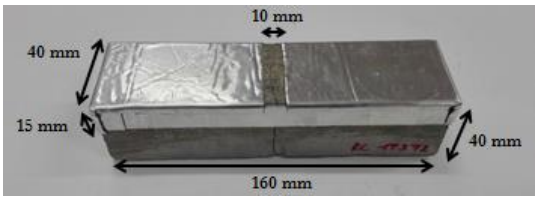

Figure II.4: Specimen preparation prior to water absorption test

After this, the (test faces of the) specimens were immersed up to a depth of 2 ± 1 mm. From that moment on, the mass of the specimens was determined at several time intervals: every half hour during the first eight hours and then again every 24 hours until 172 hours. These values enabled the calculation of the cumulative water uptake and sorption coefficients of all specimens.

4) Chloride diffusion test

For this test, all coated concrete cylinders were immersed in an aqueous NaCl solution (with a concentration of 165 g/l) for 11 weeks. After 3 weeks, all specimens were taken out of the solution for 48 hours. During this period, for 3 specimens of 2 series (PU_MAN_AFTER and WRA_MAN_AFTER) the crack was manually injected with healing agent. Subsequently, all specimens were placed back in the NaCl solution for another 8 weeks. After the total exposure period, 10 layers (40 mm x 10 mm) each with a thickness of 3 mm were ground off in the region of the crack (see Figure II.5). The powder from each layer was collected and stored for minimum 7 days in an oven at 95°C. Finally, the chloride content of each layer was determined by means of acid-soluble chloride extraction in a nitric acid solution, followed by a potentiometric titration against silver nitrate.

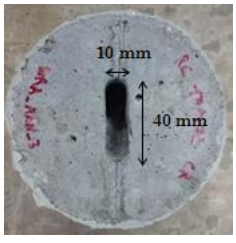

Figure II.5: Grinded region around the crack

5) Corrosion monitoring

Prior to the corrosion monitoring, all sides of the concrete beams, except the test (upper) surface and the bottom surface, were covered with aluminium butyl tape. This way, only the bottom and upper surfaces of the beams were directly exposed to the environment (a temperature of 20 °C and a relative humidity of 60 %). Using this tape, a reservoir was made on top of the beams, which was filled with a solution during the wet/dry cycles. Furthermore, the reservoir was divided in three compartments by two PVC plates (see Figure II.6). Finally, all edges of the reservoir were sealed with silicone, to ensure the liquid tightness at the edges of the reservoir.

Once prepared, the different electrochemical parameters, discussed below, were measured, once before crack creation (week -1) and once after crack creation (week 0). Subsequently, the beams were exposed to wet/dry cycles of 1/6 days for a period of 12 weeks (week 1 to 12). During the wet period, the central compartment was filled with a NaCl solution with a concentration of 33 g/l. This way, a marine environment was simulated in the region of the crack. The side compartments were filled with $Ca(OH)_2$ solution with a concentration of 1.15 g/l, in order to obtain an even moisture distribution. After 24 hours, the solutions were removed, after which the corrosion measurements were performed.

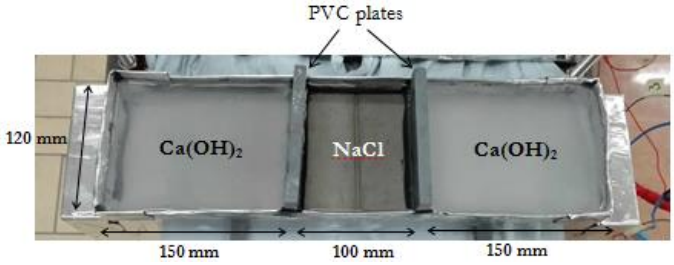

Figure II.6: Reservoirs on (uncracked) concrete beam during wet period of the wet/dry-cycles

A continuous current monitoring was performed during 12 weeks of testing. Further, every week, the following electrochemical measurements were performed, using an internal Mn/MnO_2 reference electrode:

- Corrosion potential and IR drop
- Anodic and cathodic open circuit potential
- Electrochemical impedance spectroscopy (to measure the concrete resistance)
- Anodic and cathodic linear polarisation resistance

III. RESULTS AND DISCUSSION

A. Capillary water absorption test

From the cumulative water absorption curves (Figure III.1), it was found that the water absorption for the cracked specimens was almost ten times higher than for uncracked specimens. This confirms the necessity of repairing the cracks to avoid the fast ingress of aggressive substances into the cementitious matrix.

When comparing the different healing agents, it seemed that when using WRA better healing efficiencies were obtained (109 to 115 %) than in case of PU (85 to 106 %), which still is very high. So, although very high healing efficiencies were obtained for both healing agents, the best resistances against water absorption were obtained using the water repellent

agent. The good healing performances with WRA can probably be attributed to the leakage of the healing agent on the mortar surface. Consequently, a part of the exposed test surface area was covered with water repellent agent.

When comparing the different types of healing mechanisms, the best healing performance was acquired with manual healing by surface impregnation with water repellent agent (WRA_SURF). Obviously, this can be attributed to the fact that in this case, almost no water could be absorbed by the mortar matrix, except through the crack. Nevertheless, still a significant difference could be seen when applying this layer of WRA before or after crack creation. Here, the latter case gave the best results, as evidenced by 20 % lower cumulative water absorption and the about 5 % higher healing efficiency. Moreover, after seven hours, one specimen from the test series WRA_SURF_BEFORE started to act as if it was unhealed. From that moment, a rapid increase in cumulative water absorption was observed, which can be attributed to incomplete crack healing. This difference between surface impregnation before and after the crack, can be explained by the fact that in the latter case the healing agent, applied on the test surface, can much more easily penetrate into the crack.

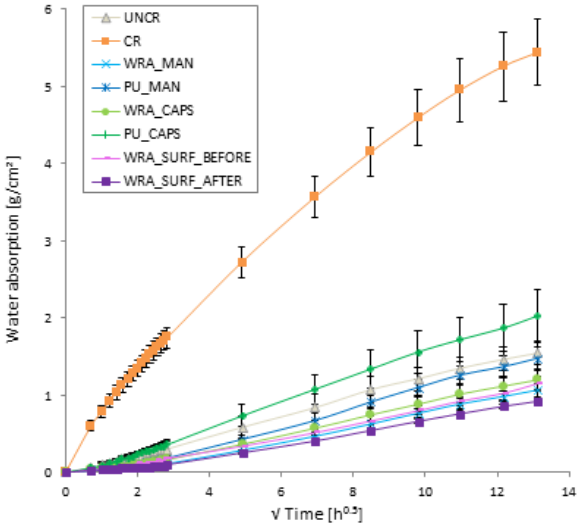

Figure III.1: Comparison of all cumulative water absorption curves in function of the square root of time. Error bars represent the standard error on the mean values.

B. *Chloride diffusion test*

The obtained chloride profiles (see Figure III.2 and Figure III.3) confirmed that crack repair was definitely necessary, since at a depth of 21 to 24 mm the chloride concentration in cracked samples was more than 25 times higher compared to uncracked samples. However, unlike for the water absorption test, the best healing performances were obtained using PU as healing agent, resulting in self-healing efficiencies not lower than 94 % over the entire crack depth. Independent of the used healing mechanism (manual or autonomous) and the penetration depth, lower chloride concentrations were found compared to WRA as healing agent, which also showed promising results in preventing chloride ingress (e.g. healing efficiencies ranging from 56 to 143 % for WRA_MAN). So, with both healing agents good healing performances were obtained, but for this test the efficiencies were higher with PU.

When comparing the different healing mechanisms, both manually injecting the healing agent (before immersion) and encapsulation of the healing agent, showed good to even excellent healing performances, with healing performances not lower than about 37 %. Using PU, equal or lower chloride concentrations were obtained than for uncracked specimens, which corresponds to healing efficiencies of 100 % for PU_CAPS over the whole crack depth and of 94 to 143 % for PU_MAN. So, it could be concluded that PU is very effective in blocking chloride ingress in concrete, no matter which healing mechanism is used. When comparing both mechanisms using WRA, it has to be noted that manually injecting WRA clearly showed better healing performances than using embedded capsules. A difference up to 70 % was found between both mechanisms.

Finally, it could be concluded that, although lower chloride concentrations were obtained than when leaving the crack unhealed, manually injecting a crack after three weeks of exposure to a chloride environment leads to bad healing performances. It can thus be concluded that a crack should be healed as soon as possible after its formation.

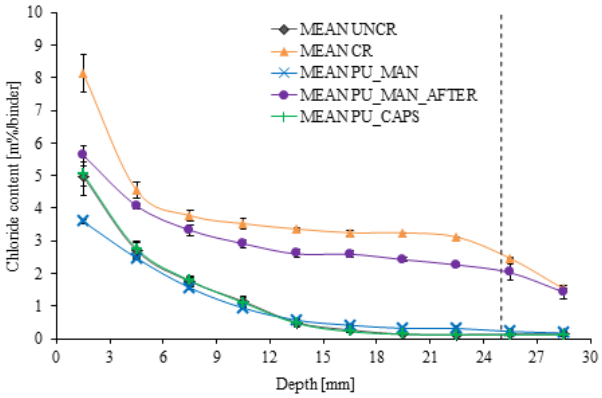

Figure III.2: Comparison of average chloride profiles of (un)cracked specimens and specimens healed with PU. Error bars represent the standard error on the mean values.

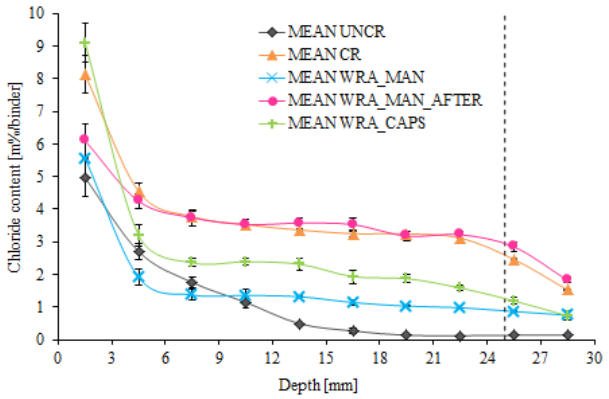

Figure III.3: Comparison of average chloride profiles of (un)cracked specimens and specimens healed with WRA. Error bars represent the standard error on the mean values.

C. *Corrosion monitoring*

The macro-cell corrosion current represents the flow of electrons between the anode and cathode and gave a direct assessment of the corrosion activity of the samples. Higher currents indicated a more active state of corrosion. Also, a clear relation was found between the corrosion current and the other measured electrochemical parameters: an increase in corrosion current, corresponded with an increase in corrosion potential, an increase in driving potential ΔE and a drop in

anodic polarisation resistance $R_{P,A}$. It was clearly visible to notice the period of severe corrosion of the specimens by comparing the different measurements per specimen.

The electrochemical measurements showed no indications of an active state of corrosion in the uncracked concrete beams over the whole exposure period. However, the presence of cracks seemed to have a big influence, since corrosion initiated from the first week and after 12 weeks of exposure, all cracked beams showed major corrosion activity, with measured corrosion currents up to 100 µA.

Although the healing effect was visible in case of PU_CAPS, e.g. 15 % higher (less negative) corrosion potential compared to cracked beams, still corrosion initiation could not be prohibited and there was also further propagation of corrosion. The same conclusion could be made for manual injection with PU: although the effect of the healing agent again was clearly visible, two out of the three beams however showed corrosion activity. From this, it can be concluded that, in most of the cases, using PU as healing agent cannot (completely) prevent corrosion initiation.

On the contrary, both autonomous healing (by encapsulation) as well as manual healing (by injection) with WRA seemed to be very effective in preventing localised corrosion at the rebar (at least for an exposure time of 12 weeks). Both mechanisms showed identical results, i.e. no macro-cell corrosion current occurred and stable values were found for the corrosion potential (about -220 mV vs. MnO_2) and the driving potential (± 160 mV). Compared to uncracked beams, even higher anodic polarization resistance (up to 50 kΩ) were obtained, corresponding to a difference up to 20 %.

Finally, manual healing by surface impregnation was also investigated. When done before crack creation, bad healing performances were found. For example, an even larger increase in driving potential was obtained compared to cracked beams, reaching to a value of about 500 mV. For some beams, corrosion initiation could be prolonged, but after an exposure period of seven weeks, corrosion initiation and subsequent propagation of corrosion occurred for all beams. From this, it can be concluded that this healing mechanism is not successful in preventing localised corrosion. When impregnation of the surface with WRA was done after crack creation, good healing performances were obtained for two out of the three specimens, with similar results as for uncracked beams. However, one beam experienced corrosion activity from week 4 onwards. This could probably be attributed to incomplete healing.

IV. CONCLUSIONS

Table IV-1 gives an overview of the ability of different healing agents and mechanisms in resisting water absorption, chloride ingress and/or corrosion initiation.

It can be seen that, although the performances of other mechanisms are certainly not bad in most of the cases, only two healing mechanisms perform well for all three tests: autonomous healing mechanism by encapsulation of water repellent agent (WRA_CAPS) and manual healing by injection of the crack with water repellent agent (WRA_MAN). Further, also surface impregnation with water repellent agent after crack creation (WRA_SURF_AFTER) showed good to excellent resistances against water absorption and corrosion initiation. However, since this mechanism was not tested against chloride ingress in the chloride penetration test, further investigation is necessary in order to confirm the good healing performances of this mechanism.

In general, water repellent agent thus seemed to be a more efficient healing agent than polyurethane. When comparing the healing mechanisms, it can be stated that both manually injecting the crack, as well as using embedded capsules can lead to overall good healing performances. Pending further research, it can be provisionally stated that this also counts for impregnating the test surface with a water repellent agent after crack creation. Consequently, it is recommended to use one of these healing mechanisms in practice.

Table IV-1: Overview of resistances of different healing agents and healing mechanisms against water absorption, chloride ingress and corrosion initiation

Healing agent	Healing mechanism	Resistance against …		
		Water absorption	Chloride ingress	Corrosion initiation
PU	PU_CAPS	Good	Excellent	Bad
	PU_MAN	Excellent	Excellent	Bad
	PU_MAN_AFTER	/	Bad	/
WRA	WRA_CAPS	Excellent	Good	Excellent
	WRA_MAN	Excellent	Good	Excellent
	WRA_MAN_AFTER	/	Bad	/
	WRA_SURF_BEFORE	Excellent	/	Bad
	WRA_SURF_ AFTER	Excellent	/	Good

ACKNOWLEDGEMENTS

The authors would like to acknowledge Prof. dr. ir. Nele De Belie, Prof. dr. ing. Kim Van Tittelboom, Ir. Bjorn Van Belleghem and Dr. ir-arch. Philip Van den Heede for their contributions to this research.

REFERENCES

[1] M. Otieno, H. Beushausen, and M. Alexander, *"Chloride-induced corrosion of steel in cracked concrete - Part I: Experimental studies under accelerated and natural marine environments," Cem. Concr. Res.*, vol. 79, pp. 373–385, 2016.

[2] B. Van Belleghem, K. Van Tittelboom, and N. De Belie, *"Efficiency of self-healing cementitious materials with encapsulated polyurethane to reduce water ingress through cracks,"* 2017.

[3] B. Van Belleghem, K. Van Tittelboom, and N. De Belie, *"Use of encapsulated healing agents to limit water uptake through cracks in mortar,"* pp. 1–10, 2017.

Table of Contents

List of figures

List of tables

List of abbreviations

Symbol	Description	Unit
AC	Alternating current	
Ag	Silver	
AgCl	Silver Chloride	
CA	Cyanocrylate	
$Ca(OH)_2$	Calcium hydroxide	
$Ca(NO_2)_2$	Calcium nitrite	
$CaCO_3$	Calcium carbonate	
C_{crit}	Critical chloride content or threshold value	[m%/cement]
CE	Counter electrode	
CS	Counter sense	
Cl^-	Chloride ion	
$Cl^-_{CR,i}$	Chloride content of cracked specimen at depth i	[m%/binder]
$Cl^-_{HEAL,i}$	Chloride content of healed specimen at depth i	[m%/binder]
$Cl^-_{UNCR,i}$	Chloride content of uncracked specimen at depth i	[m%/binder]
CO_2	Carbon dioxide	
C_i	Initial concentration of total chlorides	[%]
C_s	Free chloride concentration (vgl 2.5)	[kg/m³ of solution]
C_s	Surface concentration of total chlorides (vgl 2.6)	[%]
C_v	Free chloride concentration	[kg/m³ of concrete]
CSE	Copper – Copper sulphate electrode	
CSH	Calcium silicate hydrate	
C_x	total chloride content in the concrete or binder	[%]
Cu	Copper	
$CuSO_4$	Copper sulphate	
D	Chloride diffusion coefficient	[m²/s]
D_{app}	Apparent chloride diffusion coefficient	[m²/s]
D_{cr}	Chloride diffusion coefficient in cracked concrete	[m²/s]
D_d	Diffusion coefficient	[m²/s]
D_{H_2O}	the chloride diffusion coefficient in water	[m²/s]
$D(\theta_s)$	Hydraulic diffusivity of a solution	[m²/s]
ΔE	Driving potential	[mV]
e^-	Electron	
E_{corr}	Corrosion potential	[mV vs. REF]
ECC	Engineered cementitious composite	
EIS	Electrochemical impedance spectroscopy	
$E_{O,A}$	Resting potential of anode	[mV]
$E_{O,C}$	Resting potential of cathode	[mV]
erf	Error function	
f	Frequency	[Hz]
Fe^{2+}	Ferrous ion	
Fe_2O_3	Iron oxide	

Fe_3O_4	Iron oxide	
$Fe(OH)_2$	Ferrous hydroxide	
GFRP	Glass fibre reinforced polymer	
GGBFS	Ground granulated blast-furnace slag	
H_2O	Water	
Hg	Mercury	
Hg_2Cl_2	Mercury chloride	
I	Electric current	[A]
i	Electric current density	[A/cm²]
i_{corr}	Corrosion current density (or corrosion rate)	[μA/cm²]
I_{corr}	Corrosion current	[μA]
I_{macro}	Macro-cell corrosion current	[μA]
I_{micro} (or I_{self})	Micro-cell corrosion current	[μA]
J_c	Flux mass of chloride due to capillary suction	[kg/m²s]
J_d	Ionic diffusion flux (of chlorides)	[kg/m²s]
$K_{P,A}$	Anodic control factor	[%]
$K_{P,C}$	Cathodic control factor	[%]
K_E	Concrete control factor	[%]
k	Geometrical factor	[m]
Log	Logarithm	
LPR	Linear polarisation resistance	[kΩ]
LVDT	Linear variable differential transformer	
m	Aging factor	[-]
MDI	Methylene diphenyl diisocyanate	
MK	Metakaolin	
MMA	Methylmethacrylate	
MMO	Metal-metal oxide	
Mn	Manganese	
MnO_2	Manganese oxide	
Na_2FPO_3	Sodium monofluorophosphate	
Na_2SiO_3	Sodium silicate	
NaCl	Natrium chloride	
O_2	Oxygen	
OCP	Open circuit potential	[mV]
OH^-	Hydroxyl ion	
OPC	Ordinary Portland cement	
pH	Acidity scale	[-]
PMMA	Polymethylmethacrylate	
PU	Polyurethane	
PVC	Polyvinyl chloride	
φ	Phase angle or phase shift	[°]
Ø	Bar diameter	[mm]
q_s	Volume rate of a solution flow	[m³/(m²/s)]
R	(Electrical) resistance	[Ω]
ρ	(Electrical) resistivity	[Ωm]
R	Resistance	[Ω]
R_E	Concrete resistance	[Ω]

R_t	Transfer resistance	[Ω]
R_p	Polarisation resistance	[Ω]
$R_{P,A}$	Polarisation resistance of anode	[Ω]
$R_{P,C}$	Polarisation resistance of cathode	[Ω]
R_t	Transfer resistance	[Ω]
R_Ω	Ohmic resistance	[Ω]
REF	Reference electrode	
SAP	Super absorbent polymers	
SF	Silica fume	
SCE	Saturated calomel electrode	
SHE	Self-healing efficiency	[%]
$S_{CR,M}$	Mean sorption coefficient of cracked specimen	[kg/m²/h$^{0.5}$]
$S_{HEAL,i}$	Sorption coefficient of individual healed specimen	[kg/m²/h$^{0.5}$]
$S_{UNCR,M}$	Mean sorption coefficient of uncracked specimen	[kg/m²/h$^{0.5}$]
t	Time	[s]
t_0	Reference time	[s]
T_i	Titanium	
T_iO_2	Titanium dioxide	
$t_{service\ life}$	Service life time of a structure	[year]
$t_{initiation}$	Initiation period of concrete	[year]
$t_{propagation}$	Propagation period of concrete	[year]
θ_s	Solution saturation	[m³ solution/m³ concrete]
(UF)FA	(Ultra-fine) fly ash	
ω	Crack width	[µm]
ω	Frequency	[rad/s]
W/B	Water to binder ratio	
W/C	Water to cement ratio	
WE	Working electrode	
WS	Working sense	
WRA	Water repellent agent	
x	Depth from the concrete surface	[m]
x	Concrete cover thickness (vgl 2.8)	[m]
Z	Complex impedance	

1. Introduction

1.1 Problem statement

Concrete is the most used construction material in the world, due to its low price and favourable engineering properties. However, a limitation of (reinforced) concrete is the inevitable presence of (micro) cracks, voids and capillary pores. Cracks form preferential paths for aggressive agents to enter the concrete matrix, for example chlorides in a marine environment. As soon as a critical amount of chlorides has reached the location of the steel reinforcement, chloride-induced corrosion may occur, which is one of the main deterioration mechanisms of reinforced concrete structures. If left untreated, reinforcement corrosion accelerates the deterioration of reinforced concrete structures and may lead to several interrelated negative consequences, ultimately leading to a reduction in service life of these structures. Therefore, repair of cracks is necessary in order to avoid major damage and/or extend the service life of reinforced concrete structures. However, maintenance and/or repair works impose high direct and indirect costs.

Although cementitious materials have the natural ability to repair damage to a certain extent (only for small cracks), healing mechanisms can be implemented in order to enhance the corrosion resistance of reinforced concrete structures. This can be done either by applying manual healing or by incorporation of an autonomous healing mechanism.

The effectiveness of the healing agents in improving the corrosion resistance is of great importance and consequently attracts considerable interest. In this master's dissertation, the influence of two healing agents (polyurethane (PU) and water repellent agent (WRA)) on the corrosion behaviour and transport properties of reinforced concrete was investigated, using different healing mechanisms.

This was done through three types of tests. First, a water absorption test was performed on mortar prisms in order to investigate the capillary water uptake through the (healed) cracks. Secondly, the chloride penetration in concrete cylinders was tested by an accelerated chloride diffusion test. The final part of the investigation consisted of corrosion monitoring on cracked concrete beams which are cyclically exposed to a chloride solution with realistic concentration

The aim of this master's dissertation was to compare (different applications of) these types of healing. Moreover, a comparison will also be made between the different healing agents, mentioned above.

1.2 Outline of the thesis

This master's dissertation is divided in four main parts. The first part (Part I: State of the art) provides the necessary background information found in literature. In chapter 2, information about the corrosion process is given, concentrating on chloride-induced corrosion and the effect of cracks on this phenomenon. The different techniques to detect corrosion are then discussed in chapter 3, while chapter 4 is committed to the healing of the cracks.

Part II defines and discusses the used materials for the experiments (chapter 5) and the used methods (chapter 6). The results of these experiments are then discussed in Part III. This is done separately for each experiment. In chapter 7, the results for the capillary water absorption test are discussed after which the same is done for the chloride penetration test in chapter 8. Finally, chapter 9 deals with the corrosion monitoring results. Subsequently, all the obtained results from the three different experiments are compared in chapter 10.

The last part of this thesis, Part IV consists of an overall conclusion of this master thesis, followed by suggestions for future research.

Part I
State of the Art

2. Reinforcement corrosion

2.1 Introduction

Concrete is the most used construction materials in the world, due to its low price and favourable engineering properties. However, although concrete has a high compressive strength, it has a relatively low tensile strength and ductility. This is often counteracted by the inclusion of steel reinforcement, which has higher tensile strength and ductility. In this way, the steel is also protected by the concrete from potentially harmful environmental exposure (Michel et al., 2016). In the ideal situation, this combination should be very durable. However, a limitation of concrete is the presence of (micro) cracks, voids and capillary pores through which aggressive agents such as chlorides, CO_2, etc. can easily penetrate and deteriorate the structure (Sangoju et al., 2017).

One of the main deterioration mechanisms of reinforced concrete structures is corrosion of steel reinforcement. If left untreated, reinforcement corrosion accelerates the deterioration of reinforced concrete structures and may lead to several interrelated negative consequences, ultimately leading to a reduction in service life of these structures (Otieno et al., 2016a). In order for corrosion to occur in a basic environment as concrete, not only the presence of both water and oxygen – 'the driving forces' – are required, but also an anode (negative pole) where oxidation takes place and a cathode (positive pole) where electrochemical reduction takes place (De Schutter, 2014).

The corrosion of steel embedded in concrete is an electrochemical process in which both chemical reactions and flow of electrical current are involved. It can be divided into two separate, though coupled, chemical 'half-cell reactions' that take place simultaneously on the steel surface, the anodic reaction or the oxidation of iron and the cathodic reaction or the reduction of oxygen. These half-cell reactions are given below:

Anodic reaction – oxidation of iron:

$$Fe \rightarrow Fe^{2+} + 2e^{-} \qquad (2.1)$$

Cathodic reaction – reduction of oxygen:

$$O_2 + 2H_2O + 4e^{-} \rightarrow 4OH^{-} \qquad (2.2)$$

The anodic half-cell reaction is thus always characterised by liberating electrons (e^{-}), which are then conducted through the metal to the cathode, where they are consumed.

Fe^{2+} and OH^{-} ions react to form ferrous hydroxide ($Fe(OH)_2$) at the steel surface or different forms of hydroxides and oxides (Fe_3O_4 / Fe_2O_3 / ...) depending on the availability of oxygen and water and the pH (Gulikers & Raupach, 2006).

A schematic illustration of the corrosion process is shown in Figure 2.1. The surface of the corroding steel functions as a mixed electrode that is a composite of anodes and cathodes electrically connected through the body of the steel. Concrete pore water functions as an aqueous medium, i.e. an electrolyte, for transport of ionic species (Ahmad, 2003). Hereby, the corrosion cell can be seen as an electric circuit containing four components: an anode, a cathode, an ionic conductor (pore water) and an electronic conductor (steel bar).

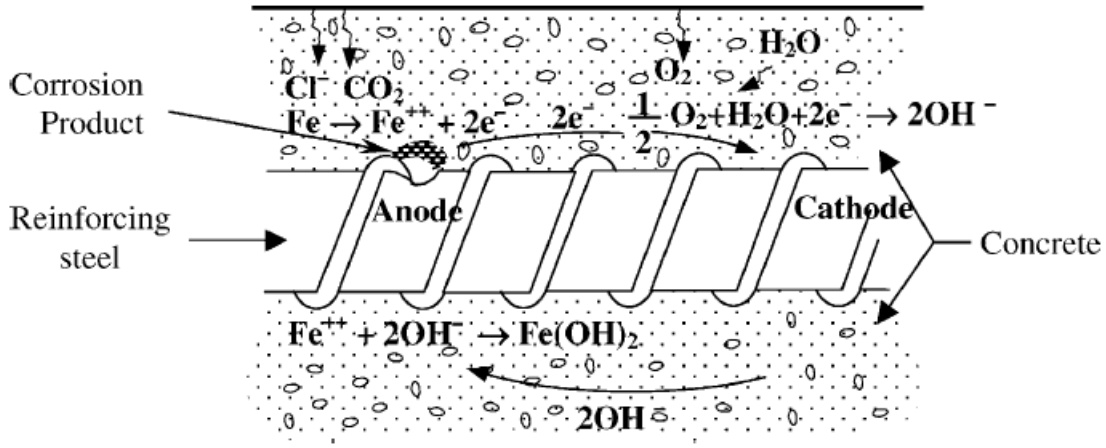

FIGURE 2.1: SCHEMATIC ILLUSTRATION OF STEEL REINFORCEMENT CORROSION IN CONCRETE (AHMAD, 2003)

Two kinds of electrochemical corrosion cells have been classified in literature: micro-cells and macro-cells (Cao et al., 2013).

- Micro-cell corrosion: pairs of immediately adjacent anodes and cathodes. The anodic reaction is totally supported by the local cathodic reaction;
- Macro-cell corrosion: spatially isolated anodes and cathodes. The anodic reaction in the active zone is supported by the cathodic reaction in the passive zone.

Accordingly, micro-cells often lead to uniform iron removal while macro-cells usually cause localised corrosion or pitting corrosion (see also paragraph 2.2). This is illustrated in Figure 2.2.

Despite the availability oxygen, water and aggressive substances, the chance is still real that corrosion does not occur. There are still two barriers which protect the steel against corrosion, i.e. the concrete cover, which is the shortest distance between the reinforcement surface and the concrete surface, and the passive layer of the steel rebar, a layer consisting of iron oxide (Fe_2O_3) which prevents the chemical reaction (2.1) (see also 2.2.1.2).

Many factors influence corrosion of steel in concrete. According to Ahmad (2003), these are the following:

- Availability of oxygen and moisture at rebar level
- Relative humidity and temperature
- Availability or ingress of aggressive substances (CO_2 or Cl^-)
- Concrete and steel quality parameters

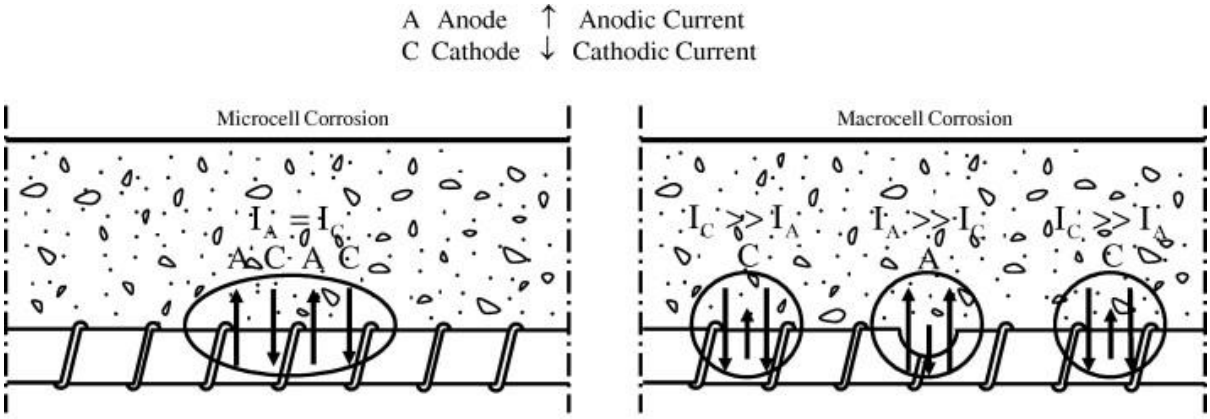

FIGURE 2.2: MICRO-CELL AND MACRO-CELL CORROSION (CAO ET AL., 2013)

2.2 Chloride-induced corrosion

As earlier mentioned, corrosion of steel in reinforced concrete structures is caused by either ingress of carbon dioxide, e.g. present in the air (carbonation-induced corrosion) or chlorides, e.g. ions present in sea water, industrial wastewater or de-icing salts (chloride-induced corrosion). Further in this thesis however, only the latter will be discussed, which is the main cause of steel corrosion in reinforced concrete structures (Otieno et al., 2016a).

A typical characteristic of chloride-induced corrosion (or localised corrosion) is pit formation on the steel, schematically illustrated in Figure 2.3. Although it depends on the exposure time, this pit (or small cavity) typically amounts a few square millimetres (Gulikers & Raupach, 2006).

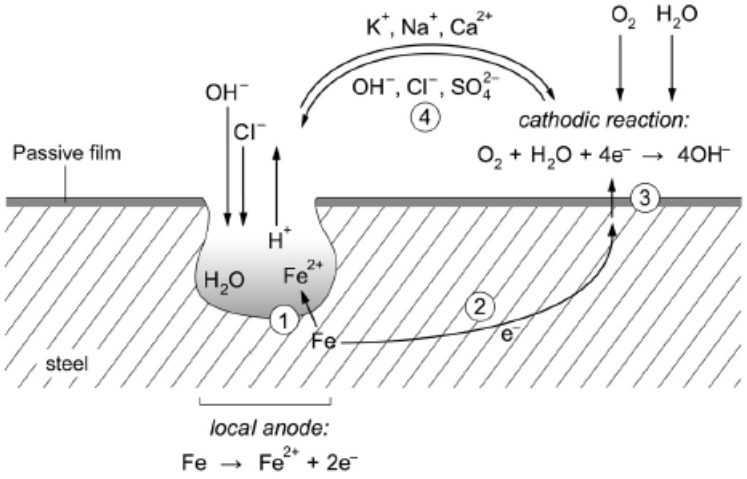

FIGURE 2.3: SCHEMATIC ILLUSTRATION OF CHLORIDE INDUCED PITTING CORROSION AND REACTION STEPS: 1. ANODIC IRON DISSOLUTION; 2. FLOW OF ELECTRONS THROUGH METAL; 3. CATHODIC REDUCTION REACTION; 4. IONIC CURRENT FLOW THROUGH THE ELECTROLYTE (ANGST, 2011).

2.2.1 Initiation and propagation

According to Tuutti's model (1982), the service life of structures exposed to reinforcement corrosion can be divided into two main time periods, the initiation period and the propagation period, as shown in Figure 2.4. The initiation period ($t_{initiation}$) can be defined as the time, starting from the exposure of the structure, until the reinforcement becomes depassivated. Thus, in case of chloride-induced corrosion, as soon as the concrete contains a critical amount of chlorides at the depth of the reinforcement. The time at which the reinforcement starts to corrode, defines the beginning of the propagation period ($t_{propagation}$) (Gulikers & Raupach, 2006). The formation of expansive corrosion products leads to tensile stresses in the surrounding concrete, finally resulting in cracking and spalling of the concrete cover, delamination and cross sectional reduction of the reinforcement. These corrosion-induced damages may cause aesthetic damages, decrease the load bearing capacity of a structure and in the worst-case lead to failure (Michel et al., 2016).

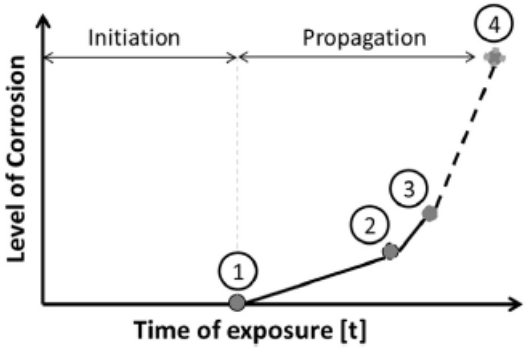

FIGURE 2.4: DETERIORATION LEVELS FOR CORROSION OF STEEL REINFORCEMENT IN CONCRETE; (1) DEPASSIVATION OF THE REINFORCEMENT (USUAL FAILURE CRITERION), (2) FORMATION OF CRACKS, (3) SPALLING OF THE CONCRETE COVER, AND (4) COLLAPSE OF THE STRUCTURE THROUGH BOND FAILURE OR REDUCTION OF THE CROSS SECTION OF THE LOAD BEARING REINFORCEMENT (JUSTNES ET AL., 2016)

Considering the above, the lifetime of a structure can be expressed as:

$$t_{\text{service life}} = t_{\text{initiation}} + t_{\text{propagation}} \qquad (2.3)$$

Herein, $t_{propagation}$ defines the time needed for unacceptable deterioration of the structure. For reinforced concrete, it has been assumed reasonable to equate this unacceptable corrosion damage to the onset of spalling of concrete cover (see (3) in Figure 2.4) (Ahmad, 2003). However, probably more important for chloride induced corrosion is the loss of steel cross sectional area or the loss of bond between the rebar and the concrete (see (4) in Figure 2.4). Unfortunately, no uniformly agreed model has been proposed to calculate the lifetime of a structure.

2.2.1.1 Chloride ingress in (uncracked) concrete

First, it has to be noted that concrete is highly reactive, which results in the fact that not all the infiltrating chlorides (or 'total chlorides') in concrete reach the steel. Many of them are trapped by the cement matrix, both physically and chemically. This process is known as chloride binding and the trapped chlorides are also called 'bound chlorides'. Subsequently, not all the chlorides inside concrete are responsible for corrosion. The chlorides that do reach the steel and which are responsible for corrosion, are called 'free chlorides' (Khitab et al., 2017). Thus, the chloride binding capacity of concrete is of great importance for protection against chloride induced reinforcement corrosion. This binding capacity mainly depends on the following factors (Angst, 2011):

- Type of cement
- pH-value
- Amount of calcium silicate hydrates (CSH)
- Temperature

Although these bound chlorides are not responsible for corrosion, they do play an important role in the corrosion process, since they affect the rate of chloride ingress, the chloride threshold value and thus the time to corrosion initiation (Montemor et al., 2003).

Chloride ingress in concrete is a complex phenomenon involving many mechanisms, e.g. capillary suction, diffusion, permeation and migration. Both capillary suction and diffusion are discussed in this section. However, in general, capillary suction is regarded as a much more efficient transport mechanism than diffusion since the chloride ions are carried with moving water rather than diffusing in static water (Angst, 2011).

The volume rate of solution flow (water + chloride ions) per unit area of concrete q_s, in $m^3/(m^2/s)$, can be expressed, using Darcy's law for one-dimensional capillary flow, as (Nagesh & Bhattacharjee, 1998):

$$q_s = -D(\theta_s)\frac{d\theta_s}{dx} \qquad (2.4)$$

where: θ_s the solution saturation [$(m^3$ of solution$)/(m^3$ of concrete$)$]
$D(\theta_s)$ the hydraulic diffusivity of the solution [m^2/s]

The flux of mass of chloride at any point in the concrete J_c, in kg/m^2s, due to capillary suction can then be written as:

$$J_c = C_s q_s \qquad (2.5)$$

where: C_s the (free) chloride concentration [kg/m^3 of solution]

In unsaturated concrete, chloride ingress is a combination of capillary suction and diffusion. Diffusion of chlorides, from higher concentration to lower concentration, is caused by a concentration gradient of the free chlorides. This concentration gradient can be expressed using

Fick's second law of diffusion and results in the following formulas to describe the chloride profile in function of time (Justnes et al., 2016):

$$C_x(x,t) = C_s - (C_s - C_i) \cdot \mathrm{erf}\left(\frac{x}{2\sqrt{D_{app}(t) \cdot t}}\right) \quad (2.6)$$

$$D_{app}(t) = D_{app}(t_0) \cdot \left(\frac{t_0}{t}\right)^m \quad (2.7)$$

where:			
	$C_x(x,t)$	total chloride content in the concrete or binder at a depth x at time s	[%]
	C_s	surface concentration of total chlorides in concrete or binder	[%]
	C_i	initial concentration of total chlorides in concrete or binder	[%]
	erf	error function	[-]
	$D_{app}(t)$	apparent chloride diffusion coefficient at time t	[m²/s]
	t_0	reference time	[s]
	m	aging factor	[-]

According to Justnes et al. (2016), the required (or maximum allowable) chloride diffusion coefficient (D) of concrete to achieve an intended service life (t) can also be expressed in function of the concrete cover thickness (x) over the reinforcement by:

$$D = (\text{concentration factor}) \cdot (\text{aging factor}) \cdot (\text{temperature factor}) \cdot \frac{x^2}{t} \quad (2.8)$$

This equation however only applies for uncracked concrete with service lives of minimum 25 years. Also, all three factors in the above equation are constants, so this equation can be simplified as follows.

$$D = (\text{constant}) \cdot \frac{x^2}{t} \quad (2.9)$$

Note that the above equations refer to the 'total' chloride profiles, while only the 'free' chlorides in the pore system actually diffuse. This is due to the fact that it is very difficult or even impossible to measure the 'free' chloride concentration. As a result, the diffusion coefficients obtained from these measured 'total' chloride profiles are often referred to as 'apparent' (Justnes et al., 2016).

Similar to equation (2.5), the ionic diffusion flux of chlorides J_d, in kg/m²s can then be written as given below (Nagesh & Bhattacharjee, 1998). This equation is also known as Fick's first law of diffusion.

$$J_d = -D_d(C_v)\frac{dC_v}{dx} \quad (2.10)$$

where: D_d the diffusion coefficient [m^2/s]
C_v the (free) chloride concentration [kg/m^3 of concrete]

The total flux J is then the sum of (2.5) and (2.10):

$$J = J_c + J_d \quad (2.11)$$

2.2.1.2 Depassivation

Steel in concrete is normally protected by the alkaline solution contained in the pores of the hydrated cement paste (with pH values higher than 13), which promotes *passivation*, i.e. the formation of a spontaneous thin protective oxide layer on the surface of the steel (Bertolini et al., 2016). This layer, often called the oxide film or the passive film, works as a physical barrier separating the metal from the adjacent electrolyte and as such prevents dissolution of the underlying metal and thus significantly reduces the corrosion rate.

The passive state remains as long as the concrete pore water in contact with the reinforcement is sufficiently alkaline and free from chloride ions. Corrosion of the steel bars takes place if the passive film is removed or is locally damaged, also called *depassivation*. So, in case of chloride-induced corrosion, chloride ions may locally break or destroy the passive film even in alkaline concrete. This occurs when chloride ions penetrate the concrete cover, and reach a critical threshold level at the depth of the reinforcement. Pitting corrosion thus initiates and propagates if moisture and oxygen are available at the passive areas of the steel surface.

2.2.1.3 Critical chloride content

Reinforcement corrosion in non-carbonated, alkaline concrete can only start once the chloride content at the steel surface has reached a certain threshold value. This value is often referred to as 'critical chloride content' or 'chloride threshold value' C_{crit} and can thus be defined as the chloride content required for depassivation of the steel. Numerous parameters affect this value of C_{crit}, of which the most important factors are the electrochemical potential of the steel, the pH of the pore solution in the concrete and the presence of voids at the steel-concrete interface (Bertolini et al., 2016). Sandberg (1999) stated that also the moisture content is believed to be an important factor in controlling the chloride threshold, as it directly influences the availability of oxygen at the reinforcement.

Although there are many ways to express the critical chloride content, most commonly it is expressed as the percentage of total chloride content relative to the mass of the cement. In Europe, it is intended to limit the tolerable chloride content to 0.4% by weight of cement. However, numerous researchers have found different values for C_{crit}. These reported values range from 0.04 to 8.34% total chloride by weight of cement (Angst et al., 2009).

2.2.1.4 Corrosion rate

During the initiation phase, the corrosion rate is assumed to be zero. During the propagation phase, the corrosion rate is not constant and is a function of many interrelated factors, such as (Otieno et al., 2016b):

- Cover depth
- Condition of the concrete cover (e.g. cracking) (see 2.3)
- Concrete quality
- Temperature
- Concrete resistivity
- Moisture content of the concrete

Depending on the corrosion state of the concrete (active or passive, see 2.2.1.2), different values for the corrosion rate can be measured. In case of a passive state, the rate of rebar corrosion appeared to be relatively low (10^{-9} to 10^{-7} A/cm^2), whereas relatively high values are noticed in case of an active state (10^{-6} to 10^{-5} A/cm^2) (Ahmad, 2003).

2.2.2 Durability strategies

Durability is of great importance for among others the design engineers, owners and researchers. Several parameters are commonly used to characterise the durability of concrete (Angst, 2011):

- Permeability
- Porosity and pore size distribution
- Ion diffusivities
- Electrical resistivity

Since slower penetration of aggressive substances implies the highest durability increase, low permeability, low porosity, low diffusivity and high electrical resistivity are beneficial. According to Bertolini et al. (2016), three main strategies against chloride-induced corrosion can be given:

1. The improvement of permeability of the concrete cover (only for uncracked concrete)
2. The use of stainless steel bars
3. The application of cathodic protection

Note that the use of stainless steel will increase costs and that not all stainless steels are resistant against chloride-induced corrosion. Another promising option to increase the durability (and sustainability) of reinforced concrete is partially replacing the cement by mineral admixtures, such as (ultra-fine) fly ash ((UF)FA), silica fume (SF), metakaolin (MK) and ground granulated blast-furnace slag (GGBFS), since this leads to an increased resistance of the concrete against chloride penetration (Shi et al., 2012). Further improvement of the durability properties of the concrete cover can be achieved by lowering W/C-factor or increasing the cover thickness. However, the presence of cracks in concrete can seriously affect these durability properties (Cao et al., 2013). The effect of cracks in concrete is discussed in the following section.

2.3 Effect of cracks

2.3.1 General

In service, cracks or micro-cracks are inevitably present in concrete as a result of several mechanisms, for example drying shrinkage, thermal gradients, freezing-thawing cycles, alkali-aggregate reaction and external loading (Wang & Ueda, 2011).

If no cracks would be present, both the initiation and propagation phases are usually a function of, among other factors, the penetrability of the concrete cover, the cover thickness, the resistivity of concrete, and the corrosion resistance of the steel bars. In the presence of cracks, studies have shown that the factors affecting the corrosion rate in uncracked concrete are still relevant but their effectiveness is significantly reduced (Otieno et al., 2016a). In this case, the corrosion resistance of the bars may be the main factor that has practical influence on the initiation and propagation phases (Otieno et al., 2010).

Cracks impair the durability of reinforced concrete structures by creating preferential paths for the penetration of corrosion-inducing species (water (H_2O), oxygen (O_2), carbon dioxide (CO_2), chlorides (Cl^-)) leading to faster initiation (and propagation) of steel corrosion and consequently a reduction in service life (Otieno et al., 2016a).

Analogously, Sangoju et al. (2017) formulated that the cracks in the concrete cover produce at least the following three specific effects:

i. They tend to facilitate the onset of corrosion by providing easy access for the penetration of dissolved Cl^- ions (and of CO_2) so as to induce depassivation (Figure 2.5);
ii. They accelerate the rate of corrosion once begun, by reducing the barrier to diffusion of oxygen, at least near the cracks themselves;
iii. They produce substantial non-uniformity in the physical and chemical environments around the steel, thus providing favourable conditions for corrosion to occur.

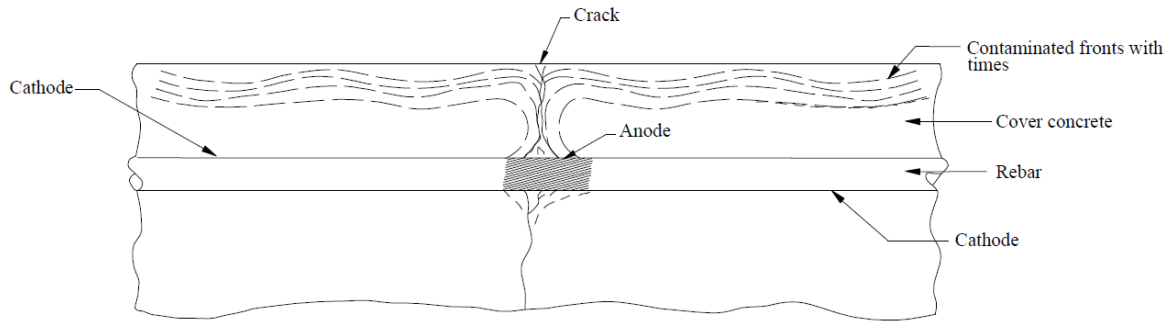

FIGURE 2.5: DEPASSIVATION OF THE STEEL NEAR THE CRACK (SANGOJU ET AL., 2017)

2.3.2 Chloride ingress in cracked concrete

As mentioned in paragraph 2.2.1.1, chloride penetration in sound saturated concrete is a one-dimensional diffusion process. Hence, for sound concrete, Fick's second law can be used to determine the free chloride concentration. For cracked concrete, however, chloride penetration is a two-dimensional diffusion process and thus a two-dimensional finite element analysis can be used to calculate the free chloride concentration (can also be determined experimentally). This was investigated by Wang & Zhang (2016). They stated that cracked concrete can be divided into two zones, a sound zone and a cracked zone. For stress-free concrete, it is assumed that the chloride diffusion coefficient in the sound zone is the same as that of sound concrete.

In the cracked zone, however, additional chlorides can penetrate into concrete, as mentioned earlier. Thus, the considerations of the influence of cracking on chloride ingress are necessary for the durability design of reinforced concrete structures. Wang & Zhang (2016) found that cracks have a significant influence on the chloride concentration around the cracked zone. With the increase of crack width, crack depth and crack amount, more chloride ions will penetrate and the chloride penetration depth increases correspondingly and thus the chloride ingress will aggravate.

The relation between chloride diffusion coefficient and crack width can be described using a piecewise function as follows (Wang & Zhang, 2016):

$$D_{cr} = \begin{cases} D_{app} & \omega < 30\ \mu m \\ 28.3 - 35.6\exp(-0.00835\omega) & 30 \le \omega \le 120\ \mu m \\ D_{H_2O} & \omega > 120\ \mu m \end{cases} \qquad (2.12)$$

where:	D_{cr}	the chloride diffusion coefficient in cracked concrete	[m²/s or mm²/h]
	D_{app}	the apparent diffusion coefficient	[m²/s or mm²/h]
	D_{H_2O}	the chloride diffusion coefficient in water	[m²/s or mm²/h]
	ω	the crack width	[μm]

As shown in (2.12), when the crack width is less than 30 μm, which is the lower limit for cracks to influence chloride diffusion, the product of subsequent hydration and self-healing (see section 4.3) of cementitious materials will block the crack. So the crack's effect can be ignored. When crack width is higher than 30 μm and less than 120 μm, which is the upper limit for cracks to influence chloride diffusion, the product of subsequent hydration cannot block the crack completely, so chloride diffusion will happen in the unblocked part. When the crack width is higher than 120 μm, the product of subsequent hydration cannot block the crack, so D_{cr} is equal to the chloride diffusion coefficient in water D_{H_2O}.

So, it can be seen that, at the same depth, the chloride diffusion coefficient in the cracked zone is much higher than that of the sound zone and thus the chloride concentration in the cracked zone is much higher than that in the sound zone.

A similar relation between the chloride diffusion coefficient and the crack width was proposed by Wang & Ueda (2011), although with different crack width criteria. They concluded that when the crack width is larger than a critical value, D_{cr} is independent of the crack width and is determined

as 10000 mm²/h, which is much larger than that in free bulk water. When the crack width is less than this critical value, D_{cr} is determined as the average value of a range from 1500 mm²/h to 4500 mm²/h, i.e. 3000 mm²/h.

2.3.3 Influencing factors

The effect of cracking on the durability of reinforced concrete structures is a complex function of their type, width, length, depth, frequency, orientation with respect to the reinforcement and self-healing potential. Some of these can be summarised as follows (Otieno et al., 2010):

- Longitudinal cracks (parallel to the reinforcement) are more likely to result in higher corrosion rates than transverse cracks (perpendicular to the reinforcement), because the corroded length will be much larger (Gulikers & Raupach, 2006).
- The corrosion rate increases with increasing frequency of intersecting cracks. Hereby, it has to be stated that, as longitudinal cracks widen and interconnect, localised corrosion (macro-cell) may gradually evolve into uniform corrosion (micro-cell) (Cao et al., 2013).
- The occurrence and benefits of crack self-healing (i.e. the time-dependent behaviour of the crack) are significant in the reduction in concrete penetrability and hence improving the protection of the embedded steel from corrosion (see section 4).

Furthermore, the influence of the crack width, concrete quality and cover depth on the corrosion rate was investigated by Otieno et al. (2016a). Hereby, concrete quality refers to the ease of ingress of corrosion-sustaining agents (mainly oxygen and moisture). This study showed that the corrosion rate (i_{corr}) increased with increase in crack width, and decreased with increase in concrete quality (represented by binder type and water-to-binder (w/b) ratio) and cover depth. The effect of the cover depth can be attributed mainly to the limited oxygen availability (as cover depth increases) to sustain the cathodic reaction during corrosion by increasing its travel path from the concrete surface to the steel level. Concerning the crack width, it is believed that adopting one unique threshold value is not very reliable, since the effect of crack width on corrosion of reinforcing steel is influenced by many factors (Blagojevic et al., 1991).

In general, blended concretes (50/50 OPC/…) seemed to be much less affected by cracking (i.e. higher resistivity) compared to plain concrete (OPC), which leads to the strong preference to blended cements for marine environments. Corex slag concretes are also less sensitive to changes in w/b-ratio (Otieno et al., 2010). Sangoju et al. (2017) further stated that the rebar corrosion is lower in concrete with lower water to cement ratios, due to decreased permeability and lower electrical conductivity.

The influence of crack reopening on corrosion of cracked concrete was also studied by Otieno et al. (2010). It could be concluded that reloading (crack reopening) of corroding reinforced concrete structures accelerates corrosion by reactivating (reopening) self-healed cracks, widening the existing ones, increasing the loading level (i.e. stress in the steel), damaging the concrete-steel interface or a combination of the aforementioned. However, the effect of reloading was more significant if the reinforced concrete structure was actively corroding before reloading.

3. Corrosion monitoring

As mentioned in paragraph 2.1, reinforcement corrosion can lead to high costs for maintenance and/or repair. So, in order to avoid high costs, monitoring corrosion at an early stage is necessary. Corrosion can be detected by different techniques. Important to notice is that quantifying corrosion using one monitoring technique is not reliable. Thus, a more accurate conclusion about the corrosion state of the reinforcement can be obtained by a combination of different techniques. Also, complementary data from the concrete structure, by specialists or skilled engineers in the field of corrosion testing and structural evaluation, is necessary (Elsener et al., 2003).

One possibility to detect active corrosion are (one or more) electrochemical monitoring techniques. In this thesis, different non-destructive monitoring techniques were used, measuring the following parameters: macro-cell corrosion current, corrosion potential, ohmic drop, open circuit potential, concrete resistance and linear polarisation resistance. These are all discussed in this section.

In addition to the above mentioned techniques, active corrosion can also be detected by weight loss measurements. However, this method is a destructive technique and is not suitable to identify the time of depassivation, since already a significant amount of corrosion is necessary in order to detect the mass difference. To identify depassivation, visual inspection of the steel surface – after splitting the concrete of course – can be useful, due to the appearance of rust on the steel surface. The accuracy of this method is however also low, since it is not possible to know how much time has passed between depassivation and visual observation of rust. Moreover, the appearance of rust spots may take some time and, once present, does not necessarily mean significant and sustained corrosion activity (Angst et al., 2009).

Depassivation can thus not be considered as an instant event, but rather as a period of time, from the first defect until active corrosion is established. It is thus impossible to identify the very start, e.g. the first local defect in the passive film. Nevertheless, electrochemical techniques come much closer to this moment than visual inspection and weight loss measurements (Angst et al., 2009).

3.1 Corrosion Potential (E_{corr})

The corrosion potential, also called half-cell potential, E_{corr} is a qualitative index which can be used to locate (areas of) corroding reinforcement as well as evaluating the efficiency of the repair work (Elsener et al., 2003). Although it is the most widely used electrochemical method for corrosion monitoring, it does not provide any quantitative information on the actual corrosion rate of the reinforcement (Ahmad, 2003).

This method consists of measuring the difference of electric potential between the electrode of interest (e.g. reinforcement steel), or working electrode (WE), and a reference electrode (half-cell). This can be done using a voltmeter with a high internal impedance, in order not to disturb

the electrode under study (Angst, 2011). Following external reference electrodes are commonly used (Elsener et al., 2003):

- Copper – Copper sulphate electrode (Cu / $CuSO_4$) (CSE)
- Saturated calomel electrode (Hg / Hg_2Cl_2) (SCE)
- Silver chloride electrode (Ag / AgCl)

The saturated copper – copper sulphate electrode is more suitable for on-site work, while the calomel and silver chloride electrodes are used more in the laboratory work. In practice, a silver chloride electrode (Ag/AgCl) is also used as an internal reference electrode.

In case of external reference electrodes, placed on the concrete surface (Figure 3.1), the corrosion potential cannot be measured directly at the concrete / rebar interface, due to the concrete cover. The potentials are thus influenced by the ohmic drop (or IR-drop) in the concrete cover (see paragraph 3.2) (Elsener et al., 2003).

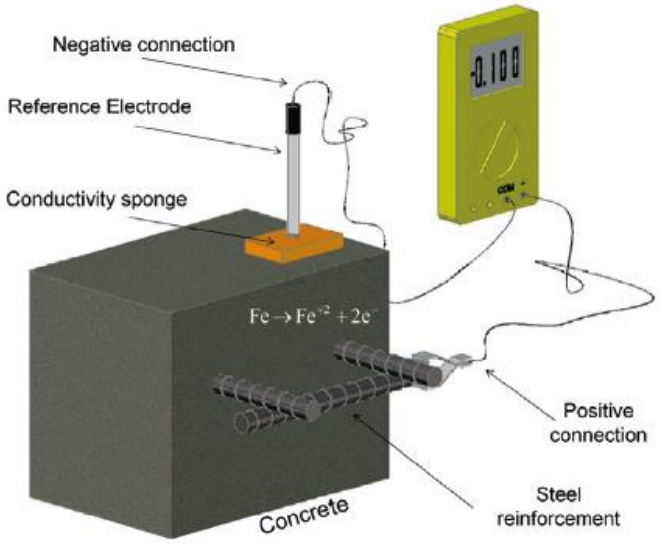

FIGURE 3.1: PRINCIPLE OF CORROSION POTENTIAL MEASUREMENT, USING AN EXTERNAL REFERENCE ELECTRODE (MEDEIROS M. H. F., 2017)

Alternatively, an internal electrode can be used instead of an external, which reduces the IR-drop. The most used internal reference electrode to perform potential measurements are metal-metal oxide (MMO), such as Mn/MnO_2- and Ti/TiO_2-electrode (Poursaee, 2014).

Electrical conduction between the reference electrode and the concrete is established by the transport of ions. This can be done by placing a conductive bridge between the reference electrode and the concrete. In case of an external reference electrode, the resistance between the reference electrode and the concrete is lowered by placing a wet sponge in between, as can be seen in Figure 3.1 (Elsener et al., 2003).

The corrosion potential depends on the type of reference electrode used and on the corrosion condition of the steel. Based on these factors, different criteria for the interpretation of these potentials can be drawn. These are depicted in Table 3-1. Actively corroding steel has a more

negative potential than passive steel in concrete. However, a low potential value does not necessarily mean significant corrosion. So, only a clear drop in potential (change from passive to active condition) can be used as criterion for depassivation (Angst et al., 2009).

TABLE 3-1: CRITERIA FOR INTERPRETATION OF CORROSION POTENTIALS (ASTM C876-91, 2009)

$Cu/CuSO_4$ electrode	**Ag/AgCl electrode**	**Likely corrosion condition**
> -200 mV	> -106 mV	Low (10% risk of corrosion)
-200 to -350 mV	-106 to -256 mV	Intermediate corrosion risk
< -350 mV	< -256 mV	High (> 90% corrosion risk)
< -500 mV	< -406 mV	Severe corrosion

The corrosion potential is also influenced by the concrete moisture and oxygen content, the water-to-cement ratio, the thickness of the concrete cover and the degree of chloride contamination. For example, both higher moisture (and oxygen) contents as well as chloride contamination, seemed to result in more negative values of corrosion potential due to the increase of the electrical conductivity of the system.

3.2 Ohmic drop (IR drop)

As can be seen in Figure 2.3, the anodic and cathodic sites are spatially separated and the electrical circuit in the macro-cell has to be closed by a ionic flow through the electrolyte. However, in the presence of an ohmic resistance against this ionic flow, the potentials of anode and cathode are not equal. In this case, energy is dissipated by the ionic current passing the resistance in the electrolyte. So, while the currents of the anodic reaction and the cathodic reaction are equal, the potentials are different. This voltage drop is usually referred to as *ohmic drop* or *IR drop* (Angst, 2011).

3.3 Corrosion current (I_{corr})

Another indication of the corrosion state of the reinforcement can be given by the corrosion current, measured between the anode and cathode of the reinforcement.

As mentioned before, the chlorides in concrete cause pitting of the reinforcing steel, which leads to substantial reductions in the cross-sectional area of the bars. In case of localised corrosion, it may be expected that the corroding spot would behave as pure anode, while the surrounding zones behave as pure cathodes. However, it was found by Andrade et al. (2008) that the anodic zones also contain cathodic zones. In other words, there exists both a macro-cell current (or galvanic current) between non-corroding and corroding zones, as well as a micro-cell current within this corroding zone. This is depicted in Figure 3.2.

So, the overall corrosion current (I_{corr}) is then equal to the sum of macro-cell corrosion current (I_{macro}) and the micro-cell corrosion current (I_{micro}):

$$I_{corr} = I_{macro} + I_{micro} \qquad (3.1)$$

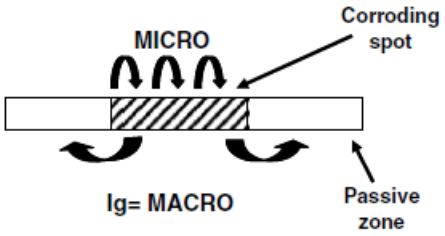

FIGURE 3.2: REPRESENTATION OF COUPLED MICRO- AND MACRO-CELL CORROSION CURRENT IN CASE OF LOCALISED CORROSION

Since a transport of ions and electrons is created by the electrochemical reactions (2.1) and (2.2) (see also Figure 2.3), the rates of these reactions are normally given as electric current densities (Gulikers & Raupach, 2006):

- Electric current (I) = electric charges per unit of time [coulomb/s = ampere]
- Electric current density (i) = electric current per unit (polarised) surface area of steel [ampere/square meter, A/m^2]
- Corrosion current density (i_{corr}) (or corrosion rate) = electric charges per unit of time [microampere/square centimetre, $\mu A/cm^2$]

The corrosion rate is measured in terms of this electrochemically measured corrosion current density, which is the most useful quantitative parameter for studying corrosion in reinforced concrete, representing the amount of corrosion of steel in concrete (Ahmad, 2003). This value indicates the difference between passivity (very low values) and active corrosion (higher values).

In order to calculate the corrosion current density, a damage model for reinforcement corrosion was proposed by Schwenk (1972) which basically follows Ohm's law, where the current can be calculated by dividing the potential difference by the resistances of the system. Since the macro-cell model neglects micro-cell corrosion, the damage model is extended by the term I_{micro} (or I_{self}). This can be seen in Figure 3.3, which shows this macro-cell corrosion model as an equivalent electrical circuit diagram.

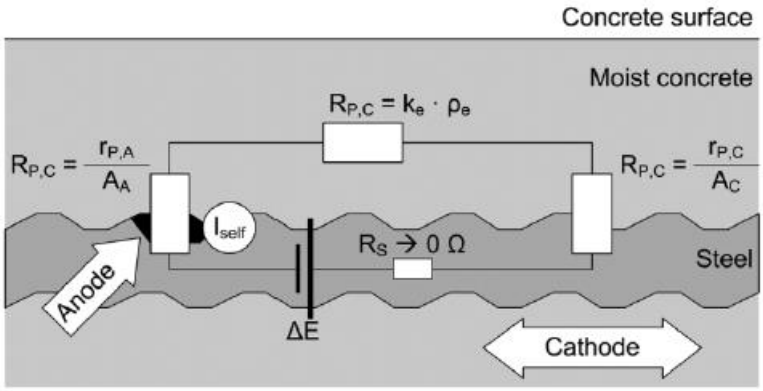

FIGURE 3.3: ELECTRICAL EQUIVALENT CIRCUIT DIAGRAM FOR MACRO-CELL CORROSION MODEL

Corresponding to this electrical circuit diagram, Schwenk (1972) defined the following equation:

$$I_{corr} = \left[\frac{E_{0,C} - E_{0,A}}{R_{P,A} + R_{P,C} + R_E} + I_{micro}\right] \qquad (3.2)$$

where:	I_{corr}	macro-cell corrosion current	[A]
	$E_{0,C}$	resting potential of cathode	[mV]
	$E_{0,A}$	resting potential of anode	[mV]
	$R_{P,C}$	polarisation resistance of cathode	[Ω]
	$R_{P,A}$	polarisation resistance of anode	[Ω]
	R_E	concrete resistance	[Ω]
	I_{micro}	micro-cell corrosion current	[A]

From equations (3.1) and (3.2), it can be seen that the macro-cell corrosion current (I_{macro}) is defined as the driving potential (ΔE), which is the potential difference between the anode $(E_{0,A})$ and the cathode $(E_{0,C})$, divided by the sum of the resistances of the system. The system resistance is composed of the resistances of the anodic and cathodic partial reactions (defined by the anodic and cathodic polarisation resistances $R_{P,A}$ and $R_{P,C}$), the resistance of the concrete (R_E) and the resistance of the steel. However, the latter can be neglected, as also indicated in Figure 3.3. Concerning the micro-cell corrosion current (I_{micro}), without going further into detail, investigations have shown that its development is influenced by parameters such as the type of cement, w/c-ratio, chloride content, temperature, moisture content and surrounding air humidity (Beck et al., 2012).

All the above mentioned parameters from equation (3.2) can be determined experimentally:

- Resting potentials (anode and cathode) → Open circuit potential measurements (see section 6.6.4)
- Polarisation resistances (anode and cathode) → Linear polarisation resistance measurements (section 3.4 and 6.6.6)
- Concrete resistance → Electrochemical impedance spectroscopy (section 3.5) or resistivity monitoring techniques (section 3.6).

3.4 Linear polarisation resistance (LPR)

The most quantitative technique to detect depassivation of the steel is the measurement of the polarisation resistance. This non-destructive technique allows to determine of the instantaneous corrosion rate and is based on the observation that within a small potential range (typically 10-20 mV) around E_{corr}, the *E-I*-relationship is approximately linear. The linear polarisation resistance R_p is then defined as the slope of this curve at E_{corr} or thus the relation between the potential (ΔE) and the current (ΔI) (Angst, 2011):

$$R_p = \left.\frac{\Delta E}{\Delta I}\right|_{E=E_{corr}} \quad (3.3)$$

This resistance to polarisation is related to the corrosion activity. For example, small polarisation resistance indicates high corrosion activity (Gulikers & Raupach, 2006).

3.5 Electrochemical impedance spectroscopy (EIS)

Electrochemical impedance spectroscopy (EIS) is a powerful technique to study the steel/concrete system. It provides information on a number of parameters, such as the presence of surface films, characteristics of the concrete, interfacial corrosion, and mass transfer phenomena (Ribeiro & Abrantes, 2016). The basic concept of EIS is that an electrochemical interface can be viewed as a combination of passive electrical circuit elements, i.e. resistance, capacitance and inductance (Montemor et al., 2003).

Like resistance, impedance is a measure of the ability of a circuit to resist the flow of electrical current, but which is not limited to certain simplifying properties and thus is a more general circuit parameter (Orazem & Tribollet, 2017). Electrochemical impedance is usually measured by imposing an external sinusoidal voltage signal (alternating current (AC)) with an small amplitude (typically in the range of 10 mV) to the working electrode. The frequency is varied over a large range (usually from 1 MHz to mHz) and the current response in the system is measured (Angst, 2011).

An expression analogous to Ohm's law allows to calculate the impedance of the system (Orazem & Tribollet, 2017):

$$Z = \frac{E_t}{I_t} = \frac{E_0 \sin(\omega t)}{I_0 \sin(\omega t + \varphi)} = Z_0 \frac{\sin(\omega t)}{\sin(\omega t + \varphi)} \quad (3.4)$$

The impedance is thus expressed in terms of a magnitude, Z_0, and a phase shift, φ. So, from this relation between the imposed voltage signal, the recorded current response and the phase difference, the impedance, Z, can be obtained for various frequencies. The impedance can also be expressed as a complex function, in which the impedance $Z(\omega)$ is split into a real part, $|Z|(\cos\varphi)$, and an imaginary part, $|Z|(\sin\varphi)$.

$$Z(\omega) = \frac{E}{I} = |Z|(\cos\varphi + j\sin\varphi) \qquad (3.5)$$

The EIS measurements are usually interpreted using a correlation between the impedance data and an equivalent circuit representing the physical processes taking place in the system under investigation or through graphical representations (Ribeiro & Abrantes, 2016). To discuss the variation of impedance with frequency, the data is often plotted in a "Nyquist plot" (complex plane plot), where real and imaginary parts of the impedance are abscissa and ordinate, respectively (Angst, 2011). This plot consists of a series of points, each representing the impedance at a particular frequency. The magnitude of this impedance can then be represented as a vector of length $|Z|$ and the direction of the impedance by the phase angle φ (or arg Z) or the angle between this vector and the X-axis.

Figure 3.4 shows a typical Nyquist diagram and its equivalent circuit. The Nyquist diagram clearly shows a semicircle, which is extrapolated at the right side until the diagram intersects with the horizontal axis. This determines the diameter of this semicircle, which represents the charge transfer resistance, R_t, which is equivalent to the polarisation resistance, R_p. So, a larger diameter of the semicircle corresponds to a higher resistance, R_p, and thus a lower corrosion rate (Ribeiro & Abrantes, 2016). From Figure 3.4 also the ohmic resistance, R_Ω, can be determined. As indicated, this is represented by the offset of the semicircle from the origin.

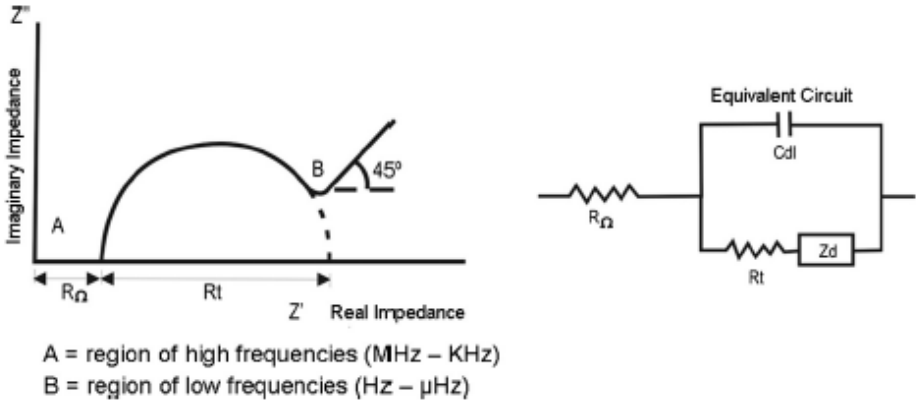

FIGURE 3.4: NYQUIST DIAGRAM AND ITS EQUIVALENT CIRCUIT (RIBEIRO & ABRANTES, 2016)

Another possible representation is the Bode plot (Figure 3.5), which shows the logarithm of the impedance modulus $(\log|Z|)$ (in ohms (Ω)) and the phase shift (φ) (in degrees) as a function of the frequency logarithm $(\log\omega \text{ or } \log f$ with ω in rad/s and f in Hz).

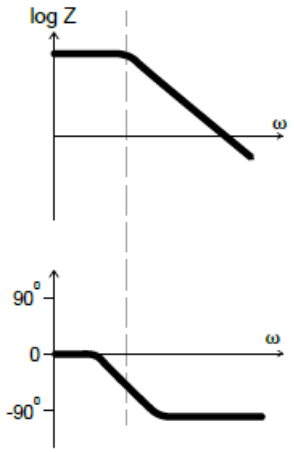

FIGURE 3.5: BODE DIAGRAM REPRESENTING THE IMPEDANCE (MODULUS AND PHASE ANGLE) OF AN ELECTROCHEMICAL CORROSION SYSTEM AS A FUNCTION OF THE ANGULAR FREQUENCY (ORAZEM & TRIBOLLET, 2017)

The main (dis)advantages of EIS are listed below (Ribeiro & Abrantes, 2016).

Advantages:

- Information regarding the corrosion kinetics
- Suitable for highly resistive environments (such as concrete)
- Provides data which indicate if corrosion occurs
- Characterizes the state of the rebar and the corrosion morphology
- Non-destructive and non-invasive technique
- Allows to monitor the evolution of the passive or active state

Disadvantages:

- Difficult to interpret the results
- More suitable for laboratory studies

3.6 **Resistivity monitoring**

The electrical resistivity of concrete can be described as the ability of concrete to withstand the transfer of ions subjected to an electrical field. The electrical resistivity of concrete is influenced by various parameters such as (Layssi, Ghods, Alizadeh, & Salehi, 2015):

- Pore structure (pore size distribution and interconnection)
- Conductivity of pore fluid
- Degree of saturation (moisture content)
- Temperature

The concrete resistivity is (empirically) inversely proportional to the corrosion rate. The rate of loss of rebar cross section in the propagation stage can thus empirically be correlated to concrete resistivity (Angst, 2011). So, the higher the resistivity, the lower the corrosion rate and thus the more resistance against corrosion. Equation (3.6) describes the relationship between the resistivity [Ωm], ρ, and the resistance [Ω] , R, of the concrete.

$$\rho = k \cdot R \qquad (3.6)$$

where k is a geometrical factor [m] which depends on the size and shape of the sample as well as the distance between the probes on the testing device (Layssi et al., 2015).

Several techniques can be used to measure the (instantaneous) electrical resistivity of concrete, including two-point uniaxial techniques, for testing concrete samples or drilled cores, and four-point (Wenner probe) techniques, for on-site evaluation. These test methods are schematically shown in Figure 3.6. In general, they are based on imposing a voltage between two (or more) electrodes and measuring the current (or vice versa) and using a cell constant to convert the measured electrical resistance, R (Ω), into electrical resistivity, ϱ (Ωm) (Angst, 2011).

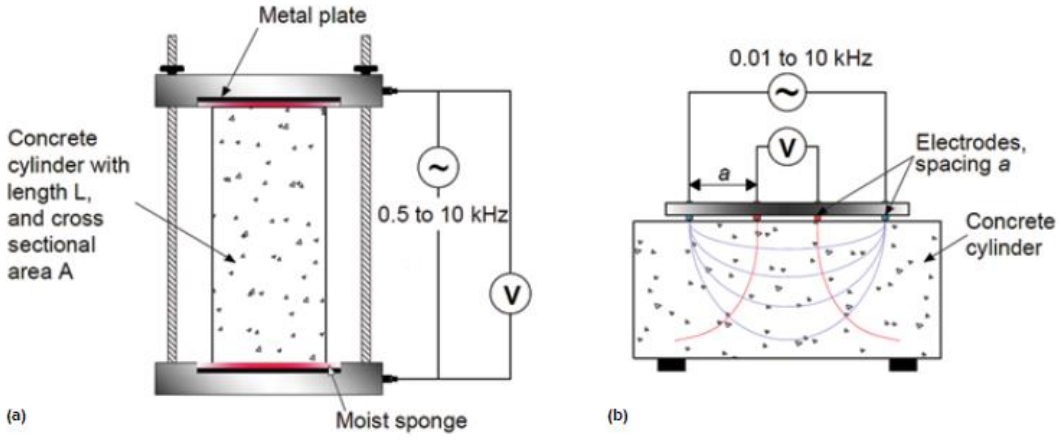

FIGURE 3.6: ELECTRICAL RESISTIVITY MEASURING TECHNIQUES: (A) TWO-POINT UNIAXIAL METHOD; AND (B) FOUR-POINT (WENNER PROBE) METHOD (LAYSSI ET AL., 2015)

4. Crack healing

Since in practice, reinforced concrete elements are almost always cracked, repair of these cracks is necessary in order to avoid major damage and/or extend the service life of these concrete structures.

However, maintenance and/or repair works impose high direct and indirect costs and some structures are even not accessible for inspection and/or repair. Fortunately, cementitious materials have the natural ability to repair damage to a certain extent. However, this natural, so called autogenous, crack healing mechanism is limited to small cracks (up to 100 μm) (De Belie et al., 2017), is only effective when water is available and is difficult to control. This is explained in detail in section 4.3. However, if the cracks are larger than 100 μm or the conditions are not favourable for autogenous healing, manual healing can be applied or autonomous healing mechanisms can be incorporated. These mechanisms are explained in sections 4.2 and 4.3, respectively. In section 4.1, first an overview is given of the most commonly used healing agents for autonomous crack healing. In section 4.4 and 4.5 two healing agents are discussed which are used in this master's dissertation: polyurethane (PU) and water repellent agent (WRA).

4.1 Healing agents

In order to suit as healing agent, several requirements need to be fulfilled. One of the most important parameters of a healing agent is its viscosity. The viscosity cannot be too high, in order to be able to fill the crack, nor be too low, since this can lead to the fact that the agent leaks out of the crack or is absorbed by the surrounding matrix. Another important property of a healing agent is the curing time. An agent should not cure too fast, such that it is able to fill the crack completely. On the other hand, a too long curing time can, similar to a too low viscosity, lead to leakage of the agent out of the crack. Further, also the way of curing, the sealing ability, some mechanical properties and the stability over time are of importance (Van Tittelboom & De Belie, 2013).

Taking into account the aforementioned parameters, an overview can be given of the most commonly used healing agents (Van Tittelboom & De Belie, 2013):

- Cyanoacrylate (CA)
- Epoxy
- Methylmethacrylate (MMA)
- Silicone
- Polyurethane (PU)
- Polyacrylate
- Tung oil
- Alkali silica solution
- Solution of $Ca(OH)_2$, Na_2SiO_3, Na_2FPO_3 or $Ca(NO_3)_2$
- Bacterial solution

Clearly, the selection of the healing agent is very important to have a good autonomous healing of cracks and can depend on the application of the healing agent.

4.2 Manual healing

Although manual crack repair is expensive, labour intensive and not always feasible due to eventual invisibility or inaccessibility of the cracks, good healing results can be achieved. This has for example been confirmed by Maes et al. (2013), through investigation of the chloride resistance of manually healed cracks (see section 4.4).

One commonly used manual healing lab technique is the injection of a healing agent in the crack, using a needle or something similar. Another possibility is to apply a protective surface treatment. This latter technique is more favourable in practice, since it is less labour-intensive and thus is cost-effective. In general, this protective surface treatment can be classified into three categories (Dai et al., 2010):

a. Surface coating (applying thin or thick polymer film)
b. Sealing (blocking the surface near the pores)
c. Surface impregnation (impregnation of water repellent agent, leaving the pores open)
d. Crack injection

Several studies have verified that surface impregnation can form an efficient barrier and as such postpone the corrosion initiation and reduce the corrosion rate of the steel reinforcement. This surface treatment can be applied before and/or after crack creation. Dai et al. (2010) stated that for reinforced structures with cracks existing before application of sealants or other surface treatments, the efficiency (and long-term effectiveness) of the healing agent mainly depends on its penetration depth. This penetration depth in concrete relies on the following factors:

- Type of (hydrophobic) healing agent
- W/C - ratio
- Initial moisture content
- Surface preparation

When cracks were formed after surface impregnation, chloride penetration could not be totally prevented (except for fine cracks) and a second surface impregnation then was unavoidable. Nevertheless, significant reduction of the corrosion rate was observed.

4.3 Self-healing concrete

With self-healing concrete, the idea is to modify the concrete structure to give it the ability of restoring cracks by itself at the moment of their appearance, in order to obtain autonomous crack healing. In this way, no manual repair works are needed anymore and further damage is avoided immediately (Van Belleghem et al., 2017a). According to Van Tittelboom et al. (2013), self-healing in cementitious materials can be classified broadly into three groups:

- Intrinsic healing
- Capsule based healing
- Vascular healing

Intrinsic self-healing concerns self-healing properties due to the composition of the cementitious matrix. In case of capsule based self-healing, the healing agent is captured in discrete capsules,

while with vascular based self-healing, the healing agent is situated in a network of hollow tubes which connect the interior and the exterior of the structure. Further, only the two former healing mechanisms will be podiscussed, since only these apply to this master's dissertation.

4.3.1 Intrinsic Self-Healing

One of the most widely studied mechanisms of crack healing in cementitious materials is autogenous healing, i.e. the natural ability to repair damage. Crack closure due to autogenous healing is mainly caused by two mechanisms. The main healing mechanism in young concrete, when water enters into concrete cracks, is hydration of unhydrated cement particles. However, if both water and carbon dioxide are present, crack closure can be obtained by dissolution and subsequent carbonation of calcium hydroxide ($Ca(OH)_2$). This becomes the major healing mechanism at later age. Further, autogenous healing can also be caused by debris present in the ingress water or loose concrete particles which block the crack.

Autogenous healing is limited to small cracks. Van Tittelboom et al. (2013) stated that the narrower the cracks are, the more likely these cracks will be completely healed by autogenous healing. Also, contact with water is needed in order to activate the mechanism (Van Tittelboom et al., 2016). Taking into account these two conditions, autogenous healing can consequently be improved, either by restriction of the crack width or by water supply. A third option to improve autogenous healing is by increasing the possibility of ongoing hydration or crystallisation. Figure 4.1 illustrates these improvements, respectively.

Restriction of the crack width can be done by using fiber reinforced strain hardening engineered cementitious composite (ECC). ECC is characterised by its high ductility and its unique crack pattern. Instead of one large single crack, multiple cracks form in the ECC matrix with a maximum crack width of 60 μm. Moreover, the highest healing efficiency was acquired with poly vinyl alcohol (PVA) fibers, due to the fact that these fibers promoted the deposition of crystallisation products (Van Tittelboom & De Belie, 2013).

Water supply can be achieved by mixing super absorbent polymers (SAP), also called hydrogels, into the cementitious material. These superabsorbent polymers absorb water which intrudes into the cracks, immediately blocking the crack through swelling. Slow release of the absorbed water, later on, leads to further hydration and precipitation of calcite, stimulating autogenous healing (Snoeck et al., 2014). Another mechanism to promote the self-healing behaviour, is by using nanoclay as an internal water reservoir (Qian et al., 2010). The water retaining capacity of nanoclay then provides internal water for further hydration.

Finally, improving hydration and crystallisation can be realised through addition of agents which are able to promote the deposition of crystals inside the crack, e.g. replacing part of the cement by fly ash or blast furnace slag. High amounts of these binders remain unhydrated, thus improving ongoing hydration. Other possibilities are adding expansive additives (De Belie et al., 2017), chemical agents or bacteria and nutrients to enhance the precipitation of $CaCO_3$ crystals at the crack (Van Tittelboom & De Belie, 2013).

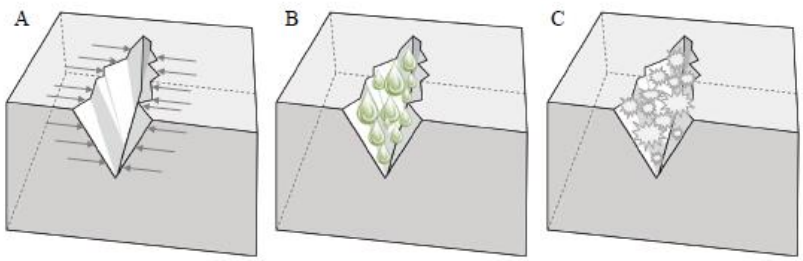

FIGURE 4.1: IMPROVED AUTOGENOUS HEALING BY (A) RESTRICTION OF THE CRACK WIDTH, (B) WATER SUPPLY OR (C) IMPROVED HYDRATION AND CRYSTALLISATION (VAN TITTELBOOM & DE BELIE, 2013).

4.3.2 Capsule Based Self-Healing

In the case of capsule based self-healing, brittle capsules filled with a healing agent are placed in the cementitious matrix, close to the reinforcement bar. Crack formation causes breakage of the brittle capsules and simultaneous release of the polymeric healing agent, which fills up the crack and forms a barrier which prevents fluid ingress through the cracks, leading to a reduced corrosion risk for the steel reinforcement (De Belie et al., 2017).

The reaction of the healing agent in the region of damage can be due to heating or due to contact with moisture, air, the cementitious matrix itself or with a second component present in the matrix or in the capsules. This is illustrated in Figure 4.2.

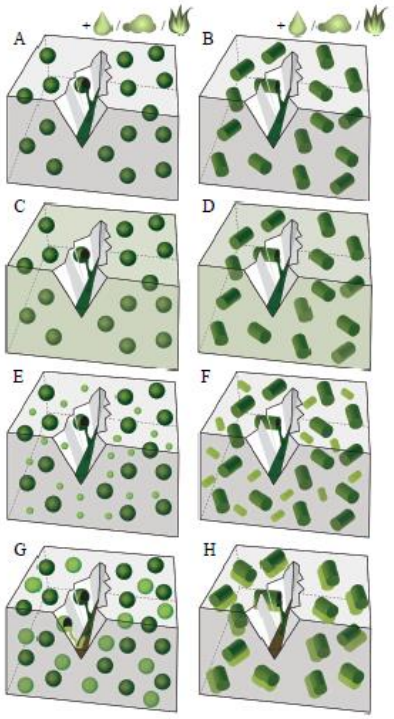

FIGURE 4.2: CAPSULE BASED SELF-HEALING APPROACHES; LEAKAGE OF HEALING AGENT FROM THE SPHERICAL/CYLINDRICAL CAPSULES INTO THE CRACK, WHERE IT REACTS DUE TO CONTACT WITH (A,B) MOISTURE OR AIR OR DUE TO HEATING, (C,D) THE CEMENTITIOUS MATRIX, (E,F) A SECOND COMPONENT PRESENT IN THE MATRIX OR (G,H) BY ADDITIONAL CAPSULES (VAN TITTELBOOM & DE BELIE, 2013).

An important point of attention is the practical implementation of this self-healing mechanism in real concrete elements. This is investigated by Van Tittelboom et al. (2016). Since the placement of these capsules in the molds obviously cannot be done during the mixing process[1], an additional handling and thus additional costs are needed. In order to reduce this extra cost, it was opted by Van Belleghem et al. (2017) to only place the capsules in the regions of the concrete element that are most vulnerable to cracking. This way, less capsules are needed. However, the region where most cracks appear, is the concrete cover of the steel reinforcement. So, in order to prevent rapid ingress of aggressive substances to the steel reinforcement, a network of capsules should be placed in this concrete cover at places where crack formation is most feared.

4.4 Autonomous healing with polyurethane (PU)

Already a lot of research has been done on self-healing concrete using polyurethane as healing agent. In this section, these experimental results are summarised.

First, the efficiency of polyurethane as a healing agent for self-healing concrete by means of manual healing of the cracks was tested by Maes et al. (2013), through investigation of the chloride resistance. A two-component PU-based healing agent was used, consisting of a prepolymer of polyurethane and an accelerator. For all samples, some positive effect was measured due to the presence of PU in the cracks. For example, in 83 % of the cases, cracks with a width of 0.1 mm and a depth of 15 mm could regain almost full resistance against chloride penetration, while for cracks with a width of 0.3 mm and a depth of 20 mm this was 67 %.

Another common application of polyurethane as healing agent is by means of encapsulation. This proved to be a very efficient technique to prevent (water and/or) chloride ingress into cracks, among others by Van Belleghem et al. (2016, 2017). In this study, cylindrical glass capsules were used containing a one component polyurethane, which resulted in a reduction of the chloride concentration of up to 30 % in the top layers (0 – 6 mm) and up to 74 % in the layers at a depth of 14 – 20 mm.

Investigations are also done on polyurethane with different viscosities (Van Belleghem et al., 2017(a,b)). With a low viscosity polyurethane (200 mPas at 25°C), a self-healing efficiency of up to 124 % was found, which corresponds to an (almost) complete healing of the crack of both relatively small and large crack widths. An improved corrosion behaviour, as well as reduction of chloride ingress and water absorption was obtained. Also, no visual damage could be observed on the anodic rebars. Unlike with this low viscosity PU, autonomous crack healing with high viscosity PU (6700 mPas at 25°C) appeared to be unsuccessful in blocking the ingress of chlorides and water[2]. Due to uncomplete crack filling, the maximum achieved self-healing efficiency amounted only 67 %.

---

[1] However, this depends on the encapsulation material. Recent studies have shown that some capsules can survive the mixing process (Araújo et al., 2018)

[2] This is not the case for all types of cracks. For artificial cracks or cracks created by tensile splitting, a satisfactory healing was found (Van Belleghem et al., 2017)

4.5 Healing with water repellent agent (WRA)

Although, manual healing (by surface impregnation) has already widely been investigated (Van Tittelboom, 2013), not much research is done yet on autonomous healing using water repellent agent (WRA) as healing agent. In recent years, a silane-based water repellent agent has proven to be a highly efficient measure to reduce water absorption and consequently suppress the initiation of steel reinforcement corrosion (Dai et al., 2010). This silane-based agent penetrates in the concrete pores and reacts with hydrated cement particles. As such, a silicon resin is formed, which can form a hydrophobic lining on the pore walls. Sodium silicate-based pore blockers were also tested by Dai et al. (2010), but appeared to be inefficient in preventing chloride penetration of concrete. Also, the long-term efficiency of WRA used for surface impregnation seemed to be highly dependent on the type of agent and whether impregnation was carried out before or after crack formation.

Part II
Materials and Methods

5. Materials

5.1 Healing agents

Two different healing agents were used for the experiments. The first one is a commercially available one-component polyurethane-based healing agent, named HA Flex SLV, from the company De Neef Conchem. It is a polyurethane (PU) precursor that essentially consists of methylene diphenyl diisocyanate (MDI) and a polyether polyol. The incomplete PU polymer contains residual isocyanate (-NCO) groups, which react with the water, present in the mortar, to form a waterproof PU polymer. The healing agent is free of volatile organic compounds and does not contain catalysts or any water-soluble products. At 25° C, it has a low viscosity of ± 200 mPas.

The other used healing agent is a commercially available water repellent agent (WRA), Sikagard 705 L, from the company Sika Belgium nv.. This WRA has a very low viscosity of 8.1 mPas (at 25 °C) and has an active silane compound which causes the water repellent effect.

5.2 Capsules

Encapsulation of the healing agents was done by cylindrical borosilicate glass capsules with an internal diameter of 3 ± 0.05 mm and a wall thickness of 0.175 ± 0.03 mm. These were cut from a tube to a length of 50 mm (for the water absorption test and corrosion monitoring test) or 35 mm (for the chloride diffusion test). After cutting to the desired length, one end of the capsules was sealed by a two component polymethylmethacrylate (PMMA) glue. Then, the healing agent could be injected in the capsules by means of a syringe with a needle. Finally, the other end of the capsules was also sealed with PMMA. Due to the brittleness of the glass, the capsules will easily break when the healing action is necessary. However, these capsules need to be placed manually into the molds before casting.

5.3 Mortar

Ordinary Portland cement mortar with a W/C-ratio of 0.5 was used for the mortar prisms, used in the water absorption test. In order to obtain this, sand with a grain size of 0-2 mm, cement type CEM I 52.5 N and (tap) water were mixed with a respective mass ratio of 6:2:1.

The following mixing procedure, conform EN 196-1, was used to prepare the mortar:

- 0” – 30”: Cement + water: mixing at 140 rpm
- 30” – 1’ : Addition of sand (while mixing)
- 1’ – 1’30”: Mixing at 285 rpm
- 1’30” – 2’: Scrape off mortar from mixing pot
- 2’ – 3’: Resting period
- 3’ – 4’: Mixing at 285 rpm

5.4 Mortar specimens with(out) self-healing properties

Mortar prisms with dimensions of 160 mm x 160 mm x 40 mm were used (same as used by Van Belleghem (2017a)). These were cast in wooden formworks and were reinforced with two bars with a diameter of 2 mm. The bars were positioned at 10 mm from the bottom of the specimens and at 10 mm from the sides. In case of specimens with self-healing properties, two capsules filled with one of the healing agents were glued on thin wires between the reinforcement bars in the centre of the prism. This can be seen on Figure 5.1. After preparation of the molds, mortar was made and the molds were filled with this mortar in two layers. After each layer, the mortar was compacted on a vibration table for 30 seconds. Subsequently, the specimens were placed in an air-conditioned room with a temperature of 20 ± 2°C and a relative humidity of at least 95% for 24 hours. After these 24 hours, the mortar specimens were demolded and placed back in that room for 28 days (curing period). Figure 5.2 shows an example of a mortar prism after demolding.

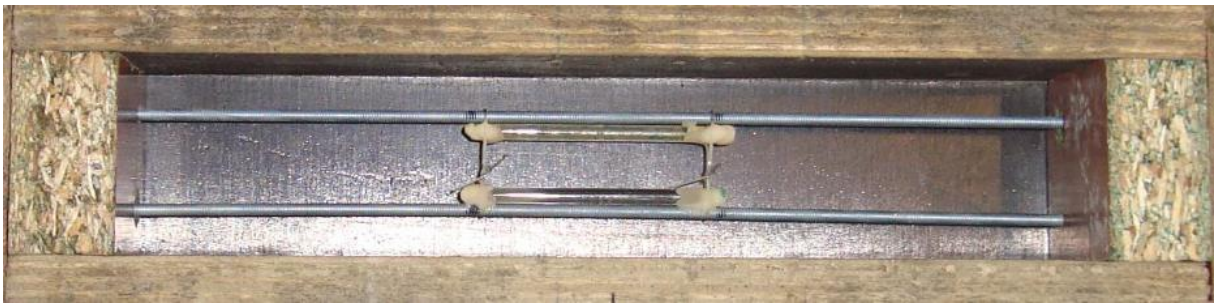

FIGURE 5.1: MOLD PREPARATION FOR A MORTAR PRISM WITH SELF-HEALING PROPERTIES (VAN BELLEGHEM ET AL., 2017B)

FIGURE 5.2: MORTAR PRISM AFTER DEMOLDING

A total of 31 specimens were made:

- 3 sound mortar prisms without a crack (UNCR),
- 22 mortar prisms with a crack but without self-healing properties (CR),
- 3 mortar prisms with embedded capsules filled with polyurethane (PU_CAPS),
- 3 mortar prisms with embedded capsules filled with water repellent agent (WRA_CAPS)

Using embedded capsules was however not the only type of healing mechanism that was tested. Also, manually injecting a healing agent (both PU and WRA) in the crack and spraying an agent (only WRA) on the upper surface was done. This will however be discussed more in detail in section 6.3.

5.5 Concrete

In this research, a fly ash containing concrete mix with a water-to-binder (W/B) ratio of 0.41 was used. Fly ash concrete was chosen because the resistance to chloride penetration is higher than for ordinary Portland cement concrete (Van Den Heede, 2014). The concrete composition is given in Table 5-1.

TABLE 5-1: CONCRETE COMPOSITION

	Fly ash concrete	
Sand 0/4	696	kg/m³
Aggregates 2/8	502	kg/m³
Aggregates 8/16	654	kg/m³
Cement CEM I 52.5 N	317.6	kg/m³
Water	153	kg/m³
Fly ash	56	kg/m³
Superplasticizer	3	ml/kg binder

The following mixing procedure was used for the concrete preparation:

- 0' – 1': Cement + aggregates: mixing
- 1' : Addition of water (while mixing)
- 1' – 3': Mixing
- 3': Addition of superplasticizer (while mixing)
- 3' – 5': Mixing

In total, three batches of concrete are made. Table 5-2 gives an overview of the concrete properties of each batch.

TABLE 5-2: PROPERTIES OF CONCRETE BATCHES

	Batch 1	**Batch 2**	**Batch 3**
Manufacturing date	23/10/'17	18/12/'17	20/12/'17
Type of specimen	Cylinders (section 5.6)	Beams (section 5.7)	Beams (section 5.7)
Density [kg/m³]	2358 ± 7.22	2371 ± 6.58	2363 ± 10.72
Compressive strength [N/mm²]	63.76 ± 2.42	61.26 ± 0.61	63.42 ± 3.55
Strength class	C40/50	C45/55	C40/50
Slump class	S4	S3	S3
Flow class	F3	F3	F3

5.6 Concrete cylinders with(out) artificial self-healing cracks

For the chloride diffusion test, 27 concrete cylinders with a diameter of 100 mm and a height of 75 mm were cast in cylindrical PVC molds, which were clamped on a wooden base (Figure 5.3a,b). In order to create artificial cracks in the specimens (see section 6.1), thin brass plates (60 mm x 50 mm, thickness 300 μm) were fixed 25 mm deep in the wooden base (Figure 5.3c). This way, the thin plate (60 mm x 25 mm) was fixed in the specimens after curing of the concrete. In case of specimens with self-healing properties, three holes with a diameter of 3.5 mm were drilled in the thin brass plates. Capsules filled with healing agent (PU or WRA) were then put through these holes and glued on nylon wires with PMMA to fix their position in the molds (Figure 5.3d). The intermediate distance between the capsules was 20 mm and they were fixed at a depth of 12.5 mm (half of the crack depth) (see clarifying sketch; Figure 5.4).

After the preparation of the molds, the concrete was made and poured in the molds in three times. After each layer, the concrete was compacted on a vibration table for 20 seconds. After casting, all specimens were placed in an air-conditioned room with a temperature of 20 ± 2°C and a relative humidity of at least 95% for 24 hours. Afterwards, the specimens were demolded and placed back in the same room. At an age of 28 days, a crack was created (see section 6.1) and all sides of the specimens, except the test surface, were coated with a two-component epoxy coating (Figure 5.5). This way, chlorides could only enter the concrete through the test surface.

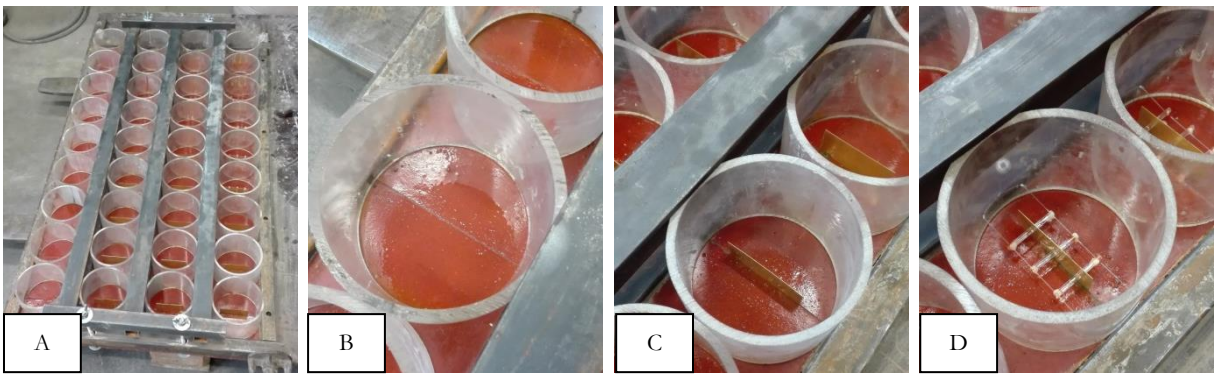

FIGURE 5.3: MOLD PREPARATION FOR THE CONCRETE CYLINDERS; (A) WOODEN BASEPLATE AND FRAMEWORK; (B) WITHOUT THIN BRASS PLATE; (C) WITH THIN BRASS PLATE FOR ARTIFICIAL CRACK; (D) WITH THIN BRASS PLATE AND EMBEDDED CAPSULES FOR ARTIFICIAL SELF-HEALING CRACK

Different types of concrete cylinders were made:

- 3 sound concrete cylinders without a crack (UNCR),
- 18 concrete cylinders with a crack but without self-healing properties (CR),
- 3 concrete cylinders with embedded capsules filled with polyurethane (PU_CAPS),
- 3 concrete cylinders with embedded capsules filled with water repellent agent (WRA_CAPS)

As was the case for the mortar prisms, autonomous capsule-based healing was not the only healing mechanism that was tested. Also manual injection of the healing agent in the crack and spraying the agent on the test (upper) surface was done. In section 6.3, this will be discussed in detail.

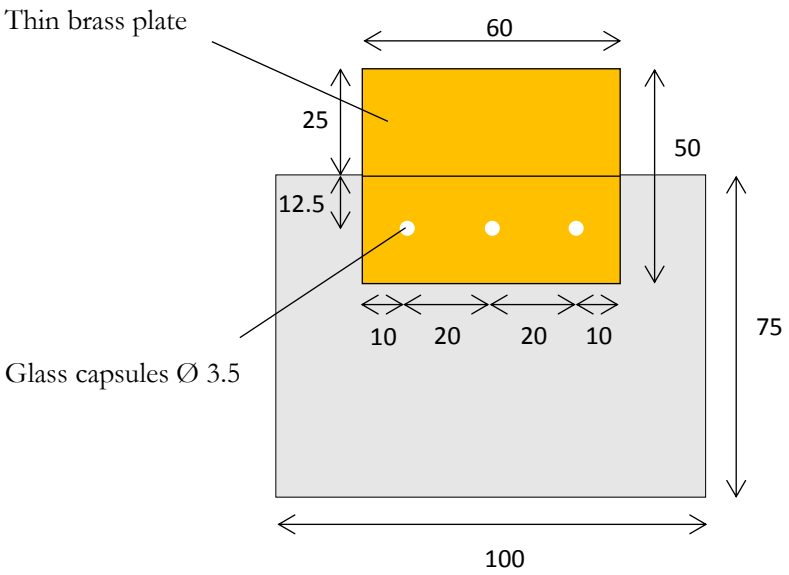

FIGURE 5.4: SCHEMATIC REPRESENTATION OF A CONCRETE CYLINDER WITH ARTIFICIAL SELF-HEALING CRACKS AFTER CASTING (DIMENSIONS IN MM)

FIGURE 5.5: COATED CONCRETE CYLINDERS (AFTER CRACK CREATION)

5.7 Concrete beams

For corrosion monitoring, 25 concrete beams with dimensions of 120 mm x 120 mm x 500 mm were made. The concrete beams were casted in wooden frameworks. In order to create a crack in the middle of the beam (see also section 6.1), a triangular notch of 3 mm was placed in the mold. Also, in order to obtain the necessary concrete cover, the reinforcement configuration was placed on two plastic rods. The experimental setup of these beams is discussed in the following sections and can be seen in Figure 5.6 and Figure 5.7.

5.7.1 Reinforcement configuration

Figure 5.6 shows the reinforcement configuration for the concrete beams, indicating the dimensions and the different materials. The steel reinforcement in the beams consists of two parts: two reinforcement cages (section 5.7.1.1), one at each side of the beam, and a central rebar (section 5.7.1.2), which respectively serve as the cathode and anode in the corrosion process. Both parts are electrically separated from each other and are both electrically connected to the exterior by means of a copper wire. In order to be able to function as cathode, both reinforcement cages are also electrically connected to each other through insulated copper wires. In order to avoid galvanic corrosion, all these copper wire connections were coated with epoxy resin (SikaCor 277). In addition to the reinforcement cages and the central rebar, four glass fibre reinforced polymer (GFRP) bars (Aslan^{TM} 100) were placed in the beams. These were needed as structural reinforcement, in order to prevent brittle failure of the beam during crack creation (section 6.1). They had a diameter of 6 mm and a length of 460 mm. Finally, as indicated in Figure 5.6, an internal reference electrode was placed close to the anode (see section 5.7.2).

5.7.1.1 Reinforcement cages (cathode)

As earlier mentioned, the first part of the steel reinforcement consists of two reinforcement cages, each at one side of the beam. Both reinforcement cages are made out of four longitudinal rebars (Ø 8 mm; length of 160 mm) which are welded to five stirrups (Ø 6 mm; 80 x 80 mm). The intermediate distance between the stirrups was equal to 36 mm. As can be seen in Figure 5.6 or Figure 5.7, the glass fibre reinforcement was also connected to these cages with steel wires. As mentioned earlier, all the copper wire connections were coated with epoxy resin.

5.7.1.2 Central rebar (anode)

The second part of the steel reinforcement is a centrally located steel bar with a diameter of 10 mm and a length of 250 mm. The rebar was partially coated with two layers of cement paste (W/C=0.4), in order to prevent crevice corrosion, and two layers of epoxy coating (SikaCor 277). In this way, only the central part of the rebar, with a length of 50 mm, was exposed to the surrounding concrete and could act as anode. The central rebar was attached to the reinforcement cages by means of straps, so they could be positioned accurately.

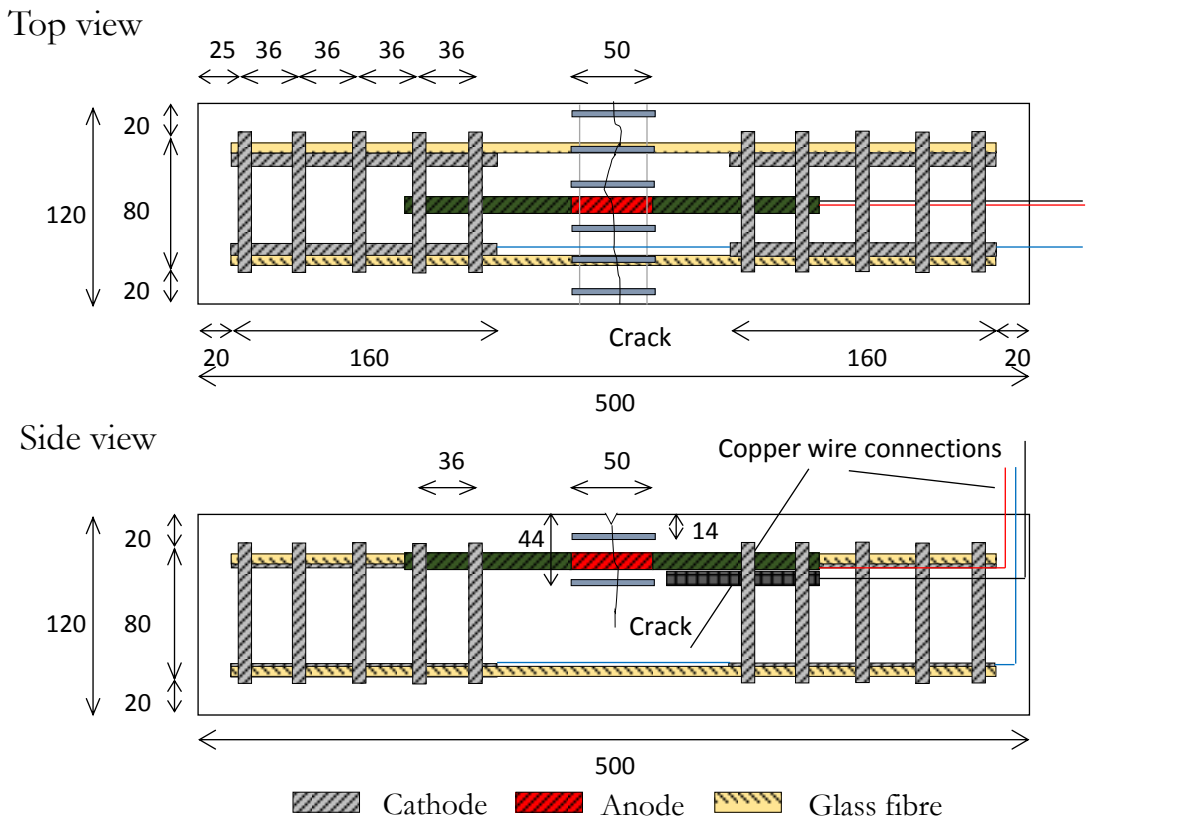

FIGURE 5.6: EXPERIMENTAL SETUP FOR AN AUTONOMOUSLY HEALED CONCRETE BEAM (DIMENSIONS IN MM)

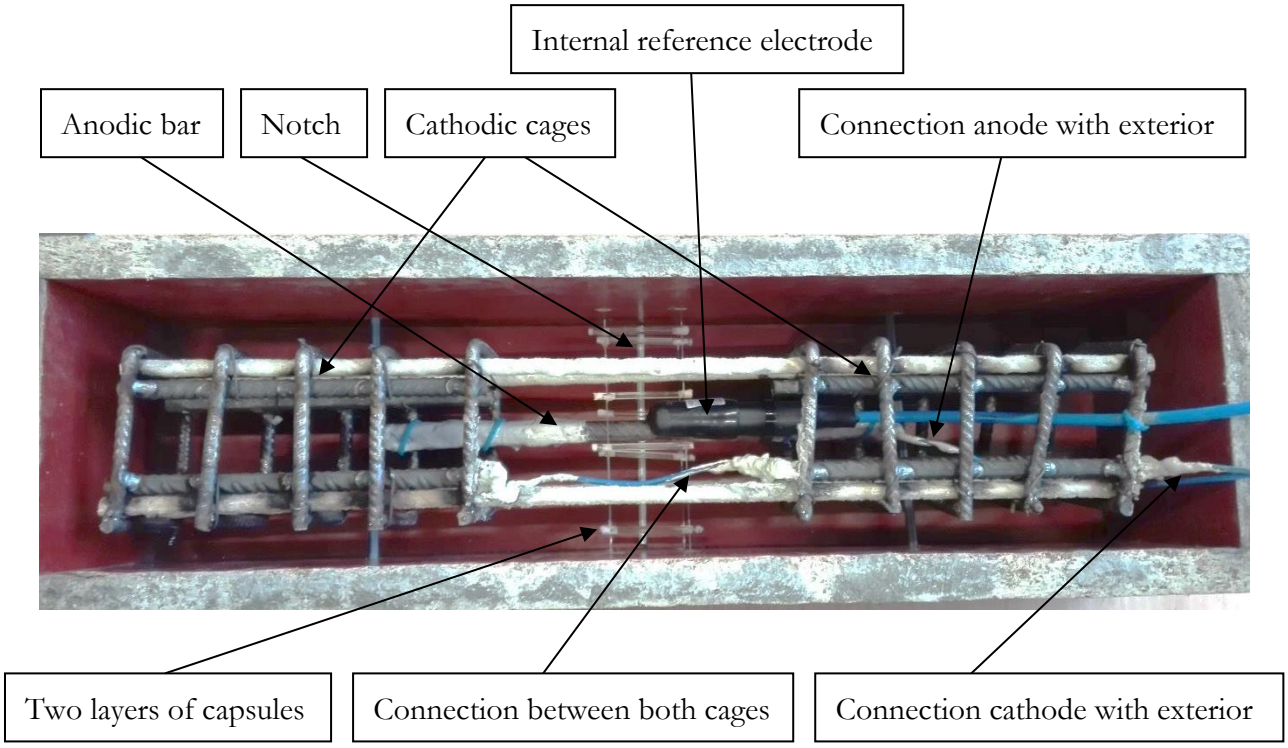

FIGURE 5.7: CONCRETE BEAM CONFIGURATION BEFORE CASTING

5.7.2 Internal reference electrode

In order to minimise the ohmic drop, an internal reference electrode was provided in each beam, instead of an using an external reference electrode. This is a commonly used Mn/MnO_2-electrode (ERE 20; Force Technology). The reference electrode is fixed at the central anodic rebar, close to the crack, by means of straps. In order to keep the measuring part of the reference electrode clean and moist, a sponge is placed on this part, which is then kept in place by a shell. Just before concrete pouring, the sponge and shell were removed.

5.7.3 Concrete beams with self-healing properties

In case of beams with self-healing properties, two layers of six capsules, filled with a healing agent, were placed in the center of the beams. One layer of capsules was placed above the anodic rebar, while the other was placed below the rebar, with a distance to the test (upper) surface of respectively 14 mm and 44 mm. The capsules were glued on thin wires, attached to the molds, with an intermediate distance of 20 mm. The position of the capsules can be seen in Figure 5.8.

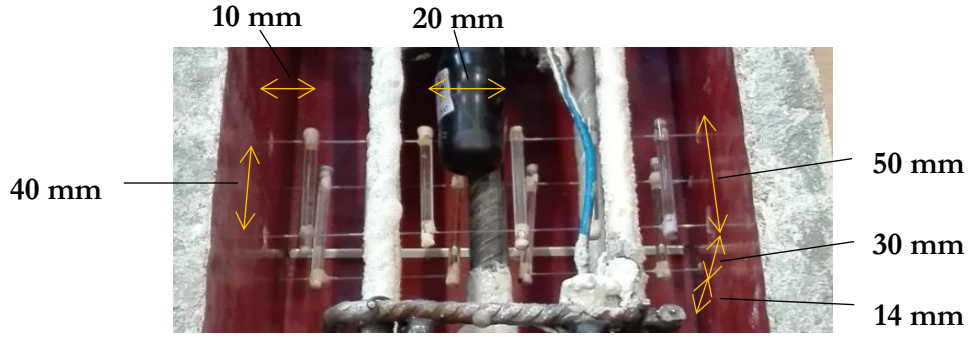

FIGURE 5.8: POSITION OF THE TWO LAYERS OF CAPSULES IN THE MOLD

So again, different types of concrete beams were made (see also section 6.3):

- 3 sound concrete beams without a crack (UNCR),
- 16 concrete beams with a crack but without self-healing properties (CR),
- 3 concrete beams with embedded capsules filled with polyurethane (PU_CAPS),
- 3 concrete beams with embedded capsules filled with water repellent agent (WRA_CAPS)

After casting, demolding and curing, the anodic and cathodic part of the reinforcement in the concrete beams are connected to each other through the external copper wires.

6. Methods

6.1 Crack creation

6.1.1 Mortar prisms

The cracks in the mortar prisms were created by means of three-point bending. In order to register and control the crack width during the bending test, a linear variable differential transformer (LVDT) was attached at the bottom of the sample using a small metal block and a thin metal plate (Figure 6.1a,b and c). A crack width of 300 μm was chosen since most design codes limit the crack width to that value. In order to obtain the target crack of 300 μm, the following loading procedure was followed:

1. Loading until 1 kN at a speed of 0.01 kN/s (= load controlled)
2. Loading until crack width of 0.5 mm at a controlled speed of 0.0006 mm/s (= displacement controlled)
3. Unloading at a speed of 0.1 kN/s

The crack width decreased during unloading (to a width of approximately 300 μm) due to the presence of the reinforcement bars. Finally, the crack width was measured using a stereomicroscope (see section 6.2.1).

FIGURE 6.1: MORTAR PRISM (A) BEFORE, (B) DURING AND (C) AFTER CRACK CREATION

6.1.2 Concrete cylinders

For the concrete cylinders, also a target crack width of 300 μm was chosen. However, in this case, artificial cracks were created. 24 hours after casting, the specimens were demolded and the thin brass plates were carefully removed. This was done by clamping the brass plates in a bench vise and carefully pull the concrete cylinder upwards (Figure 6.2a,b). This way, a crack was thus created with a length of 60 mm, a depth of 25 mm and a width of 300 μm. No microscopic measurements of the crack width were performed in this case, since it was assumed that all artificial cracks have a width of 300 μm (Van Belleghem et al., 2016).

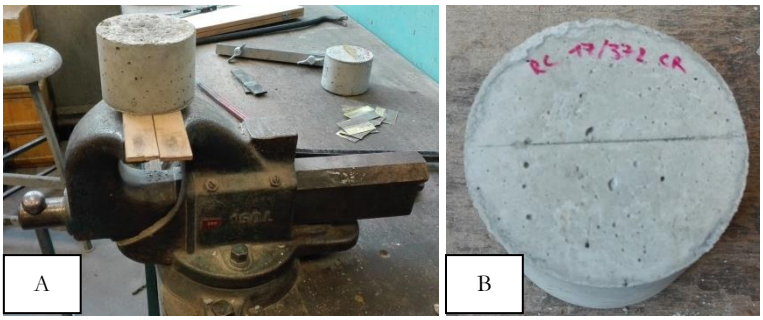

FIGURE 6.2: CONCRETE CYLINDERS DURING (A) AND AFTER (B) CRACK CREATION

6.1.3 Concrete beams

After the curing period of 28 days, a target crack width of 300 µm was created in the concrete beams by means of a three-point bending test. However, unlike for the mortar prisms, the concrete beams were kept in the three-point bending test frame in order to keep the crack open. (see Figure 6.3). This cracking of the beams by manually tightening the frames in which the beams are kept, ensures the (visual) control of the crack width. Due to the presence of the triangular notch in the middle of the beam, it was intended to create the crack at this position, so the crack always crossed the anodic bar. In order to achieve the target crack, the crack widths were measured with a portable microscope. However, an accurate crack width measurement was finally done with a stereomicroscope (see section 6.2.2). Detailed information about this specimen preparation is given in section 6.6.

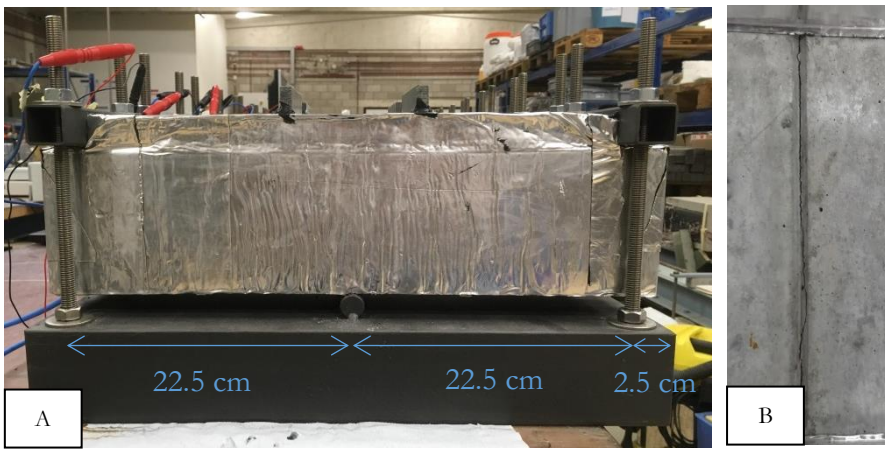

FIGURE 6.3: TEST FRAME TO LOAD THE CONCRETE BEAMS IN THREE POINT BENDING (A) AND AN EXAMPLE OF A CREATED CRACK (B)

It has to be noted that, despite the glass fibre reinforcement, present in the beams, additional cracks were inevitable in some beams. This is probably due to a too large amount of reinforcement. These additional cracks were small transversal cracks, which were connected to the main crack in or near the notch.

6.2 Crack width measurements

6.2.1 Mortar prisms

The crack width of the mortar prisms was measured microscopically using a stereomicroscope (Leica 8 APO with DFC 2956 camera) (see Figure 6.4a,b,c). Seven microscopic images were taken along the length of the crack with an intermediate distance of 5 mm. The crack width was then measured three times on each image using the program ImageJ. Finally, for each prism, the average crack width was calculated, which then represented the width of the crack.

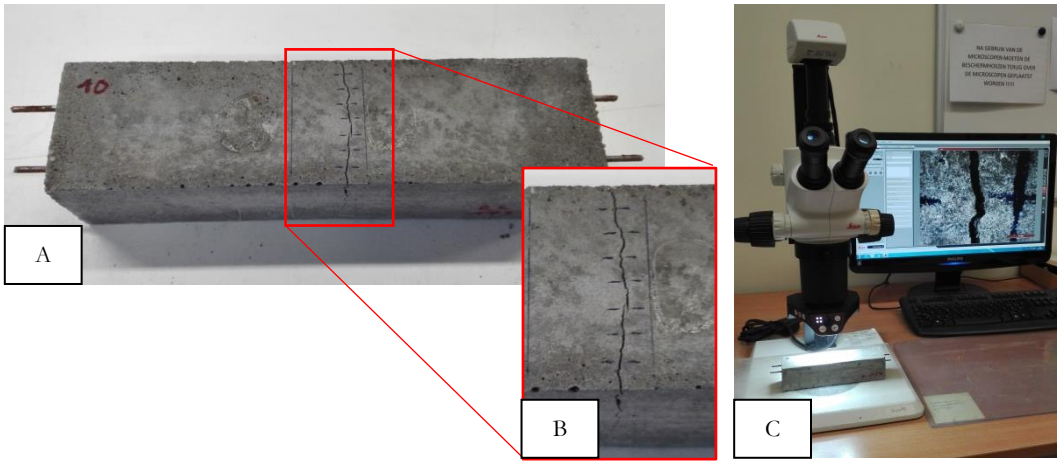

FIGURE 6.4: CRACK WIDTH MEASUREMENT OF THE MORTAR PRISMS; (A) CRACKED MORTAR PRISM, (B) CLOSE UP OF CRACK, INDICATING THE MEASURED POINTS; (C) STEREOMICROSCOPE

6.2.2 Concrete beams

Similar as for the mortar prims, the crack width of the concrete beams was measured microscopically using a stereomicroscope and ImageJ. The only difference is that only five images were taken along the length of the crack. The crack width of the beams was measured twice, once before starting the wet-dry cycles (see section 6.6) and once after 7 weeks of exposure.

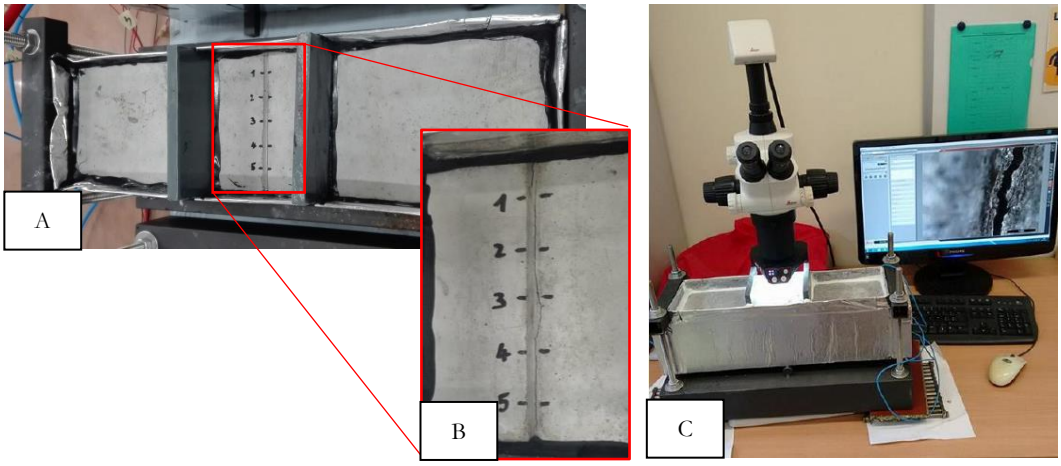

FIGURE 6.5: CRACK WIDTH MEASUREMENT OF THE CONCRETE BEAMS

6.3 Crack healing

As mentioned in previous sections, different healing mechanisms were tested in these experiments. The first method that was tested was autonomous healing, using embedded capsules filled with a healing agent. For these specimens, crack creation (section 6.1) caused the embedded capsules to break, so the healing agent was released inside the crack. The capsule breakage could be noticed by a popping sound and a sudden drop in the force during the bending test (in case of crack creation by three point bending). After capsule breakage, the specimens were stored in a climate room at a temperature of 20 ± 2°C and a relative humidity of 60% for 48 hours. During this period, the specimens were put with the crack surface facing downwards, to let the healing agent flow inside the crack, and the healing agent was given the time to harden.

A second healing mechanism was manual healing of the crack by injecting the healing agent in the crack using a syringe and a needle. This was done once with polyurethane (PU) and once with water repellent agent (WRA) as healing agent. In order to prevent leakage of the healing agent on the surface, the zone around the crack was taped before injection of the agent.

Another healing mechanism that was tested, was spraying (two layers of) the healing agent on the entire test surface of the specimens, either before or after crack creation. This was only done with the water repellent agent. Again, in order to only apply the healing agent on the upper surface, the other surfaces were taped.

Below, an overview is given of the different test series used in the experiments For each test series, minimum three replicate specimens were made.

- Uncracked specimens (UNCR),
- Cracked specimens without self-healing properties (CR),
- Cracked specimens with embedded capsules filled with polyurethane (PU_CAPS),
- Cracked specimens with embedded capsules filled with water repellent agent (WRA_CAPS)
- Cracked specimens of which the crack is manually injected with polyurethane (PU_MAN)
- Cracked specimens of which the crack is manually injected with water repellent agent (WRA_MAN)
- Cracked specimens of which the test surface is sprayed with water repellent agent, before cracking (WRA_SURF_BEFORE)
- Cracked specimens of which the test surface is sprayed with water repellent agent, after cracking (WRA_SURF_AFTER)

Note: The latter two types of specimens (WRA_SURF) were not used for the chloride diffusion test. Instead, two other types of specimens were tested of which the crack is manually injected with a healing agent (once with PU and once with WRA). However, in this case, the healing agent was injected after the specimens were immersed in a NaCl-solution for 3 weeks. These types were named as 'PU_MAN_AFTER' and 'WRA_MAN_AFTER'.

Figure 6.6 to Figure 6.8 show some examples of the different healing mechanisms applied on the different test specimens (mortar prisms, concrete cylinders and concrete beams). In case of specimens with autonomous capsule-based crack healing, it was seen that, almost immediately after breakage of the capsules, the healing agent (both WRA and PU) was released in the crack, where it hardened due to reaction with moisture. Also, some leakage of the healing agent occurred at the mortar surface. In addition to the low viscosity of the healing agents, this can also be attributed to the high capillary forces in the crack due to the limited crack width. Also, the crack volume is smaller than the amount of healing agent, present in the capsules. In spite of this leakage however, it can be seen visually that the crack is well healed along the whole length.

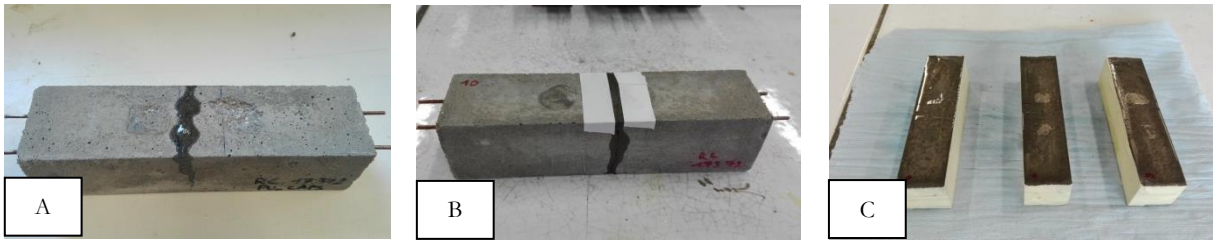

FIGURE 6.6: DIFFERENT HEALING MECHANISMS APPLIED ON THE MORTAR PRISMS; (A) CAPSULE BREAKAGE, (B) CRACK INJECTION, (C) WRA SPRAYED ON TEST SURFACE

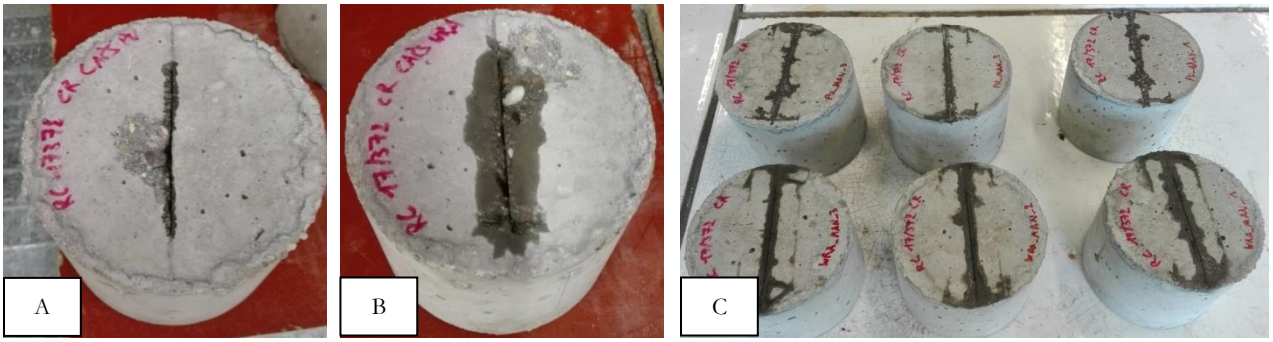

FIGURE 6.7: DIFFERENT HEALING MECHANISMS APPLIED ON THE CONCRETE CYLINDERS; (A) CAPSULE BREAKAGE (PU), (B) CAPSULE BREAKAGE (WRA), (C) CRACK INJECTION (PU & WRA)

FIGURE 6.8: CRACK HEALING BY MEANS OF CRACK INJECTION, APPLIED ON THE CONCRETE BEAMS

Finally, Table 6-1 gives an overview in which batch the different concrete beams were made.

TABLE 6-1: OVERVIEW OF CONCRETE BEAM BATCHES

Type	Specimen		Batch	
UNCR	1, 2, 3		1	
CR	4, 5, 6	25	1	2
PU_MAN	7, 8, 9		1	
PU_CAPS	10, 11, 12		1	
WRA_CAPS	13, 14, 15		2	
WRA_SURF_BEFORE	16, 17, 18		2	
WRA_SURF_AFTER	19, 20, 21		2	
WRA_MAN	22, 23, 24		2	

6.4 Water uptake through capillary absorption

The first test that was executed was a capillary water absorption test, for which the mortar prisms were used. The test was performed in a climate room at 20 ± 2°C and 60% relative humidity, based on the European standard NBN EN 13057.

6.4.1 Specimen preparation

After crack creation and before the start of the test, the specimens were dried in an oven at 40 ± 2°C until a constant mass was reached, i.e. when over a period of 24 hours the mass change was less than 0.1 %. Then specimens were taken out of the oven and placed in a climate room at 20 ± 2°C and 60% relative humidity for 24 hours. During this period, both the side surfaces and the test (bottom) surface were partly covered with aluminium butyl tape (Figure 6.9). In this way, only a region of 10 x 40 mm around the crack (or in the middle of the bottom surface in case of uncracked specimens) was exposed to water during the absorption test. Thus, water could only be absorbed by the crack.

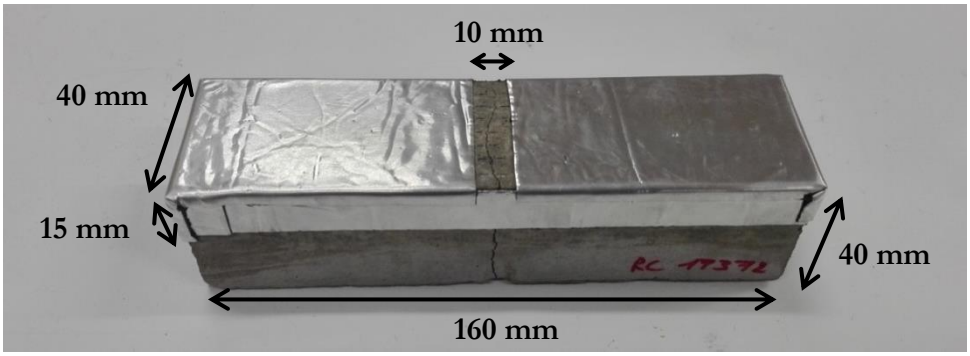

FIGURE 6.9: SPECIMEN PREPARATION PRIOR TO CAPILLARY WATER ABSORTPION TEST

6.4.2 Capillary absorption test

Before starting the water absorption test, the initial mass of all specimens was determined by weighing them on a scale with an accuracy of 0.01 g. After this, the specimens were placed with their test face on line supports in a plastic box containing water, so that they were immersed up to a depth of 2 ± 1 mm. From that moment on, the mass of the specimens was determined at several time intervals: every half hour during the first eight hours and then again every 24 hours until 172 hours.

The cumulative water uptake was then calculated by subtracting the initial mass of a sample from the determined mass. This value was then divided by the exposed surface area (10 mm x 40 mm) in order to obtain the cumulative water absorption per unit of surface area (g/cm^2). Finally, for each specimen, this value was then plotted in function of the square root of immersion time ($h^{0.5}$). Additionally, the sorption coefficient S ($kg/m^2/h^{0.5}$) was also derived. This is the gradient of the line from the intercept of the water absorption curve to the cumulative mass of the water uptake per unit area recorded at 24 hours.

6.5 **Chloride diffusion test**

In order to evaluate the chloride penetration into the different specimens, an accelerated chloride diffusion test according to the standard NT Build 443 was performed. For this test, all coated specimens were immersed in an aqueous NaCl solution (with a concentration of 165 g/l) for 11 weeks. This test was done in a climate room, at 20 ± 2°C.

As mentioned in section 6.3, after 3 weeks, all specimens were taken out of the solution for 48 hours. During this period, for 3 specimens of 2 series (PU_MAN_AFTER and WRA_MAN_AFTER) the crack was manually injected with healing agent. Subsequently, all specimens were placed back in the NaCl solution for another 8 weeks.

After the total exposure period, 10 layers (40 mm x 10 mm) each with a thickness of 3 mm were ground off in the region of the crack. The powder from each layer was collected and stored for minimum 7 days in an oven at 95°C. This can be seen on Figure 6.10.

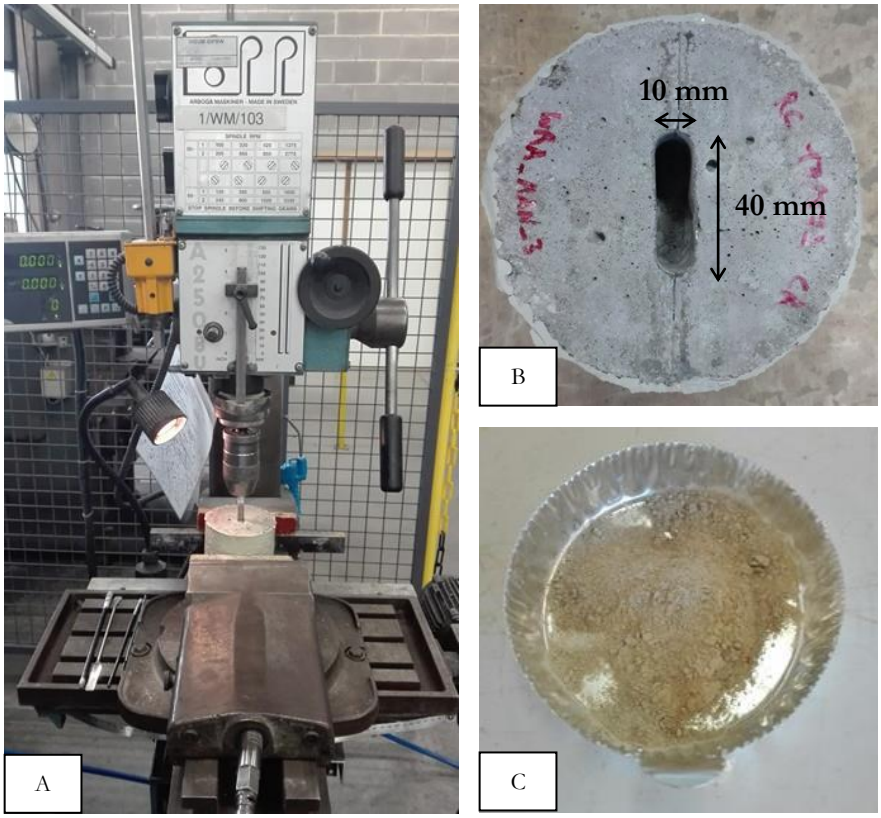

FIGURE 6.10: GRINDING OFF LAYERS IN THE REGION OF THE CRACK; (A) GRINDING MACHINE, (B) GRINDED REGION, (C) OBTAINED POWDER

Finally, the total chloride content of each powder (each layer) was determined by means of acid-soluble chloride extraction in a nitric acid solution, which contained the following steps (see Figure 6.11):

- Determination of the weight of the powder for each layer
- Addition of 5 ml nitric acid (0.3 mol/l) and 40 ml demineralized water
- Manual stirring + heating to boiling
- Filtration (particle retention of 12-15 µm) and dilution with demineralized water to 100 ml
- Addition of 10 ml demineralized water and 40 ml nitric acid to 10 ml of the obtained extract

With the obtained solution, a potentiometric titration against silver nitrate was performed, during which the chloride concentration was determined by exactly neutralizing the chlorides with silver nitrate of known concentration. Finally, the known chloride concentration can be plotted in function of the penetration depth to obtain the chloride profiles for each specimen.

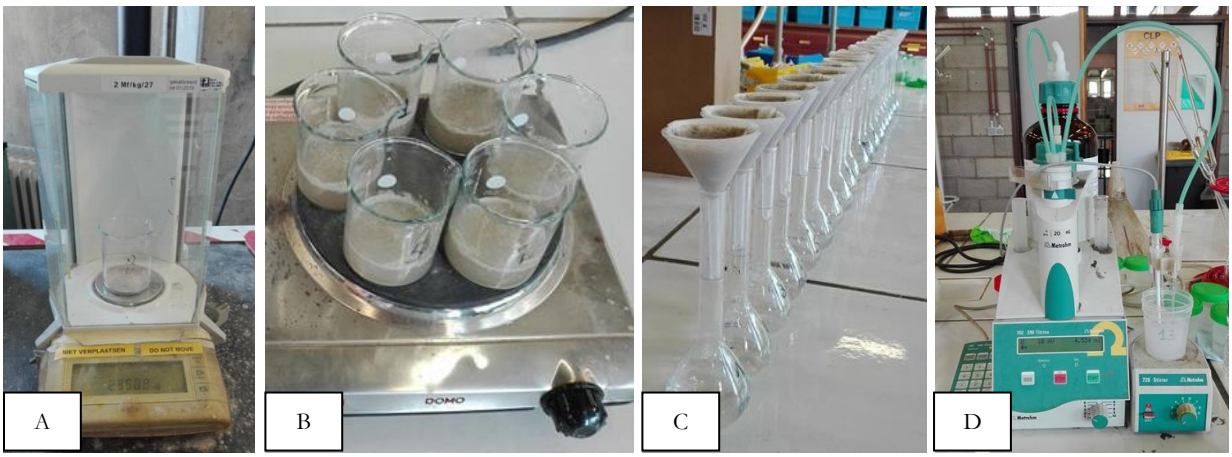

FIGURE 6.11: DIFFERENT STEPS FOR DETERMINATION OF CHLORIDE CONCENTRATION OF POWDERS; (A) WEIGHING POWDERS; (B) HEATING TO BOILING; (C) FILTRATION; (D) POTENTIOMETRIC TITRATION

6.6 Corrosion monitoring

First of all, all sides of the beams, except the test (upper) surface and the bottom surface, were covered with aluminium butyl tape. This way, only the bottom and upper surfaces of the beams were directly exposed to the environment (a temperature of 20 °C and a relative humidity of 60 %). Using this tape, a reservoir was made on top of the beams, which was filled with a solution during the wet/dry-cycles. Furthermore, the reservoir was divided in three compartments by two PVC plates: a central compartment with dimensions of 100 mm x 120 mm, and two outer compartments of 150 mm x 120 mm (see Figure 6.12). Finally, all edges of the reservoir were sealed with silicone, to ensure the liquid tightness at the edges of the reservoir.

Once prepared, the different electrochemical parameters, discussed below, were measured, once before crack creation (uncracked state; week -1) and once after crack creation (cracked state; week 0). Subsequently, the beams were subjected to a cyclic exposure to a chloride solution (1

day wet, 6 days dry) for a period of 12 weeks (wet/dry-cycles; week 1 to 12). During the wet period, the central compartment was filled (up to a height of 20 mm) with a NaCl solution with a concentration of 33 g/l. This way, a marine environment was simulated in the region of the crack. The side compartments were filled (up to a height of 20 mm) with $Ca(OH)_2$ solution with a concentration of 1.15 g/l, in order to obtain an even moisture distribution. After 24 hours, the solutions were removed, after which the corrosion measurements were performed.

Due to the electrical separation of anode and cathode within the concrete beams, the electrochemical corrosion characteristics of both anodic and cathodic partial reactions could be measured. The electrochemical measurements of are explained in the following sections, in the same chronological order as they are measured.

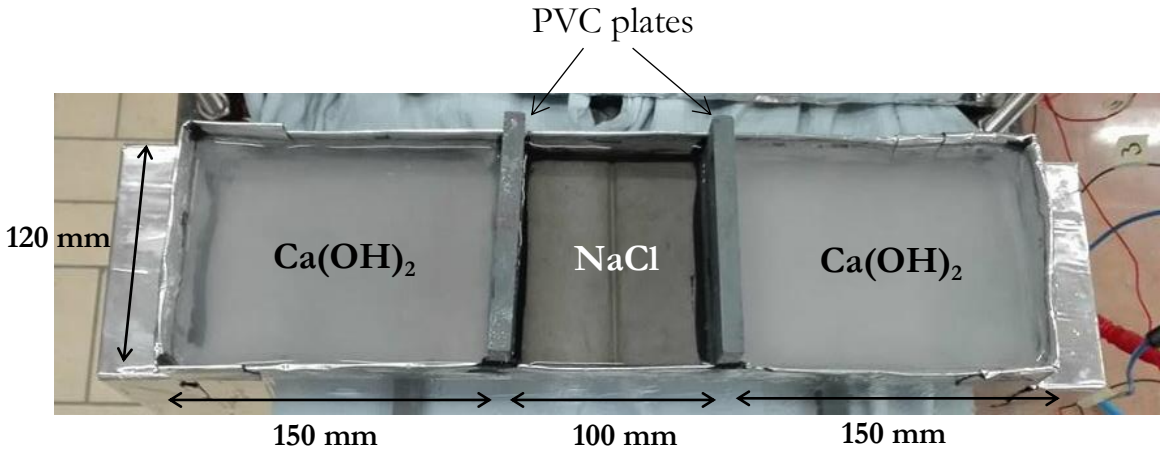

FIGURE 6.12: RESERVOIRS ON (UNCRACKED) CONCRETE BEAM FOR THE WEEKLY EXPOSURE TO NaCl SOLUTION IN THE MIDDLE COMPARTMENT AND $CA(OH)_2$ SOLUTION IN THE OUTER COMPARTMENTS

All the following electrochemical measurements (except for the corrosion current) were performed with a potentiostat (Gamry Interface 1000E) using the internal Mn/MnO_2 reference electrode in the beams. However, prior to these measurements, the anode and cathode needed to be connected to each other. Figure 6.13 shows the used potentiostat with its different cell cables. The white cable of the potentiostat is the reference electrode (REF). During a measurement, this cable is always connected with the internal reference electrode of the concrete beams. The green and blue cell cables are respectively the working electrode (WE) and the working sense (WS). The red and orange cables are respectively the counter electrode (CE) and the counter sense (CS). Finally, the floating ground cell (black) (not visible on the figure) was always connected to a Faraday shield.

6.6.1 Corrosion current

The first characteristic that was measured, was the macro-cell corrosion current (I_{macro}) This was measured daily using a current monitoring system, to which the anode and cathode were constantly connected. Only for performing the other measurements (see following sections), the anode and cathode were disconnected from this monitoring system. When connected to this current monitoring system, I_{macro} was measured approximately every hour.

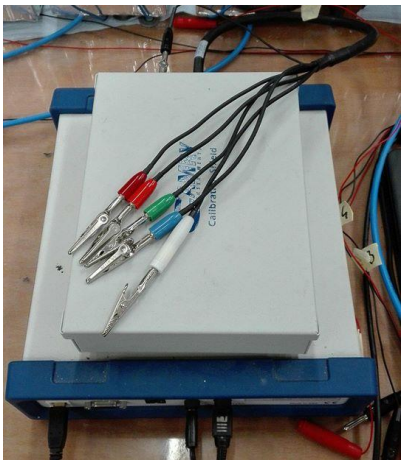

FIGURE 6.13: POTENTIOSTAT USED FOR ELECTROCHEMICAL MEASUREMENTS

6.6.2 Corrosion potential

The first characteristic, measured with the potentiostat, is the corrosion potential (E_{corr}) of the beams. This parameter was measured by connecting the interconnected anode and cathode to the working electrode (WE) and sense (WS). Figure 6.14 shows the configuration for this measurement.

FIGURE 6.14: CABLE CONFIGURATION FOR CORROSION POTENTIAL MEASUREMENT

The value, obtained after a measurement of 300 seconds (with a sample period of 0.5 s) was then taken as the corrosion potential.

6.6.3 IR drop

Secondly, the IR drop was measured. The initial setup for this measurement was similar as for the corrosion potential (anode and cathode connected with the working electrode and working sense). The total time of this test was 60 seconds with a sample period of 0.01 seconds. After about 40 seconds, the anode and cathode were disconnected, leaving the anode still connected to the working electrode. As indicated in Figure 6.15, this generated a drop in the corrosion potential curve. This drop is defined as the IR drop. After this disconnection, the anode and cathode were left to depolarize for about 15 hours.

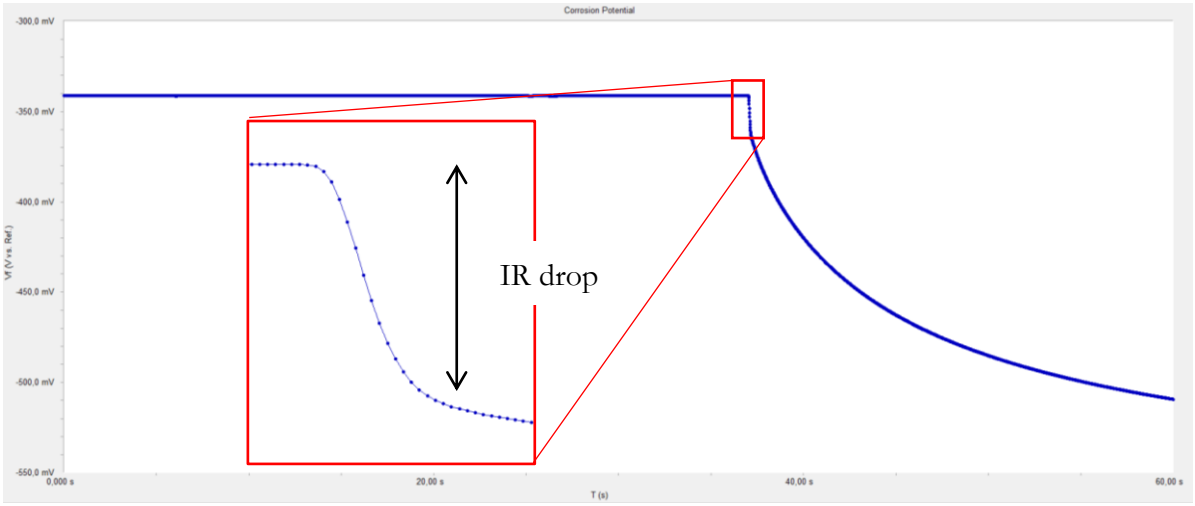

FIGURE 6.15: CORROSION POTENTIAL CURVE, INDICATING THE IR DROP

6.6.4 Open circuit potential

The open circuit potential of the anode ($E_{O,A}$) and cathode ($E_{O,C}$) was determined by measuring the voltage difference between the internal reference electrode and respectively the anode and cathode. Practically, this was done by connecting the working electrode (WE) and working sense (WS) with the anode and cathode respectively. Similar as for the corrosion potential measurements, the total time of this test was 300 seconds with a sample period of 0.5 seconds.

In case of active corrosion, the OCP value of the anode is expected to be more negative than the corrosion potential, due the loss of electrons during the anodic reaction. Since the corrosion potential is the potential at equilibrium between the anodic and cathodic reaction. As a result, the OCP value of the cathode should, contrary to the anode, be less negative than the corrosion potential. The difference between the two OCP values is defined as the driving potential (ΔE). A higher driving potential indicates a more active corrosion state of the rebar.

6.6.5 Electrochemical impedance spectroscopy (EIS)

Subsequently, electrochemical impedance spectroscopy was performed, to determine the development of the concrete resistance (R_E). This measurement made use of sinusoidal signals with an amplitude of 10 mV vs. OCP for frequencies ranging from 1 MHz to 0.1 Hz. This concrete resistance was then obtained from the Nyquist plot as the value of the real component (X-axis) of the point where the imaginary part (Y-axis) is minimum. This is illustrated in Figure 6.16.

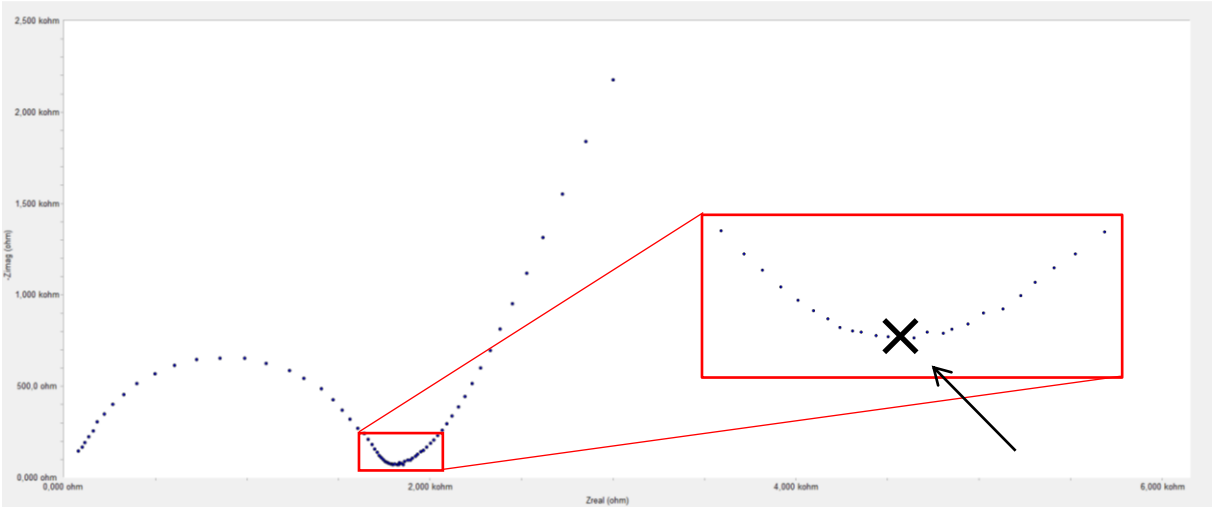

FIGURE 6.16: NYQUIST PLOT FOR EIS MEASUREMENT, INDICATING THE MINIMUM OF THE IMAGINARY PART (Y-AXIS)

For this measurement, the working electrode (WE) and working sense (WS) were connected to the anode, while the counter electrode (CE) and counter sense (CS) were connected with the cathode. This cable configuration can also be seen in Figure 6.17.

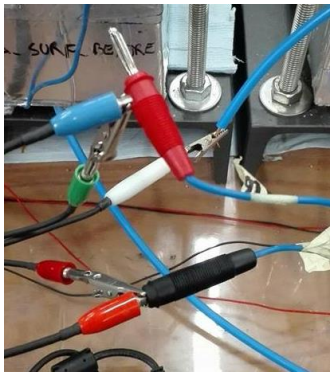

FIGURE 6.17: CABLE CONFIGURATION FOR CONCRETE RESISTANCE MEASUREMENT

6.6.6 Linear polarisation resistance

Finally, the linear polarization resistance of both anode and cathode, respectively $R_{P,A}$ and $R_{P,C}$, were determined. This polarization ranged from -20 mV vs. OCP to +20 mV vs. OCP, at a scan rate of 0.125 mV/s. For the anodic polarization resistance, the same configuration is used as for the concrete resistance (Figure 6.17). For the cathodic polarization resistance, the working electrode (WE) and the working sense (WS) are connected to the cathode, while the counter electrode (CE) and counter sense (CS) are connected to an inox mesh, which is placed on the concrete surface (on the crack) inside a wet cloth in order to make good electrical contact. This can be seen in Figure 6.18.

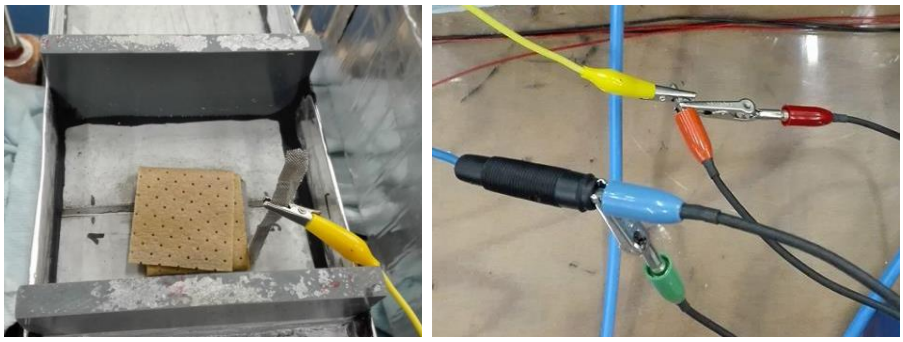

FIGURE 6.18: CABLE CONFIGURATION FOR CATHODIC POLARISATION RESISTANCE MEASUREMENT

Figure 6.19 shows an example of the E-I-curve, obtained with these measurements. The linear polarization resistance is then defined as the slope of the tangent of this curve at zero current.

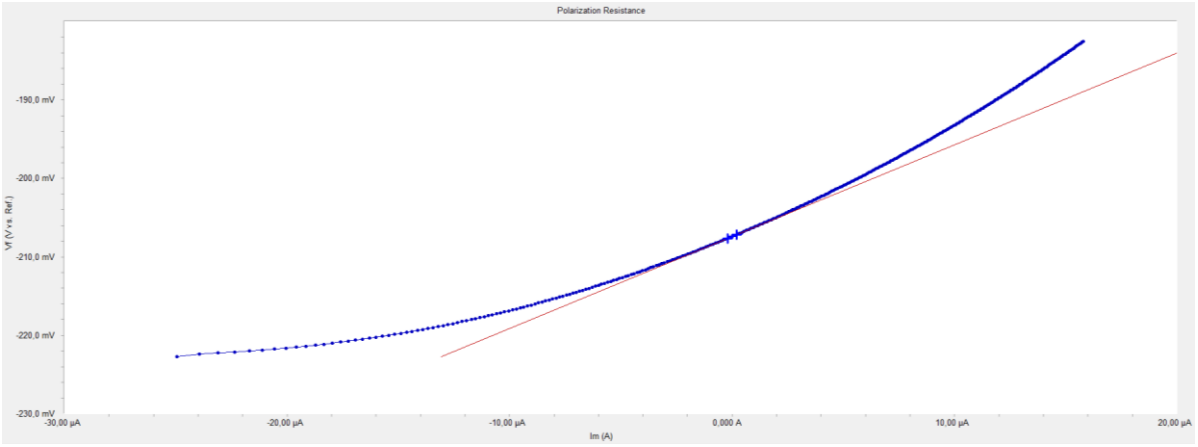

FIGURE 6.19: LPR MEASUREMENT: CURVE WITH A TANGENT AT ZERO CURRENT DENSITY

Part III
Results and discussion

7. Capillary water absorption test

In this section, the obtained results of the capillary water absorption test are discussed. First, the crack widths of all specimens are given in section 7.1. Subsequently, the absorption behaviour of all the specimens are discussed and compared according to three parameters: the cumulative water absorption in function of time (section 7.2), the capillary sorption coefficient (section 7.3) and the self-healing efficiency (section 7.4).

7.1 Crack widths

The crack width of each specimen was measured before the start of the capillary water absorption test. The mean crack widths and its corresponding standard deviation for each test series were then calculated and are shown in Figure 7.1. These mean crack widths range from 297 µm (for cracked specimens) to 517 µm (for WRA_MAN). Thus, for most test series, the aimed crack width of 300 µm was exceeded and overall mean crack width of 378 ± 70 µm was obtained.

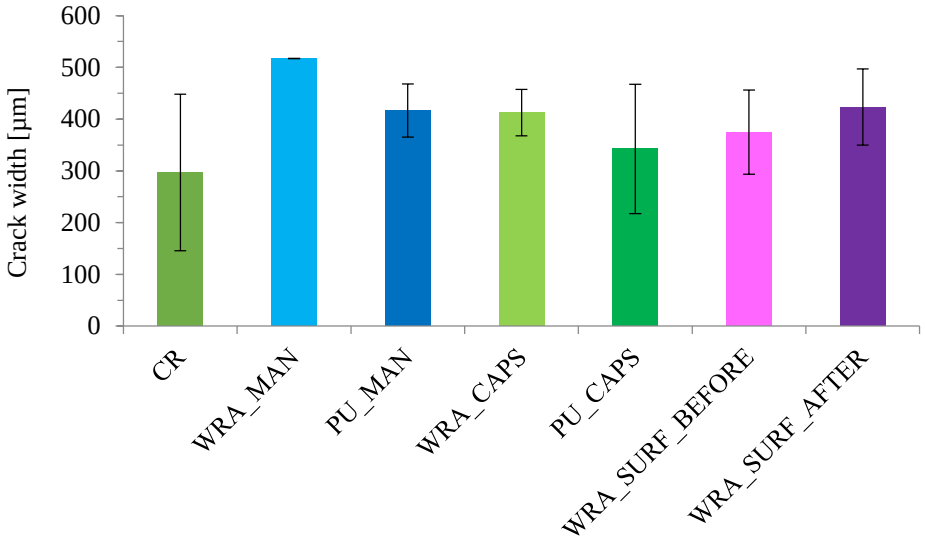

FIGURE 7.1: MEAN CRACK WIDTH FOR EACH TEST SERIES. ERROR BARS REPRESENT THE STANDARD ERROR ON THE MEAN VALUES.

7.2 Cumulative water absorption in function of time

In this section, the mean cumulative water absorption curves of all specimens are discussed. The mean cumulative water absorption curves of the (three) specimens of each test series are given separately in Figure 7.2. However, in order to properly compare these results, these curves are plotted together on the same graph. This is shown in Figure 7.3.

7.2.1 (Un)cracked specimens

By comparing the results for cracked and uncracked specimens, the influence of a crack on the ingress of water is very clear. In case of cracked specimens, the water absorption rate increases very rapidly at the beginning of the absorption test and starts to decrease after about 24 hours of testing, as the specimens get more saturated. During the whole test (172 hours of exposure), the total water absorption for cracked specimens is almost ten times higher than for uncracked specimens. This large difference indicates the need for crack repair in order to prevent water ingress (or other aggressive substances) into the mortar. Also, a larger standard error can be found for the cracked specimens, which can be attributed to the difference in crack widths, as well as other influences such as crack depth, tortuosity, micro-cracking, etc..

7.2.2 Specimens healed with PU

As mentioned in section 6.3, two healing mechanisms were applied using PU as healing agent, namely autonomous healing using embedded capsules (PU_CAPS) and manual healing by injecting the PU in the crack (PU_MAN). In Figure 7.3, it can be seen that both curves have a linear trend. Crack healing using embedded capsules resulted in a larger capillary water absorption than noticed for uncracked specimens, while the cumulative water absorption curve for crack healing by manually injection is located under the curve for uncracked mortar (see also sections 7.3 and 7.4). During the first 48 hours, both curves show approximately the same behaviour as the curve for uncracked samples. However, the slope of the curves is different, so that the curve for uncracked specimens is situated in between the aforementioned curves. During the continuation of the test, the cumulative water absorption rate for uncracked specimens decreases, causing this curve to gradually get closer to the one for manual crack healing and further away from the one of autonomous healing. At the end of the test, the capillary water absorption for the specimens with capsules is about 1.33 times (or 33 %) higher than for the specimens with manually injected cracks (and uncracked specimens). However, better quantitative information about this can be found in sections 7.3 and 7.4. Also, a remarkable difference can be observed between the standard errors of both curves. At the end of this test, this error is almost three times larger for the specimens with capsules than for the manually injected specimens. Both differences, in water absorption and in standard error, can be attributed to incomplete crack healing of some specimens with capsules, e.g. due to the fact that (1) a capsule was not broken, (2) the fact that not all the healing agent was released out of the capsules or (3) due to the insufficient leakage of the agent in the crack.

Remarkably, all the healed specimens showed an increase in water absorption rate (see section 7.3) after this first eight hours. For example, in case of PU_CAPS, the water absorption rate showed an increase from about 0.46 $g/cm^2/h^{0.5}$ during the first eight hours to about 0.62 $g/cm^2/h^{0.5}$ during the rest of the exposure time. This is a difference of 0.16 $g/cm^2/h^{0.5}$ or almost 1.35 %. The same phenomenon has already been observed by Van Belleghem et al. (2017a). Two possible reasons for this increase were given in this paper. A first possible reason is that, due to the low viscosity of the healing agents, only the part of the crack below the level of the capsules was healed. This way, penetration of water in the mortar matrix next to the crack could lead to water ingress in the unhealed part of the crack and hence an increasing water absorption. Another given possibility was that, due to some damage to the bond between the mortar and the reinforcement bars, which may have been caused by crack creation, an increase in water absorption occurred when the water front in the mortar matrix next to the crack reached the position of the reinforcement bars (in this case: after eight hours). Both possibilities can also be possible in this research, however, further research is required to verify whether one of these hypothesis is correct. This can be done by either splitting the specimens and evaluating the crack faces for polyurethane coverage (for the first possible reason) or through visualization of the water uptake with X-ray or neutron radiography (for the second possibility).

7.2.3 Samples healed with WRA

The same healing mechanisms as discussed before, with PU as healing agent (see previous section), were also tested using water repellent agent (WRA_CAPS and WRA_MAN). However, two extra types were examined using WRA, namely by spraying the water repellent agent on the upper (test) surface, once before and once after crack creation, respectively defined as WRA_SURF_BEFORE and WRA_SURF_AFTER. It can be observed from Figure 7.3 that the cumulative water absorption curves of these four different types of healing mechanisms are very similar. They all have a linear trend and are all completely situated under the curve obtained for uncracked specimens.

The lowest cumulative water absorption was obtained with the specimens of which the test surface has been sprayed with WRA after crack creation (WRA_SURF_AFTER). At the end of the test, for this test series a cumulative water absorption value 1.67 times (or 40 %) smaller than for uncracked specimens was obtained.

The other three types of WRA-healed specimens resulted in slightly higher water absorption values, with a maximum increase of about 30 % for specimens with embedded capsules (WRA_CAPS). Similar as for PU_CAPS, the higher water absorption values for WRA_CAPS can probably be attributed to a limited healing efficiency for one or more specimens.

In the beginning of the test, the curve for manually injected specimens (WRA_MAN) almost coincided with the curve for WRA_SURF_AFTER. However, after about 24 hours, the absorption rate of the manually injected specimens started to increase a little more rapidly. This slightly higher water absorption rate can be attributed to the fact that in case of specimens with manually injected cracks, water was able to penetrate in the mortar matrix next to the crack, while this was prohibited for specimens with WRA on the entire test surface. In the continuation of the

test, the curve for manually injected cracks then runs close to and parallel with the one of the specimens of which the test surface is sprayed before crack creation (WRA_SURF_BEFORE).

Just like with PU as healing agent, an increase in water absorption rate after the first eight hours can be observed for all specimens (see also section 7.3). The only type of specimen for which this is not valid, is WRA_SURF_BEFORE, which can be attributed to the deviating values in the period from 5 to 8 hours. Again, further investigation through evaluation of the crack faces, in this case for the WRA penetration front, is necessary.

Another remarkable fact was noticed when looking at the results of the specimens of which the test surface was sprayed with WRA before crack creation (WRA_SURF_BEFORE) (see Figure 7.2). At the beginning of the test, all three specimens had similar linear results. However, after seven hours (indicated with a dashed line), a rapid increase in cumulative water absorption (followed by a gradual decrease) could be observed for one of the specimens, while the two other curves remained linear during the continuation of the test. This can probably be explained by incomplete crack healing. Since the surface was impregnated with the healing agent before the crack was created, the healing agent was only applied on the upper surface. So, after crack creation, the inside of the crack could only be healed by penetration of the healing agent through the mortar matrix (before and after crack creation). However, since probably not the entire mortar matrix was (evenly) healed, it is possible that parts of the crack were not healed. So, the time until this rapid increase in water absorption rate (here: seven hours), was probably the time water needed to reach an unhealed part of the crack. So, from that moment on, water could (freely) penetrate in the crack (and subsequently the entire mortar prism and the specimen started to act as if it was unhealed. The resemblances between this curve and the one for cracked specimens (same slope and trend) can also be seen on Figure 7.2.

Note: Due to the deviating results for that one prism, this specimen was excluded for the calculations of the mean cumulative water absorption curve and its corresponding standard error (see Figure 7.3). So, for type WRA_SURF_BEFORE, only two specimens were considered, instead of three (or more).

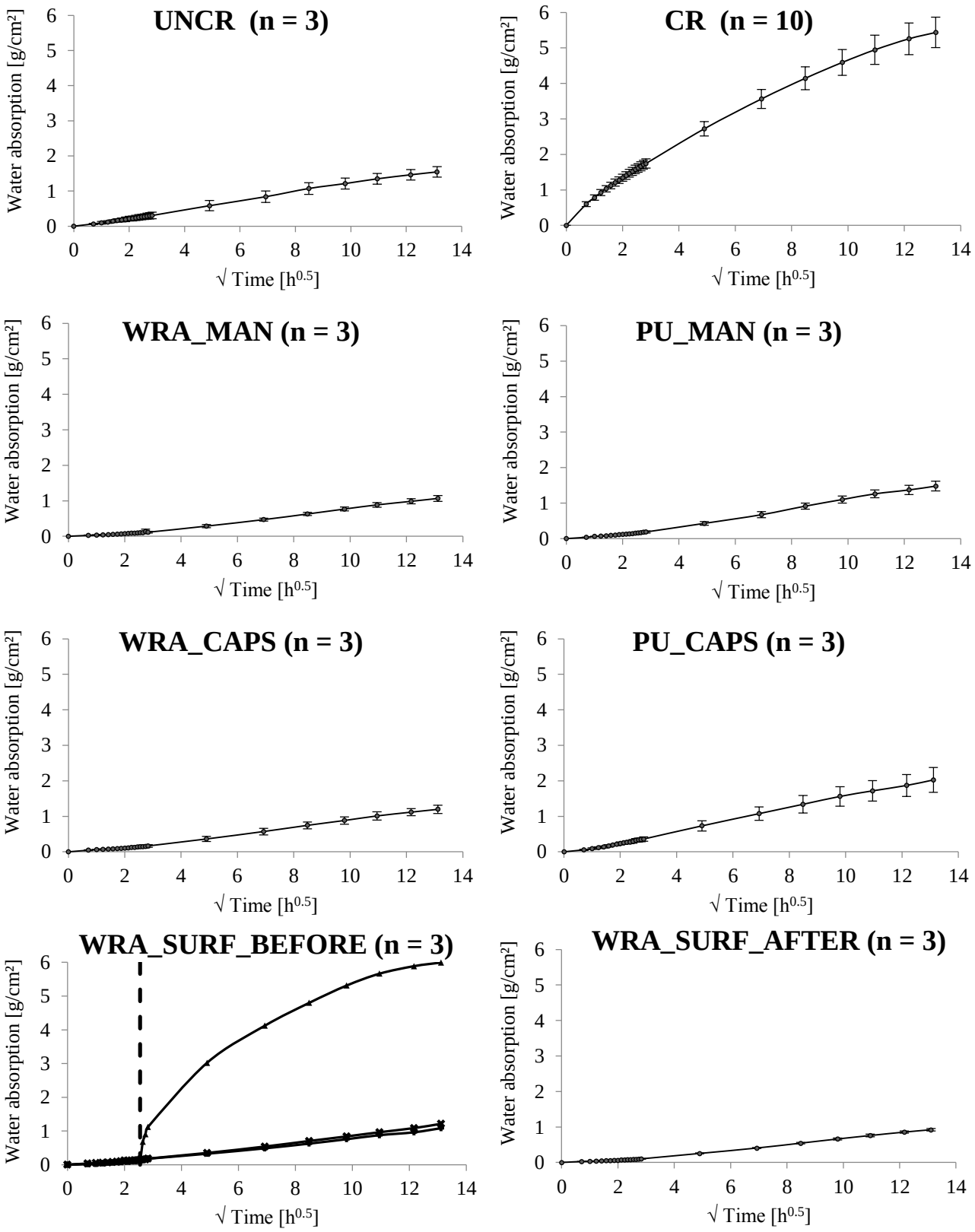

FIGURE 7.2: CUMULATIVE WATER ABSORPTION CURVES IN FUNCTION OF THE SQUARE ROOT OF TIME FOR ALL SPECIMENS. ERROR BARS REPRESENT THE STANDARD ERROR ON THE MEAN VALUES. N INDICATES THE AMOUNT OF SPECIMENS PER TEST SERIES

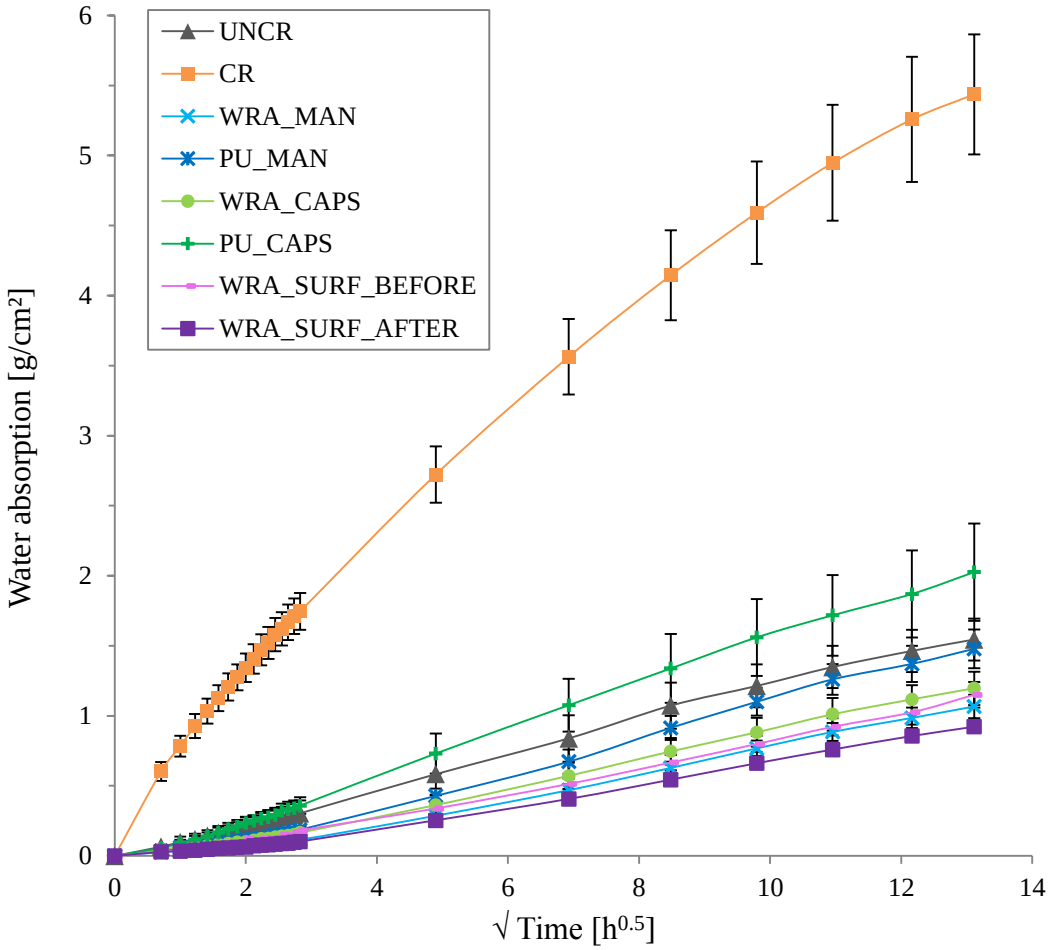

FIGURE 7.3: COMPARISON OF ALL CUMULATIVE WATER ABSORPTION CURVES IN FUNCTION OF THE SQUARE ROOT OF TIME. ERROR BARS REPRESENT THE STANDARD ERROR ON THE MEAN VALUES.

7.3 Capillary sorption coefficient

Figure 7.4 shows the capillary sorption coefficients of all tested specimens. This coefficient is once calculated between the start of the experiment and eight hours of exposure (initial sorption coefficient) and once for the remaining exposure time (secondary sorption coefficient). This way, the earlier mentioned phenomenon of an increasing water absorption rate could be investigated quantitatively.

First, the results for the uncracked and cracked mortar specimens are discussed. Due to the presence of the crack, the cracked specimens obviously have a much higher sorption coefficient than the uncracked ones, of which the crack width is equal to zero. The initial sorption coefficient for the uncracked specimens is equal to 1.08 kg/m²/h$^{0.5}$. For cracked specimens, this amounts 6.17 kg/m²/h$^{0.5}$, which is more almost six times higher than for uncracked specimens. Also, a large difference was noticeable between the initial and secondary sorption coefficient. The initial sorption coefficient was equal to 6.17 kg/m²/h$^{0.5}$, while a secondary sorption coefficient was found of 3.59 kg/m²/h$^{0.5}$, which is a decrease of almost 42 %. This can be attributed to the fact that, before the start of the test, the specimens were almost completely dry, so almost no

water was present in them. So then, when the water started to freely penetrate in the prism, a lot of water could be absorbed by the prism. However, the further in time, the more water has penetrated in the prisms and consequently the more these prisms approach the state of saturation. The more saturated the prisms get, the harder it gets for the water to penetrate, since only the deeper and smaller voids in the mortar matrix still need to be filled.

When looking at the sorption coefficients for the mortar prisms of which the cracks are healed, all types of healing mechanisms show similar results, no matter which healing agent was used. All these sorption coefficients, both initial and secondary, were much lower than for cracked specimens and most of them were even lower than for uncracked specimens. For example, the initial sorption coefficient of WRA_SURF_AFTER amounted 0.36 kg/m²/h$^{0.5}$, which was three times lower than for uncracked specimens and even more than 17 times lower than for cracked specimens. Based on Figure 7.4, also the increase in water absorption rate after the first eight hours, explained in section 7.2.2, can be confirmed. All healing mechanism showed a significant difference between the initial and secondary sorption coefficient, due to partial crack healing (only below level of capsules) or damage to the bond between the mortar and the reinforcement, as was already explained in section 7.2.2. The largest difference was found for WRA_MAN, which showed an increase of more than 125% from an initial sorption coefficient of 0.41 kg/m²/h$^{0.5}$ to a secondary coefficient equal to 0.92 kg/m²/h$^{0.5}$.

Finally, although the values of the sorption coefficients of all the healed specimens were not higher than 1.26 kg/m²/h$^{0.5}$, still a little differences could be noticed between the healing mechanisms with PU and WRA. The mean sorption coefficients for specimens healed with PU (0.96 kg/m²/h$^{0.5}$ for PU_MAN and 1.08 kg/m²/h$^{0.5}$ for PU_CAPS) seemed to be higher compared to the WRA-healed specimens (0.67 kg/m²/h$^{0.5}$ for WRA_MAN, 0.58 for kg/m²/h$^{0.5}$ for WRA_SURF_AFTER and 0.79 kg/m²/h$^{0.5}$ for WRA_CAPS and WRA_SURF_BEFORE). This corresponded to differences in mean sorption coefficient ranging from 21.5 % to 86 %.

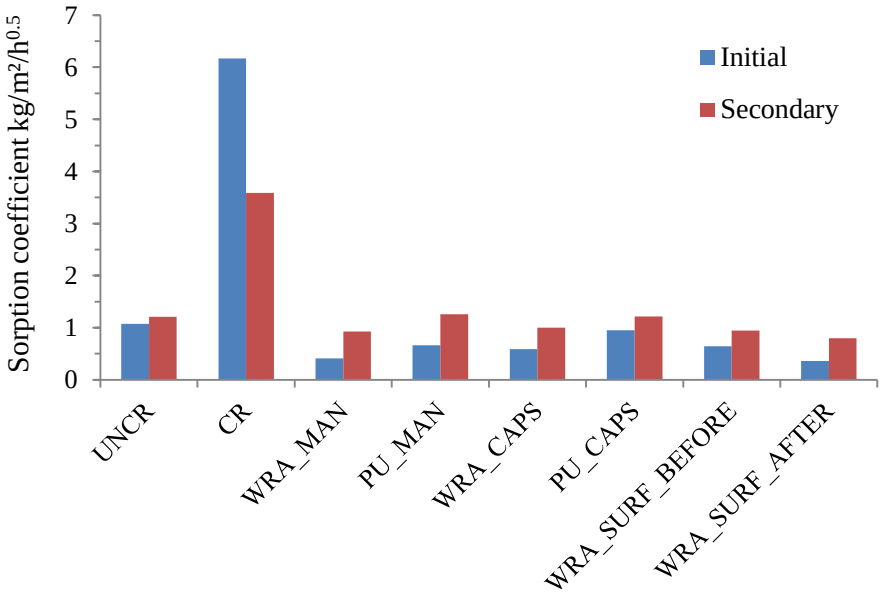

FIGURE 7.4: INITIAL (0 H – 8 H) AND SECONDARY (8 H – 172 H) SORPTION COEFFICIENTS FOR EACH TYPE OF HEALING MECHANISM

7.4 Self-healing efficiency

In order to make a quantitative evaluation of the self-healing performance, the self-healing efficiency (SHE) can be determined for each type of healing mechanism, according to the definition given in Van Belleghem et al. (2017). However, the calculation of this value depends on the application. The self-healing efficiency of a mortar specimen [%] in case of a water absorption test was defined by equation (7.1).

$$SHE = \frac{S_{CR,M} - S_{HEAL,i}}{S_{CR,M} - S_{UNCR,M}} \qquad (7.1)$$

where: $S_{CR,M}$ the mean sorption coefficient of the cracked specimen [kg/m²/h$^{0.5}$]
$S_{HEAL,i}$ the sorption coefficient of an individual healed specimen [kg/m²/h$^{0.5}$]
$S_{UNCR,M}$ the mean sorption coefficient of the uncracked specimen [kg/m²/h$^{0.5}$]

The self-healing efficiency of each specimen is depicted in Figure 7.5. Except for the one beam of the test series WRA_SURF_BEFORE, which only had an efficiency of about 14 %, overall high healing efficiencies were obtained by the applied mechanisms. Only for PU_CAPS, with a mean value of 91.86, the healing efficiency was below 100 %. However, this still indicates a good healing behaviour. The average healing efficiencies of the other test series all ranged between 109 % and 115 %. As could already be predicted after the previous sections, this largest efficiency was obtained with test series WRA_SURF_AFTER.

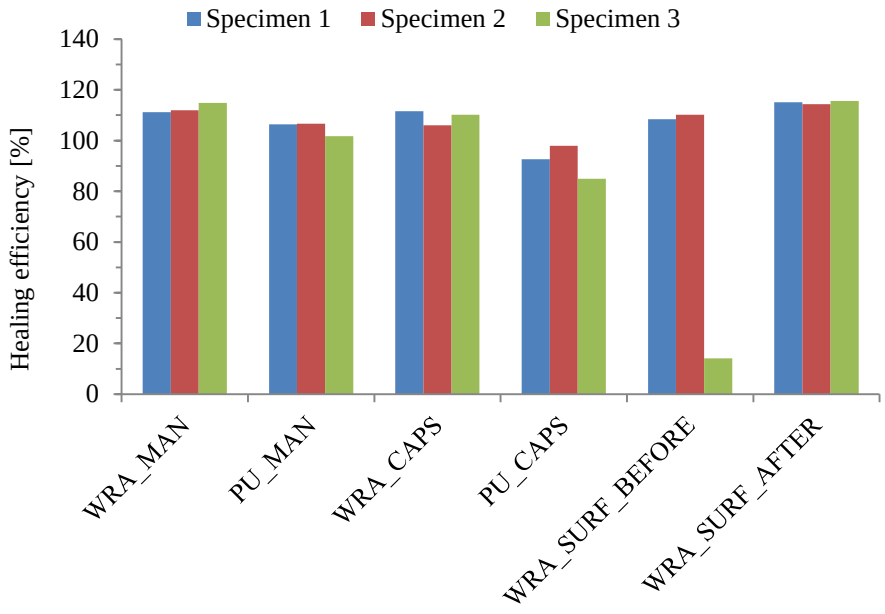

FIGURE 7.5: HEALING EFFICIENCY FOR ALL SPECIMENS

8. Chloride diffusion test

In this section, the results of the chloride diffusion test are discussed and compared. This is done based on two parameters: the chloride concentration [m%/binder] in function of the depth (see 8.1) and the self-healing efficiency (see section 8.2). These both parameters are plotted in function of the crack depth [mm]. However, it has to be noted that for all graphs in this section, the data points at a certain depth are the mean values of the grounded layers with a thickness of 3 mm (see section 6.5). So, these data points actually correspond to the depths ranging from 1.5 mm lower to 1.5 mm higher depths than this certain mean depth at which the data points are situated. So for example, a data point situated in the graph at a depth of 4.5 mm actually corresponds to depths from 3 mm to 6 mm.

8.1 Chloride penetration in function of depth

For all specimens, the chloride concentration [m%/binder] was calculated and plotted in function of the penetration depth [mm]. In section 8.1.1, the results for the cracked and uncracked specimens are discussed and compared with each other, after which the same is done for the different healing mechanisms, using PU (see section 8.1.2) and WRA (see section 8.1.3) respectively as healing agent. Afterwards, a comparison is made between the chloride profiles of all specimens in section 8.1.4.

8.1.1 (Un)cracked specimens

Firstly, the effect of cracks on the ingress of chlorides is discussed. Figure 8.1 shows the obtained profiles after the total exposure regime for the three replicate specimens of the uncracked (a) and cracked (b) test series.

For uncracked specimens (UNCR), the mean chloride concentration at the surface amounts 4.97 ± 0.57 m%/binder and this chloride content dropped fast when going deeper into the concrete matrix. At depths of 15 mm or more, the chloride concentration was already lower than 0.27 m%/binder. For cracked concrete specimens (CR), at every depth the mean chloride concentration is higher compared to the uncracked samples. At the surface, the mean chloride content of the cracked specimens was equal to 8.13 ± 0.61 m%/binder, which is about 1.64 times higher than what was found for the uncracked specimens. At a depth of 21 to 24 mm, this was 3.12 ± 0.15 m%/binder, which is more than 25 times higher compared to the uncracked samples. So, clearly, the presence of cracks has a big influence on the ingress of chlorides.

When looking at the mean chloride profiles, a significant difference can be seen between the cracked and uncracked specimens. While the chloride content of the uncracked specimens rapidly decreases to small values, the chloride concentration of cracked samples decreases in the beginning but from a depth of about 3 mm to 24 mm, a nearly constant level of about 3.3 - 3.5 m%/binder was reached. This can be explained by the fact that chlorides can penetrate freely in the crack, so after a while the crack is filled with the same amount of chlorides. At depths

larger than 25 mm, the chloride concentration started to decrease again. The reason for this decrease is that the crack ends at a depth of 25 mm. So, the chloride concentration at depths larger than the crack depth was only established by penetration of chlorides, probably from inside the crack, through the concrete matrix. Thus, although still a certain amount of chlorides successfully penetrated through these larger depths, a significant difference could be noticed compared to smaller depths from 0 mm to 25 mm, since for these smaller depths, most of the chloride concentration was established by chlorides present in the crack.

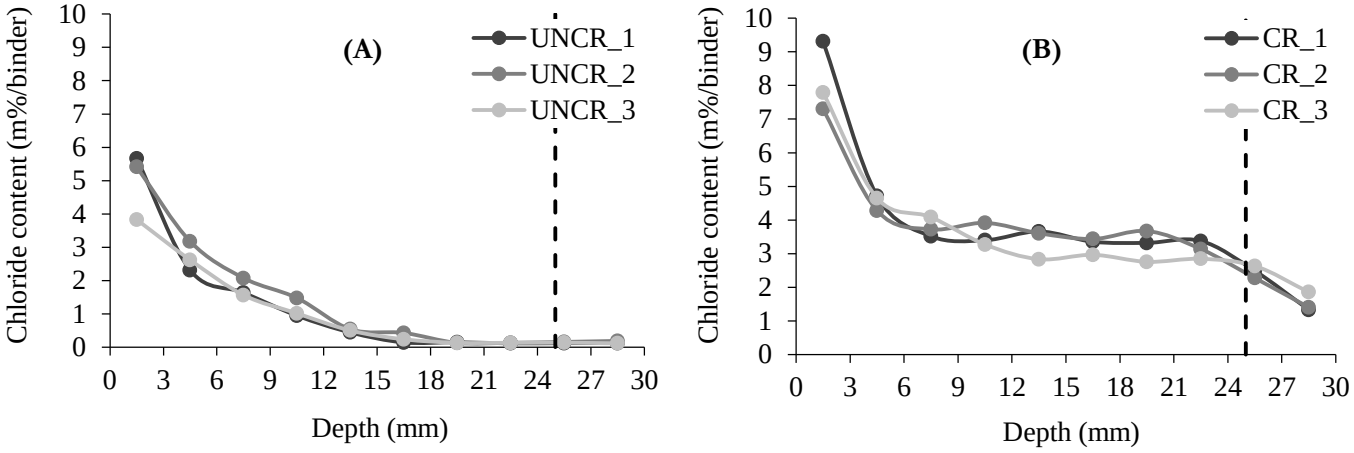

FIGURE 8.1: CHLORIDE PROFILES OF (A) UNCRACKED AND (B) CRACKED SPECIMENS. DASHED LINE INDICATES THE END OF THE CRACK

8.1.2 Specimens healed with PU

The (mean) chloride profiles of the specimens healed with PU are given in Figure 8.2. As can be seen, very promising results were obtained by manually injecting the crack with PU before placing the samples in the solution (PU_MAN). At the surface, a small chloride concentration, compared to the other healing mechanisms, was found, namely 3.60 ± 0.07 m%/binder. This was even less than for uncracked specimens (see also section 8.1.4). Moreover, this chloride content rapidly decreased, resulting in a concentration of less than 0.5 m%/binder from a depth of 15 mm or higher. Also, a very small standard error was obtained for PU_MAN, which shows that PU_MAN causes consistent crack healing, more than other mechanisms.

Approximately the same result was found for the specimens with embedded capsules filled with PU (PU_CAPS). The only noticeable difference is the higher chloride concentration at the test surface. This was equal to 5.04 ± 0.37 m%/binder, which is about 1.4 times higher than for the manually injected specimens. A possible reason for this phenomenon is the presence of a hardened layer of PU on the surface around the crack in case of manually injected cracks. Due to the impossibility of perfectly filling up the crack (e.g. due to the tortuosity inside the crack) and the possibility of a bit too large injected volume of PU, some of the healing agent had leaked out of the crack and hardened on the surface. As this hardened PU-layer partly covered the surface, penetration of chlorides in the crack could be prevented. On the contrary, for samples with capsule-based healing, there was (much) less leakage on the surface, as can be seen in Figure 8.3.

Another possible explanation is the fact that, due to the presence of the embedded capsules, the thin brass plates were fixed more in the concrete cylinders. This way, it was harder to remove these plates and more force was needed. Consequently, for some specimens, this resulted in spalling of the concrete at the surface (see also Figure 8.3), which made it easier for chlorides to penetrate at these surfaces.

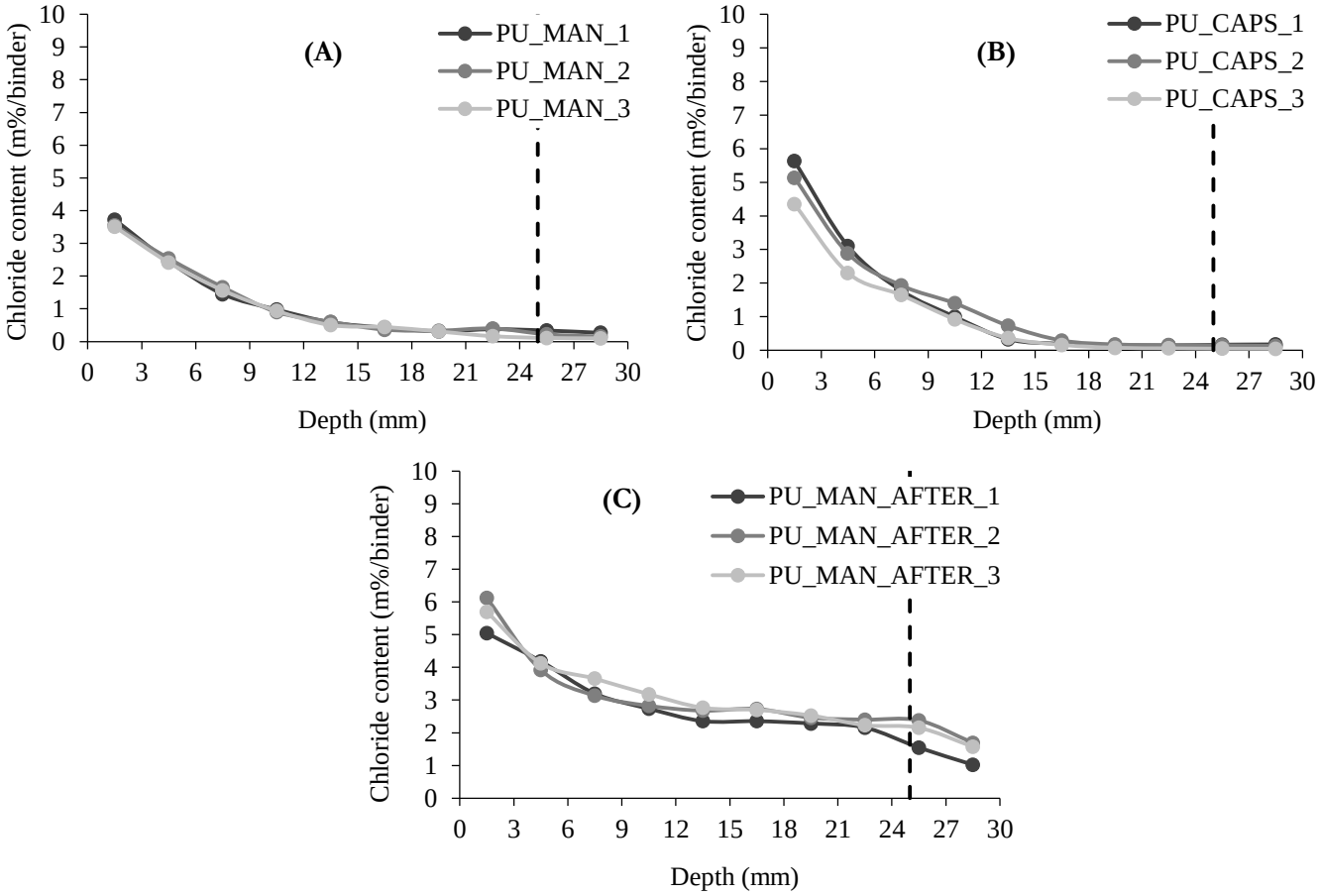

FIGURE 8.2: CHLORIDE PROFILES OF SPECIMENS HEALED WITH PU THROUGH (A) MANUAL INJECTION, (B) ENCAPSULATION AND (C) MANUAL INJECTION AFTER THEE WEEKS OF EXPOSURE. DASHED LINE INDICATES THE END OF THE CRACK

FIGURE 8.3: DIFFERENCE IN LEAKAGE OF THE HEALING AGENT AND SPALLING OF THE CONCRETE BETWEEN SPECIMENS WITH (A) MANUALLY INJECTED CRACKS AND (B) EMBEDDED CAPSULES

Unlike for manually injecting the crack with PU before immersion in the NaCl-solution, less good results were obtained for samples of which the cracks were manually injected after three weeks of immersion. First of all, a high chloride concentration at the surface was found, namely 5.62 ± 0.31 m%/binder, which is similar as for the specimens with embedded capsules. Also, the chloride concentration for this healing after three weeks of exposure showed no rapid decrease. Instead, at a depth of 12 mm, it reached an almost constant value of about 2.3 to 2.6 m%/binder. Finally, the concentration decreased again after reaching the end of the crack. Clear similarities can be observed between this latter test series and the results for the cracked specimens. The only differences were the lower chloride concentration at the surface (decrease of 31 %), mainly due to the surface coverage of the hardened PU layer, and the overall decrease in chloride content over the whole measured depth of about 23 %. Both differences can also be explained by the fact that the PU injected after a few weeks, actually was effective in blocking the further penetration of chlorides (respectively at the surface by the hardened PU and in the crack), but by that time already a lot of chlorides were present in the crack and the concrete matrix. This led to rather low healing efficiencies (see section 8.2). It can thus be concluded that it is of great importance to heal a crack as soon as possible after its formation.

8.1.3 Specimens healed with WRA

Just like for the healed specimens using PU as healing agent, a comparison can be made between the different healing mechanisms with WRA as healing agent. The chloride profiles for specimens healed with WRA can be found in Figure 8.4.

First, the chloride profile of specimens with manually injected cracks (before immersion) is discussed. It can be seen that a high chloride concentration of 5.56 ± 1.11 m%/binder has been found at the surface, which is probably caused by spalling of the concrete. However, at a depth of about 3 mm, this value is already four times lower. From this depth, an slightly decreasing curve can be seen, with chloride concentrations ranging from about 1.4 to 0.8 m%/binder.

Using embedded capsules filled with WRA resulted in a higher chloride concentration at the crack surface compared to manual injection of the crack. In this case, the concentration at the surface was equal to 9.11 ± 0.59 m%/binder, which is even higher than for cracked specimens. These high values may again be attributed to spalling of the concrete. This was even more pronounced than for the samples with PU-capsules, probably explaining the higher chloride concentrations at the surface. A constant concentration of about 2.35 m%/binder is reached between depths of 6 mm and 15 mm, after which an almost linear decrease can be seen in the curve until a value of 0.73 ± 0.14 m%/binder.

With the last healing mechanism, i.e. injection of WRA in the crack after 3 weeks of immersion, less good results were obtained. Although the chloride concentration at the surface was lower than the two aforementioned healing mechanisms, namely 6.11 ± 0.51 m%/binder, this chloride content did not decrease a lot. Instead, between a depth of 6 mm and 25 mm, a rather constant high chloride concentration of 3 to 4 m%/binder was found. At depths of 25 mm or more, again a more rapid decrease in chloride concentration occurred, due to the end of the crack.

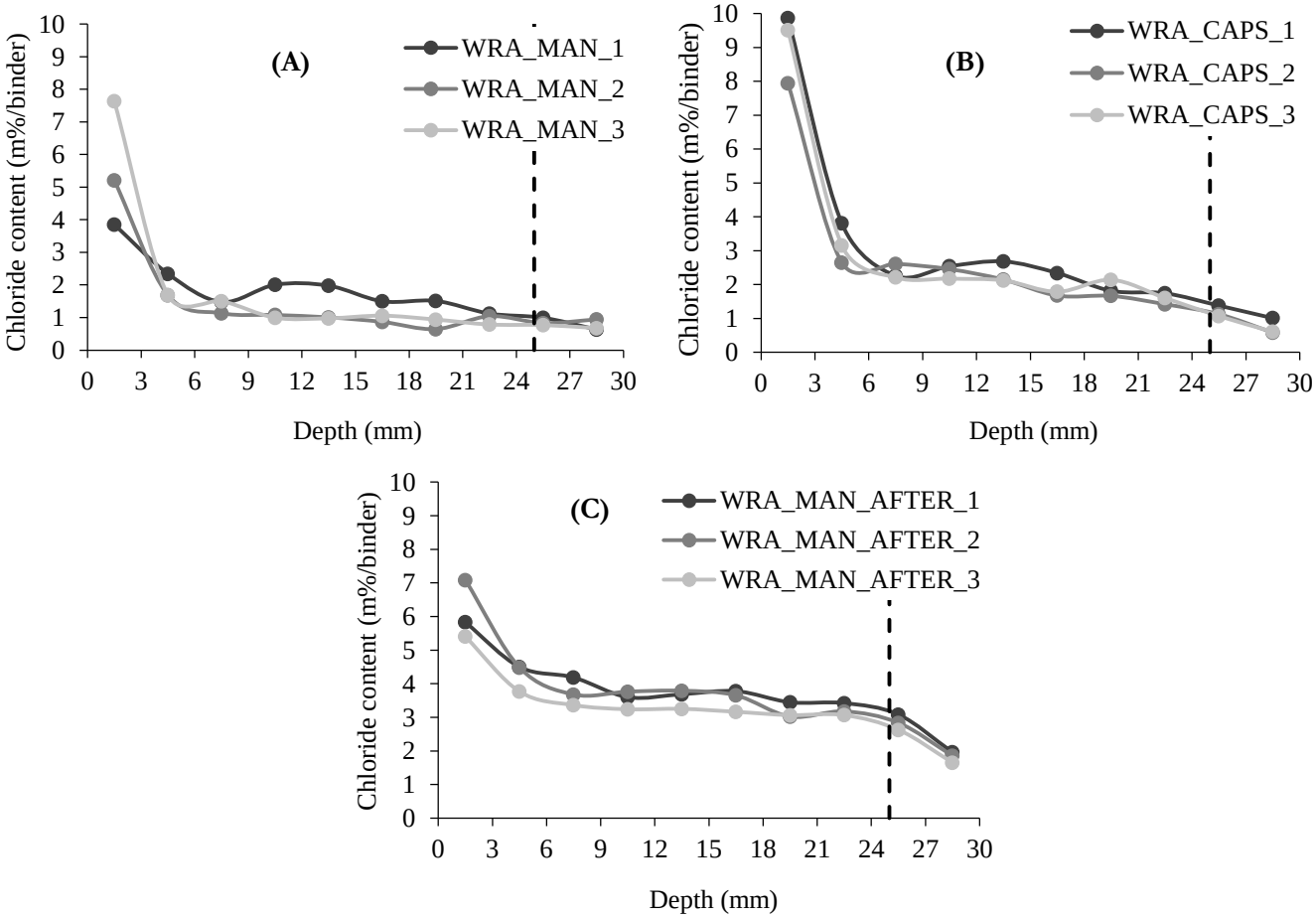

FIGURE 8.4: CHLORIDE PROFILES OF SPECIMENS HEALED WITH WRA THROUGH (A) MANUAL INJECTION, (B) ENCAPSULATION AND (C) MANUAL INJECTION AFTER THREE WEEKS OF EXPOSURE. DASHED LINE INDICATES THE END OF THE CRACK

8.1.4 Global comparison

The mean chloride profiles discussed in section 8.1.1 to 8.1.3 can be plotted together, to properly compare the different types of healing mechanisms. To prevent confusion, not all these curves are plotted on the same graph. A distinction is made between the chloride profiles of specimens with PU as healing agent and the ones with WRA. For each case, they are compared to the chloride profiles of cracked and uncracked specimens. These plots can be seen on Figure 8.5 (for PU) and Figure 8.6 (for WRA).

When looking at Figure 8.5, it can be concluded that both manually injecting PU in the crack (before immersion) (PU_MAN), as well as capsule-based healing (PU_CAPS) show very promising results. The chloride profile of the latter mechanism almost completely coincides with the one for uncracked specimens, while the former mechanism gives even lower chloride concentrations than for uncracked specimens up to a depth of 12 mm. Deeper in the crack, a bit higher chloride concentrations are obtained compared to uncracked specimens, but the difference is not larger than 0.189 m%/binder. Moreover, the largest difference between UNCR and PU_MAN can be found at the surface, where the concentration for specimens with manually

injected PU is even 1.38 times smaller than for uncracked specimens. This corresponds with the aforementioned PU-layer on the crack surface, preventing the chlorides to enter the crack.

From Figure 8.6, it can be seen that (semi) good results are obtained with the same type of healing mechanisms, but with WRA as healing agent. However, not such low chloride concentrations are found as with PU. Compared to uncracked specimens, manually injecting WRA in the crack (before immersion) gives better healing performances between depths of 6 mm and 9 mm. At the surface, a difference of about 0.6 m%/binder is found, while for higher depths both curves run rather parallel with a maximum difference of 0.9 m%/binder, which corresponds to a chloride concentration for WRA_MAN about 8 times higher than for uncracked specimens.

Using WRA as healing agent in embedded capsules led to a chloride profile which showed a comparable curve as the one for cracked specimens, but with lower chloride concentrations (difference of about 1.3 m%/binder). When comparing to the chloride profiles for uncracked samples, it can be seen that, over the whole crack depth, the obtained chloride concentrations with encapsulated WRA were never lower than those for uncracked specimens. At the surface, it even has a higher chloride concentration than for cracked specimens. Here, the chloride concentration is almost two times as high as for uncracked specimens. The smallest difference between both curves occurs at a depth from 3 to 6 mm, where the concentration for WRA_CAPS is about 1.19 times higher than for UNCR, but 1.42 times lower than for CR. At larger depths, this difference increases again, with its maximum at a depth from 18 to 21 mm. There, the concentration for specimens with encapsulated WRA is about 14 times higher than for uncracked specimens, but 1.74 times lower than for cracked ones. To get a more clear and comparable view of the quantitative values, the healing efficiency can be calculated. This is done in section 8.2.

At last, based on Figure 8.5 and Figure 8.6, it can be concluded that manually injecting a healing agent (PU or WRA) after 3 weeks of immersion, does not result in very good healing performances. When using PU (PU_MAN_AFTER), the chloride concentration at each depth was lower than for cracked specimens, which means that, from the moment of injection until the end of the exposure time, the PU was probably successful in blocking the ingress of chlorides. Nevertheless, the chloride concentrations are (very) high, with at certain depths (between 18 and 24 mm) a concentration of more than 18 times the one for uncracked samples. Even worse results were obtained for the mean of the WRA_MAN_AFTER series. At depths larger than 6 mm, the curve for WRA_MAN_AFTER almost completely coincides with the one for CR, or even is situated above it. Thus, no actual healing of the crack is obtained in this case. The low self-healing efficiency for these test series is discussed in section 8.2. However, according to the chloride content, it can already be concluded that it is important and beneficial to heal a crack as soon as possible after its formation.

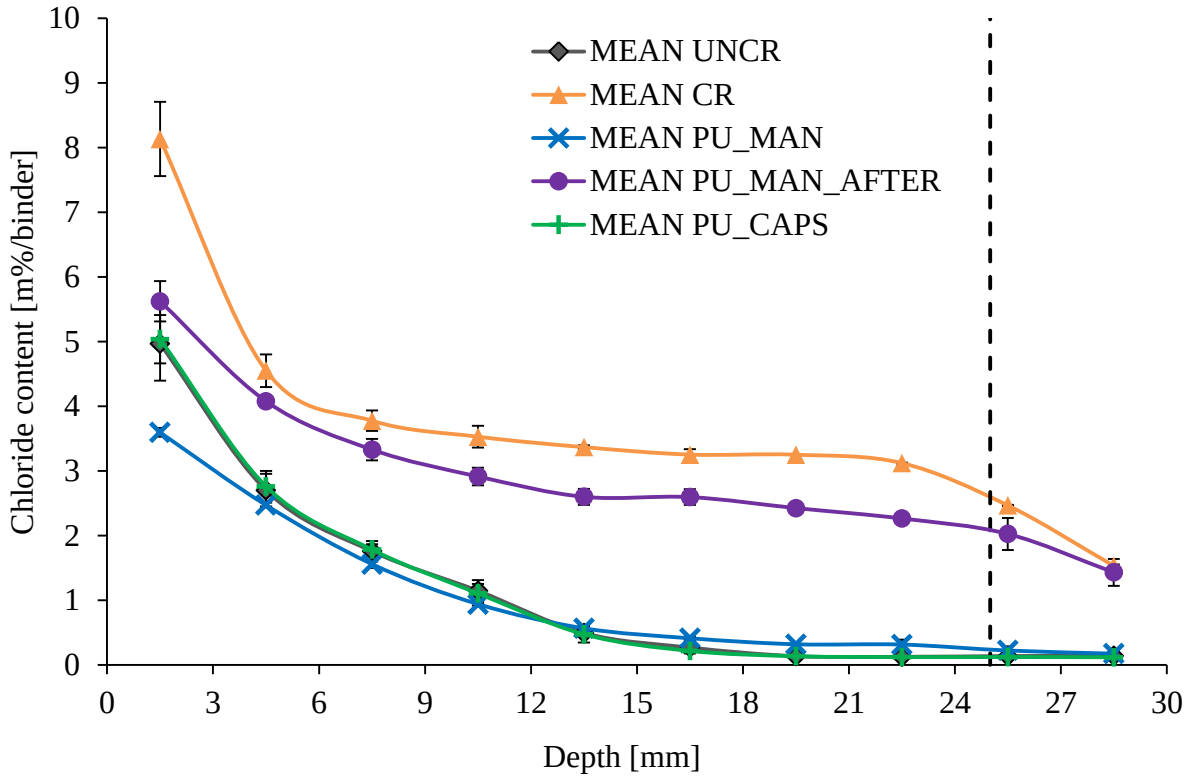

FIGURE 8.5: COMPARISON OF AVERAGE CHLORIDE PROFILES OF (UN)CRACKED SPECIMENS AND SPECIMENS HEALED WITH PU. ERROR BARS REPRESENT THE STANDARD ERROR ON THE MEAN VALUES.

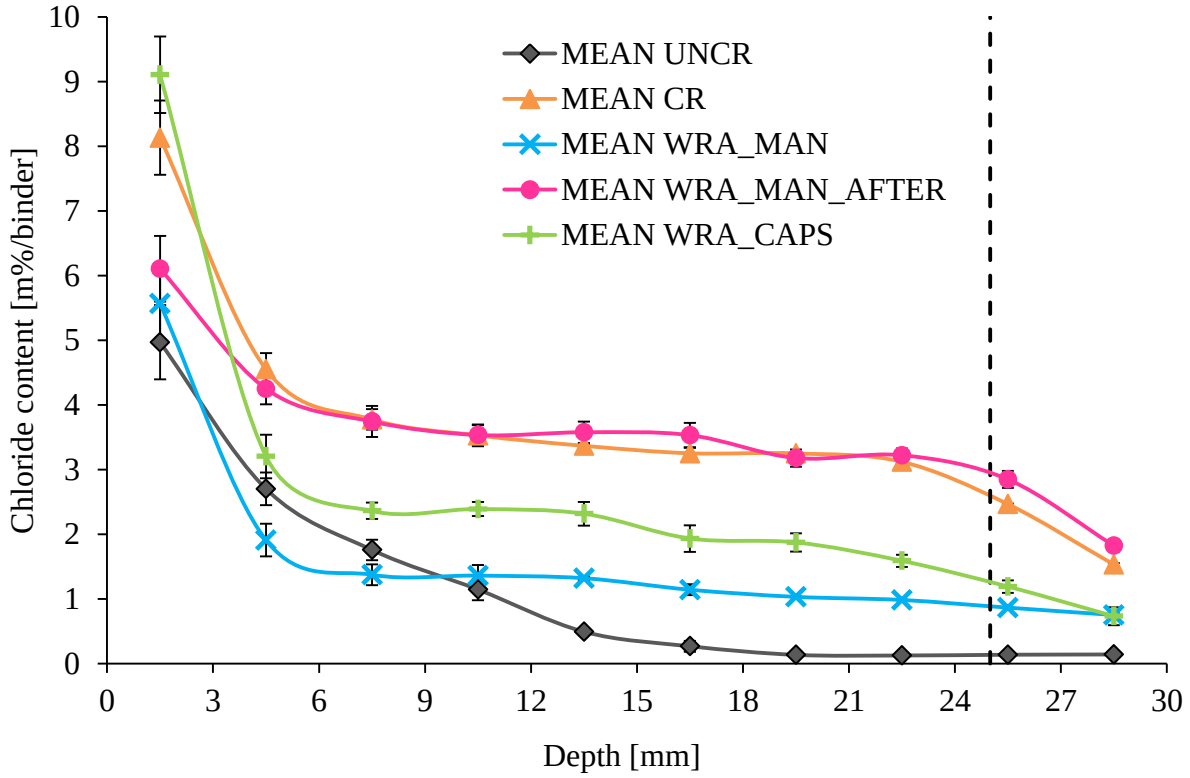

FIGURE 8.6: COMPARISON OF AVERAGE CHLORIDE PROFILES OF (UN)CRACKED SPECIMENS AND SPECIMENS HEALED WITH WRA. ERROR BARS REPRESENT THE STANDARD ERROR ON THE MEAN VALUES.

8.2 Self-healing efficiency

Similar as for the capillary water absorption test, the self-healing performance of each specimen can be derived by calculating the self-healing efficiency at every depth i below the exposed surface (SHE_i) (Equation (8.1)).

$$SHE_i = \frac{Cl^-_{CR,i} - Cl^-_{HEAL,i}}{Cl^-_{CR,i} - Cl^-_{UNCR,i}} \quad (8.1)$$

where: $Cl^-_{CR,i}$ the chloride content of the cracked specimen at depth i [m%/binder]
$Cl^-_{HEAL,i}$ the chloride content of the healed specimen at depth i [m%/binder]
$Cl^-_{UNCR,i}$ the chloride content of the uncracked specimen at depth i [m%/binder]

The obtained self-healing efficiencies for all test series are depicted in Figure 8.7. It can be seen that almost all test series experience a varying healing efficiency in the first few millimetres. This clearly corresponds to the obtained chloride concentrations at the surface of the test series. For example, both WRA_MAN and WRA_CAPS had a (very) high chloride content at the surface followed by a rapid decrease of the chloride concentration. This corresponds with a (very) low healing efficiency at the surface and a subsequent large increase in healing efficiency at a depth of 4.5 mm. WRA_CAPS even has a negative healing efficiency at the surface of about -30 %, which means that instead of preventing the chlorides from entering the crack, more chlorides ingress was observed (chloride content higher than 9 m%/binder). This can probably be attributed to the fact that, apparently, there was no leakage of the healing agent at the surface.

The contrary can be noticed for PU_MAN, PU_MAN_AFTER and WRA_MAN_AFTER, which all have a higher healing efficiency at the surface than at larger depths. For both test series, this again can be attributed to the leakage of the healing agent on the test surface after manually injecting the cracks. After these first millimetres (from about 12 mm for WRA_MAN and WRA_CAPS, while from 3 mm for the other mechanisms), all healing efficiencies became rather constant. Only for PU_CAPS, an almost constant healing efficiency of 100 % was obtained. However for WRA_MAN as well as for WRA_MAN_AFTER and PU_MAN_AFTER, a decreasing trend in healing efficiency was noticeable for depths larger than the crack depth (25 mm and more). Since the only way the healing agent could be present at these larger depths is by penetration through the concrete matrix, which is (clearly) more difficult than penetrating directly in the crack, no or less healing agent was present at these depths, resulting in the obtained lower healing efficiencies.

When comparing the different test series with each other, it can be observed that both WRA_MAN_AFTER and PU_MAN_AFTER show low (to even negative) healing efficiencies. It can thus be concluded that applying a healing agent after a few weeks (here: three) of exposure to chlorides is not recommended. From this, the importance of healing the crack as soon as possible after crack creation becomes very clear. The beneficial effect for the self-healing efficiency by healing the crack before exposure to chlorides can be noticed from the healing efficiencies of the other test series. Except for the negative value for WRA_CAPS at the surface,

all other healing are higher than for the aforementioned series which were healed at a later time. However, still rather low healing efficiencies are generally obtained for WRA_CAPS. After the earlier mentioned rapid increase from -30 % at the surface up to about 70 % between depths of 3 mm to 9 mm, the healing efficiency ranges between 35 % and 55 %. Although this still gives better results than for unhealed or untreated specimens, better healing performances can obtained with by applying other healing mechanisms. For example, by manually injecting the crack with WRA (WRA_MAN) instead of encapsulating the WRA, already large differences in healing performances were obtained, especially in the first millimetres. At the surface, this difference was equal to 120 %, which gradually decreased to differences of about 70 % between 3 mm and 6 mm depth, 50 % between 6 mm and 9 mm depth and so on, until both curves finally reached a healing efficiency of about 56 %.

The largest healing efficiencies were however obtained by applying PU in the crack before exposure. Autonomous healing using embedded capsules led to a constant high healing efficiency over the whole crack depth of 100 %. This means, as was already found in the previous section, that the PU_CAPS test series showed approximately same behaviour as uncracked specimens. From depths larger than 12 mm, manually injecting PU in the crack showed nearly the same healing efficiencies. At lower depths, even better healing performances were obtained compared to uncracked specimens. For example, at the surface, this healing mechanism led to a healing efficiency of more than 140 %, which was the highest measured value of all specimens. As mentioned in previous section, this can be attributed to the surface coverage in the zone around the crack by a hardened PU layer, resulting from excess injected agent.

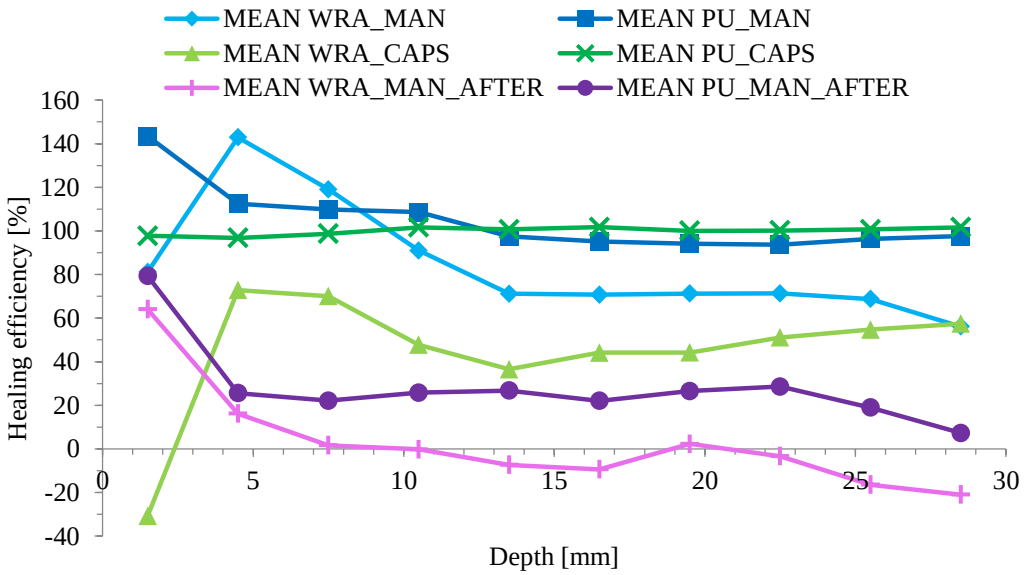

FIGURE 8.7: SELF-HEALING EFFICIENCY IN FUNCTION OF THE CRACK DEPTH FOR EACH TEST SERIES

9. Corrosion monitoring

In this section, an overview of the measurements of all electrochemical parameters as a function of time is given and discussed. First of all, the crack widths of all specimens are given in section 9.1. Subsequently, the different types of specimens for which corrosion was monitored are discussed and compared: uncracked specimens (section 9.2), cracked specimens (section 0), specimens autonomously (by encapsulation) and manually (by injection) healed with PU (section 0) and specimens healed with WRA through autonomous healing (by encapsulation) and manual healing (by injection and surface impregnation) (section 0). For each of these types, the following non-destructive electrochemical parameters, discussed in section 3) were measured:

- Macro-cell corrosion current I_{corr}
- Corrosion potential E_{corr}
- Driving potential ΔE
- Anodic polarisation resistance $R_{P,A}$
- Cathodic polarisation resistance $R_{P,C}$
- Concrete resistance R_E

However, not all parameters seemed to give a clear indication of the corrosion state. Therefore only the ones who did, all except for the cathodic polarisation resistance, are discussed in detail in sections 9.2 to 0. The cathodic polarisation resistance is then discussed separately in section 9.6.

Note: Due to the fact that the corrosion potential cannot be measured directly at the concrete/rebar interface, an error was caused due to the resistance of the electrolyte, also known as the ohmic drop or IR drop (see section 3.2). After 12 weeks of monitoring, a clear relation could be noticed between this parameter and the parameters which gave an indication of corrosion, such as the macro-cell corrosion current or the corrosion potential. The higher the corrosion activity of the beams, corresponding to lower values for the corrosion potential, the higher the measured IR drop. So, to compensate this error, the corrosion potential has been reduced by the IR drop.

9.1 Crack width

The crack width of each beam was measured at week 1, before the start of the experiment. To check whether the crack widths remained open, an extra measurement was performed at week 7. The mean crack widths and its corresponding standard deviation for each test series are calculated and are shown in Figure 9.1. Clearly, the aimed crack width of 300 μm was exceeded for all the series, since at week 0, the mean crack width for all specimens was equal to 467 ± 19 μm. After seven weeks, a decrease in crack width could be observed for most of the test series, ranging from 15 μm (for WRA_CAPS) to 218 μm (for PU_CAPS). However, for two test series an increase (up to 43 μm) was found, namely for both series of which the test surface was impregnated with WRA. For test series PU_MAN, no crack measurement could be done after seven weeks, since the crack was not clearly visible anymore (with the microscope) due to the hardened PU at the crack opening.

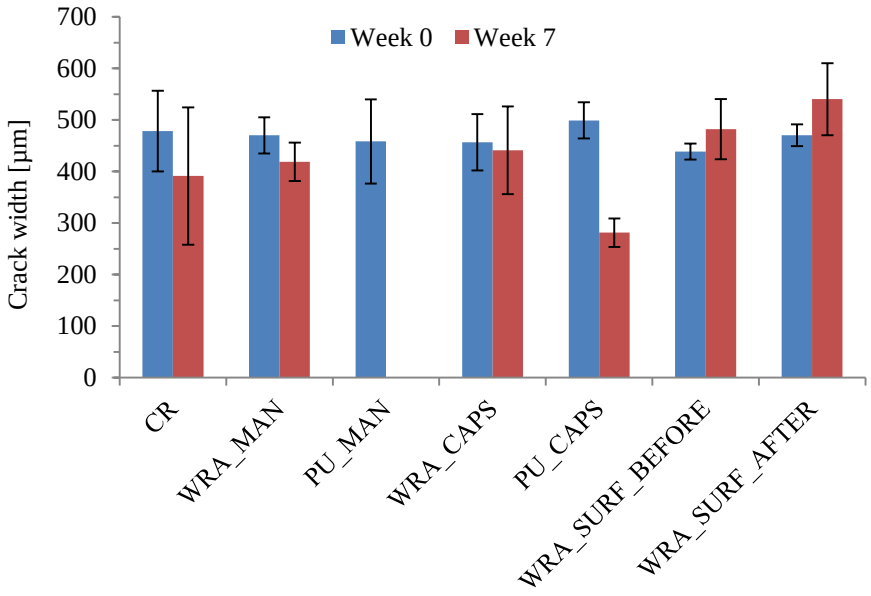

FIGURE 9.1: CRACK WIDTHS AT WEEK 0 AND WEEK 7 FOR THE DIFFERENT TEST SERIES. ERROR BARS REPRESENT STANDARD ERROR ON THE MEAN VALUES.

9.2 Uncracked specimens

The measurements of the electrochemical corrosion parameters for the uncracked specimens are depicted in Figure 9.2. Uncracked specimens are characterized by a macro-cell corrosion current (Figure 9.2a) of nearly zero during the whole experiment (12 weeks of wet/dry-cycles). Before the start of the wet/dry-cycles, the measured corrosion potential was equal to about -250 mV vs. MnO_2, while during the rest of the test a stable value of -200 mV vs. MnO_2 was obtained (Figure 9.2b).

Further, a relatively low and stable driving potential of about 150 mV (Figure 9.2c) and a high but rather stable anodic polarization resistance (between 20 kΩ and 30 kΩ) throughout the whole experiment were noticed. Note that the driving potential is not equal to zero. This is due to the depolarization of the anode and cathode before the open circuit potentials or resting potentials were measured (see section 6.6). So, due to all these measured values, one can conclude that there was no active state of corrosion in the uncracked concrete specimens over the whole exposure period. Finally, due to the ongoing hydration of the young concrete, a general increase of the concrete resistance could be noticed for all uncracked beams, ranging between 0.3 to 0.4 kΩ at the start of the experiment up to 1.6 kΩ at the end.

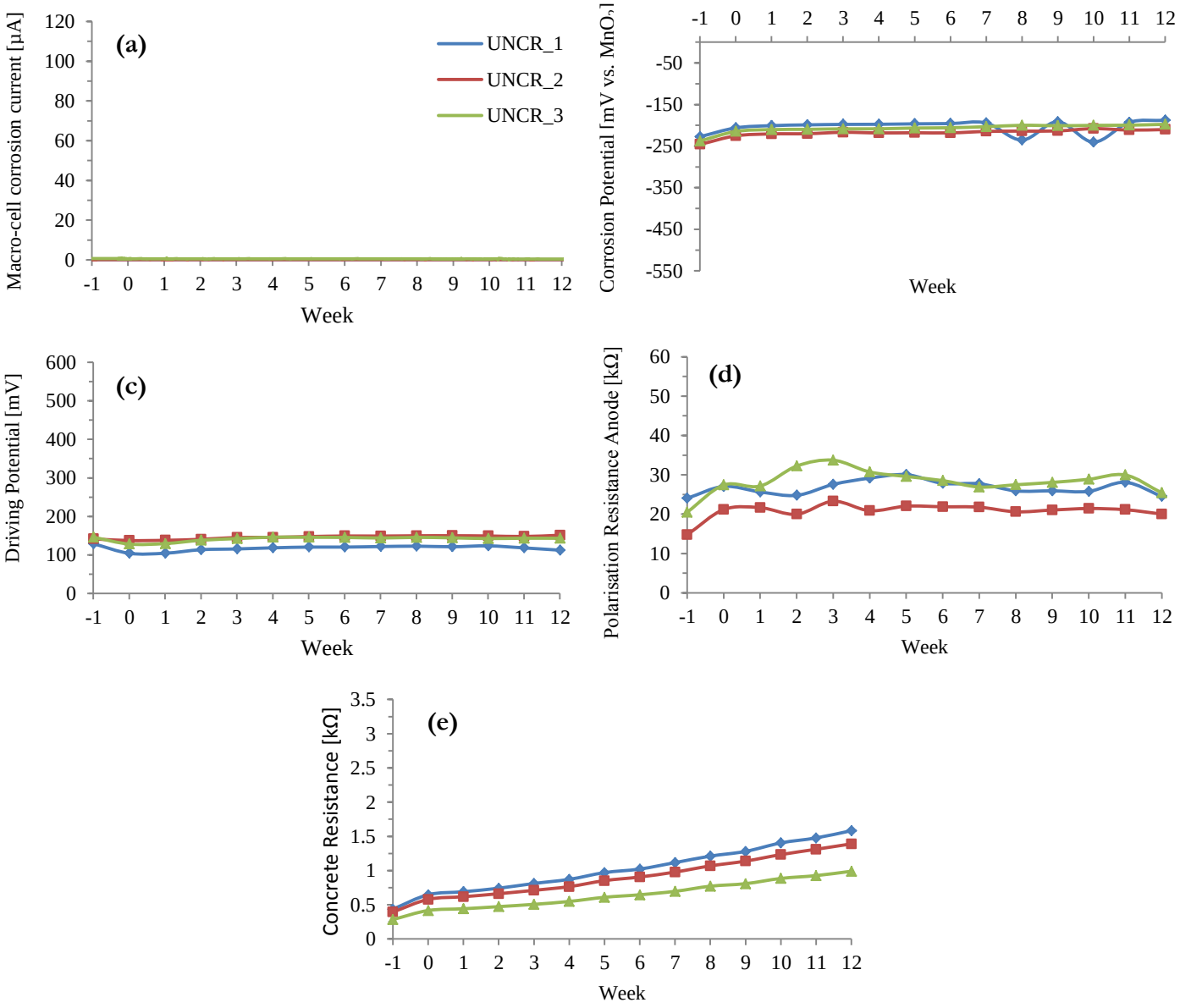

FIGURE 9.2: ELECTROCHEMICAL CORROSION PARAMETERS FOR THE UNCRACKED SPECIMENS; (A) MACRO-CELL CORROSION CURRENT , (B) CORROSION POTENTIAL, (C) DRIVING POTENTIAL, (D) ANODIC POLARISATION RESISTANCE, (E) CORROSION RESISTANCE

9.3 Cracked specimens

For cracked specimens, the obtained results for the electrochemical corrosion parameters are given in Figure 9.3. When looking at the macro-cell corrosion current (Figure 9.3a), it is clear that the presence of cracks has a big influence on this parameter. At first, between the uncracked state (week -1) and the cracked state (week 0), no significant changes could be noticed for the measurements, except for immediate increases in anodic polarisation resistance, from 10 to 15 kΩ, and concrete resistance, up to 1 kΩ. This phenomenon can possibly be explained by the larger difficulty for the applied current to flow through the concrete and the anodic rebar, due to cracking of the concrete beam. In general, it can thus be concluded that, due to the high polarisation resistance and the low corrosion current, it can be concluded that no corrosion activity is induced by cracked concrete exposed to the environment.

However, the moment the first wetting period has started (week 1), an almost immediate increase of the macro-cell corrosion current occurred for all specimens, which indicated corrosion initiation during this first wet/dry-cycle. These increases reached values ranging from about 40 μA for specimen CR_1 to even around 100 μA for specimens CR_3 and CR_4. For CR_2 however, it took about a day for this increase to occur, which then reached about the same value as for CR_1. Following this increase during a wet period, the macro-cell corrosion current slightly decreased again during the dry period. This phenomenon of respectively increasing and decreasing current repeated periodically during the rest of the experiment, each time a wet period started.

However, no clear general trend of the macro-cell corrosion could be noticed for the beams. Beams CR_1 and CR_3 showed both a general increase of the current during the first five weeks of wet/dry-cycles, to a value of 65 to 70 μA. This indicates the slightly more active state of corrosion of these beams. From week five, a slightly decreasing trend occurred, which remained until the end of the experiment. This overall decrease in current can possibly be explained by the fact the formation of corrosion products on the rebar in case of local or pitting corrosion. These corrosion products may block the penetration of additional chlorides at that location, resulting in a decreasing current.

This was quite different for the other beams. The first six weeks, beam CR_4 showed a slightly decreasing trend, reaching its lowest value of 25 μA at week six. Between week six and seven, there was a quite steep increase in current to about 50 μA, after which, similar as for CR_1 and CR_3, a general slightly decreasing trend could be noticed until the end of the experiment. The quite steep increase at week six clearly indicates the more active state of corrosion of beam CR_4. During the first week, an increase in macro-cell corrosion current was also visible for beam CR_2, indicating corrosion initiation. This current then gradually decreased until week six, probably due to the formation of corrosion products, where it even reached a value lower than 10 μA. After a little increase to 30 μA at week seven, the current subsequently showed an increase again from week eight onwards. So, at week eight, also beam CR_2 reached a more active state of corrosion. At the end of the test, the current of all the beams ranged between 30 and 50 μA.

A clear relation could be found between the macro-cell corrosion current and the corrosion potential (Figure 9.3b), the driving potential (Figure 9.3c) and the anodic polarisation resistance (Figure 9.3d). Clearly, high values of the macro-cell corrosion current were accompanied with relatively high values of the driving potential and relatively low values for the corrosion potential and anodic polarisation resistance. For example, the large increase in macro-cell corrosion current after the first wet period coincided with an increase in driving potential from 120 mV to 400 mV at week two. Meanwhile, the corrosion potential showed a decrease from -220 mV vs. MnO_2 to around -440 mV vs. MnO_2 for beams CR_1 and CR_2 and -380 mV vs MnO_2 for the other ones, at week two. Finally, the anodic polarisation resistance of all the beams also showed a decrease from 25-30 kΩ, before the first wetting period, to an almost constant value of 2.5 kΩ for the rest of the experiment. Furthermore, the sudden increases of the macro-cell corrosion current for beams CR_4 and CR_2, at week six and eight respectively, corresponded to clear drops of the corrosion potential and rises of the driving potential at these times.

So, after twelve weeks of monitoring, all cracked beams showed major corrosion activity. This led to lower values for the corrosion potential and the anodic polarisation resistance, while higher values were found for the driving potential. It can thus be confirmed that the presence of a crack in a concrete beam leads to deterioration of the passive layer of the rebar, due to more and easier penetrating chlorides, which subsequently results in corrosion activity.

Following the earlier mentioned increase of the concrete resistance due to crack creation, a drop after the first wetting period (week 1) occurred. This drop can be attributed to the ionic conductivity of the electrical current applied on the beams. Starting from week 1, a linear increase, similar as for the uncracked beams, was then found until the end of the experiment, ranging from 0.3 kΩ at week 1 to 0.8 kΩ at week 12. However, during this linear increase, the concrete resistance of the cracked beams was found to be only half of the values for uncracked beams. This can be explained by the easier penetration of the NaCl solution in the concrete matrix of the cracked specimens, which led to a higher moisture content and hence to a lower resistance.

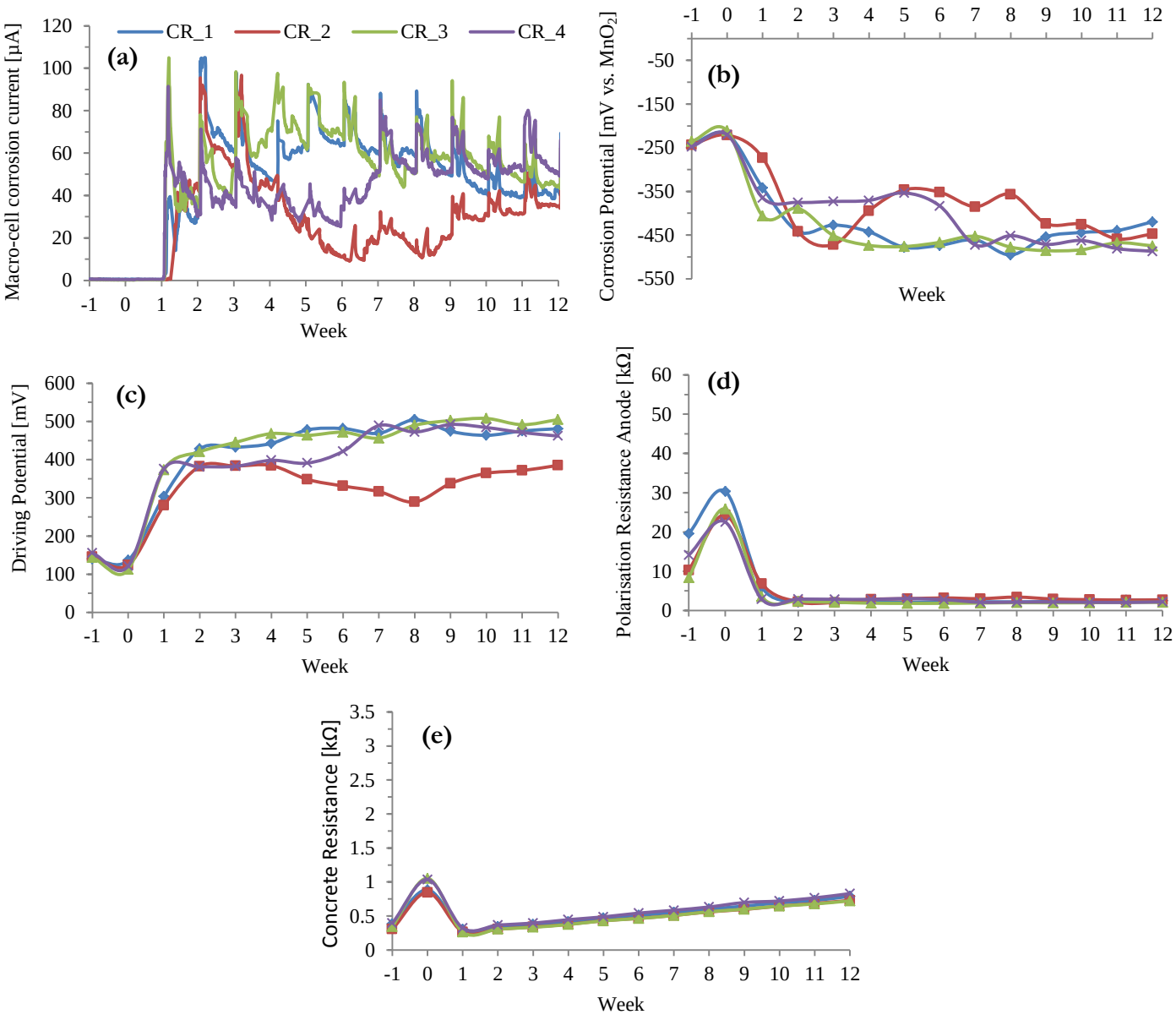

FIGURE 9.3: ELECTROCHEMICAL CORROSION PARAMETERS FOR THE UNCRACKED SPECIMENS; (A) MACRO-CELL CORROSION CURRENT , (B) CORROSION POTENTIAL, (C) DRIVING POTENTIAL, (D) ANODIC POLARISATION RESISTANCE, (E) CONCRETE RESISTANCE

9.4 Specimens healed with PU

Two types of healing mechanisms with PU were tested in this experiment: manual injection of the crack (PU_MAN) and encapsulation of the healing agent (PU_CAPS). In this section, both of these mechanisms are discussed and compared, both to each other as well as to the (un)cracked specimens. Prior to this comparison, it has to be noted that, due to a bad connection with the anode, no parameters, except for the cathodic polarisation resistance (see section 0), could be measured for beam PU_CAPS_3 and consequently, this beam was omitted from this discussion.

9.4.1 Autonomous healing (by encapsulation)

Similar as for the cracked beams, both beams with encapsulated PU showed corrosion initiation immediately after the first wetting period. This can be seen on Figure 9.4a by the large increase in macro-cell corrosion current to 60 μA and 90 μA, for beams PU_CAPS_1 and PU_CAPS_2 respectively, during the first week of exposure. This steep rise in macro-cell corrosion current was accompanied by a steep rise in driving potential (Figure 9.4c), respectively up to 340 μA and 450 μA, and a drop in corrosion potential (Figure 9.4b) to about -410 mV vs. MnO_2. After the first wet period, the anodic polarisation resistance (Figure 9.4d) already decreased to a value about 3 kΩ. It can thus definitely be stated that, from the start of the experiment, an active state of corrosion was present and hence that corrosion initiation could not be prevented by autonomous crack healing with encapsulated polyurethane.

Subsequently, the macro-cell corrosion current showed a decreasing trend during the rest of the experiment, which probably can be attributed to the formation of corrosion products. The same periodically returning peaks and drops of the current could be noticed as for the cracked beams (except for PU_CAPS_1 at week three). However, in this case, the peaks were less pronounced. Also, the values of the corrosion current at the end of the experiment were lower than for the cracked specimens, with values below 19 μA. Both beams thus seem to corrosion behaviour as for specimens with untreated cracks, although less corrosion activity was found in the propagation phase. For PU_CAPS_1, this can be confirmed by the rather constant values of -380 mV vs. MnO_2 for the corrosion potential and about 340 mV for the driving potential. Nevertheless, for PU_CAPS_2, a slightly increasing corrosion potential from -380 to -320 mV vs. MnO_2 and a slightly decreasing driving potential from 450 mV to 390 mV, together with the decreasing trend and the less pronounced peaks, show the (small) effect of the healing mechanism.

Finally from Figure 9.4e, it can be seen that the same concrete resistance behaviour was found as for the cracked beams, although the peak after crack creation for PU_CAPS_1 was about 70 % higher than obtained for cracked beams, reaching a value of 1.7 kΩ.

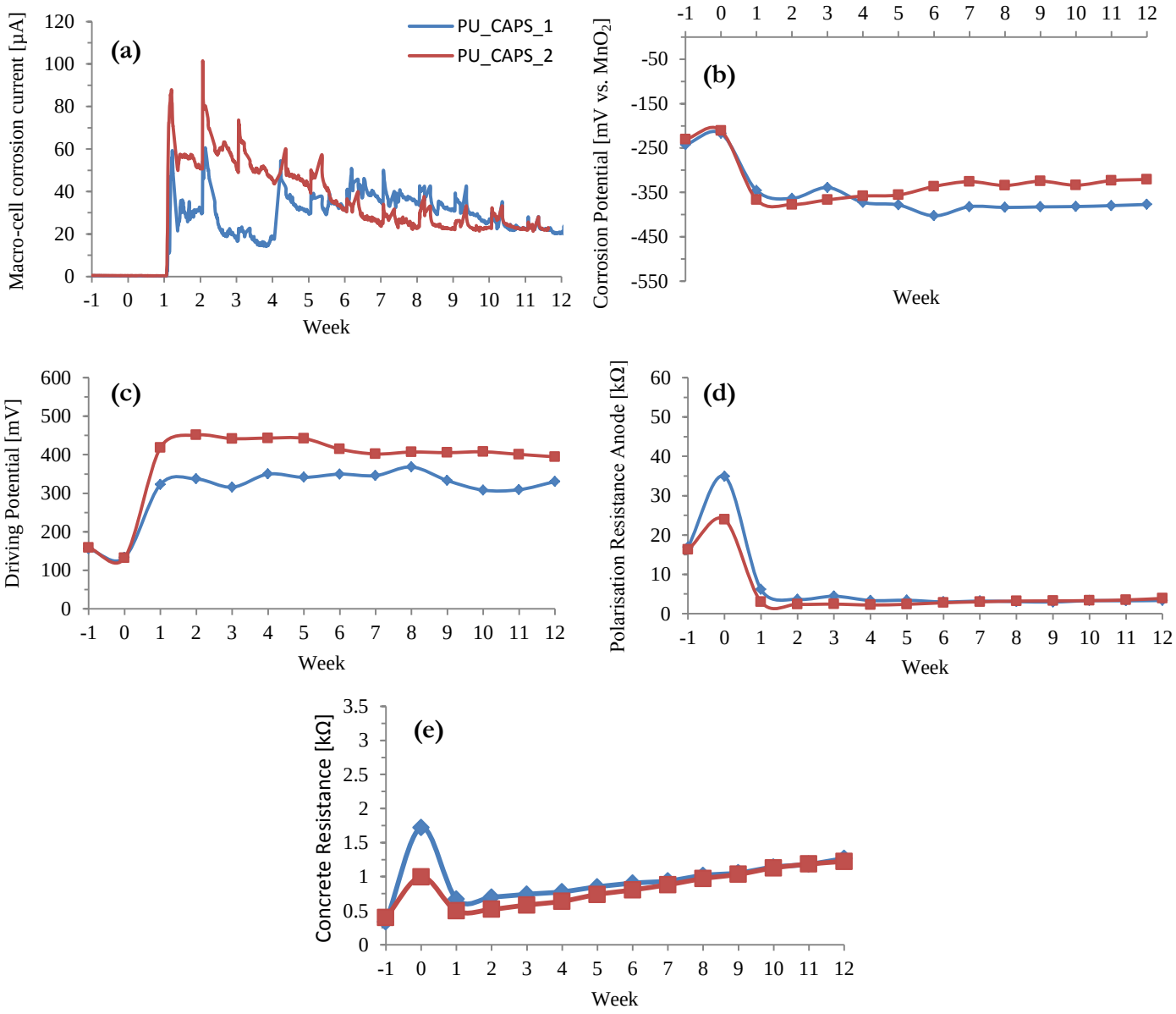

FIGURE 9.4: ELECTROCHEMICAL CORROSION PARAMETERS FOR SPECIMENS AUTONOMOUSLY HEALED BY ENCAPSULATION OF PU; (A) MACRO-CELL CORROSION CURRENT , (B) CORROSION POTENTIAL, (C) DRIVING POTENTIAL, (D) ANODIC POLARISATION RESISTANCE, (E) CONCRETE RESISTANCE

9.4.2 Manual healing (by injection)

From Figure 9.5, it can be seen that only two out of the three specimens where the crack was manually injected with polyurethane (PU_MAN_1 and PU_MAN_2) showed corrosion initiation.

Most similarities with the cracked beams were obtained for PU_MAN_2. Although, the noticeable corrosion behaviour of this beam started only after 3 weeks of exposure. In the first two weeks, little to no indications of corrosion could be seen from the macro-cell corrosion current (Figure 9.5a). However, small indications could be seen from the other graphs: a small increase of the driving potential to 237 mV (Figure 9.5c) and a corresponding drop of the anodic polarisation resistance to 13 kΩ (Figure 9.5d). The delay of the corrosion behaviour can be explained by (leakage of) the healing agent at the surface, which blocks the chlorides to penetrate in the cracks. Nevertheless, after two weeks, the chlorides were able to penetrate via the concrete matrix next to the crack into a less healed part of the crack. So, after the wet period of week three, a steep rise of the macro-cell corrosion current up to 75 μA occurred, together with a corresponding rise of the driving potential to almost 420 mV, a drop of the corrosion potential to about -480 mV vs. MnO_2 and a drop in the anodic polarisation resistance to about 3.5 kΩ. During the continuation of the experiment, the same trends can be found as for the cracked specimens (slightly decreasing I_{corr} and stable values for E_{corr} (-520 mV vs. MnO_2), ΔE (440 mV) and $R_{P,A}$ (2.5 kΩ)). It can thus be concluded that, for this specimen, the healing agent was only successful in blocking the crack in the beginning and as such, prolonging the non-active corrosion state for two weeks. But in the end, it was not able to prevent the chlorides from entering the crack.

A better healing performance was obtained for beam PU_MAN_1. Although the healing agent could not prevent corrosion initiation at the start of the experiment, a (much) less active state of corrosion was noticed based on the different electrochemical parameters. The corrosion initiation after the first wet period was characterized by a steep, but much smaller, increase of the macro-cell corrosion as was the case for specimens with untreated cracks. Here, a peak value of 35 μA was reached. Subsequently, the current decreased again and during the rest of the exposure time, no significant peaks were visible. On the contrary, a rather constant value was obtained for the macro-cell corrosion current, ranging between 8 μA and 20 μA. This healing effect could also be noticed from the corrosion potential, which, due to the corrosion initiation after the first wet period, showed a little decrease to -340 mV vs. MnO_2 followed by an almost constant value equal to -310 mV vs. MnO_2 during the rest of the experiment. This value is situated closer to the value for uncracked beams than for cracked beams. Further, compared to PU_MAN_2, a smaller increase of the driving potential to a constant value of about 360 mV and a smaller decrease of the anodic polarisation resistance to 5.5 kΩ also give a (less pronounced) indication of the healing effect of the manually injected polyurethane.

One specimen (PU_MAN_3) showed similar results as obtained for the uncracked beams: a macro-cell corrosion current of nearly zero, a stable corrosion potential value of -200 mV vs. MnO_2, a relatively low and stable driving potential of about 150 mV and a high but rather stable

anodic polarization resistance (not lower than 25 kΩ) throughout the whole experiment. No active state of corrosion of the rebar was thus reached for this beam.

Thus, in general, although the healing effect is clearly visible for PU_MAN_3, no consistency can be found in the results for manually injecting the crack with PU: one beam showed no corrosion behaviour, one beam did reach an active state of corrosion but only after two weeks of exposure, while the corrosion state of the third beam was situated in between the aforementioned two. These findings can also be noticed when looking at the concrete resistance, by the difference in peak height.

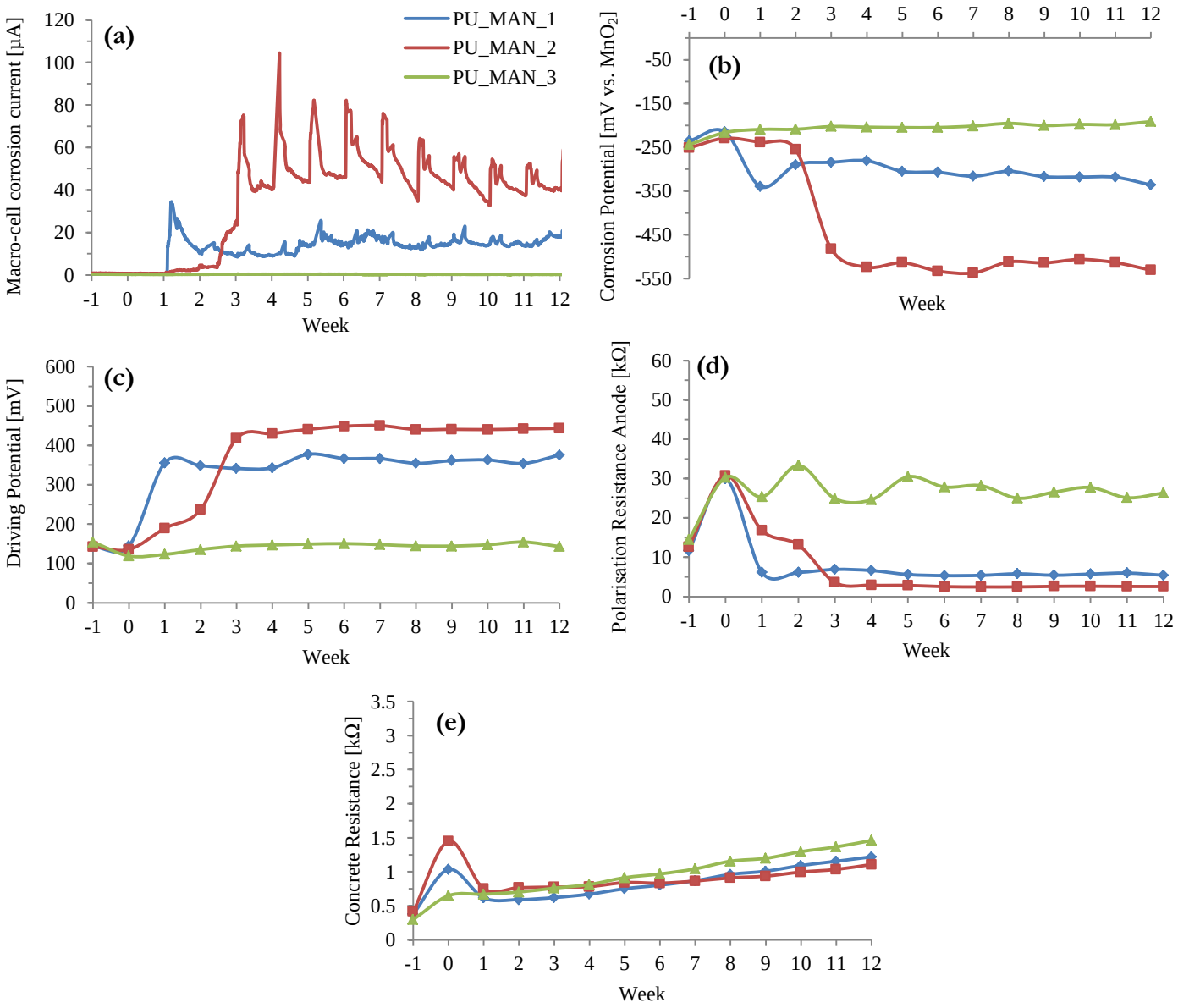

FIGURE 9.5: ELECTROCHEMICAL CORROSION PARAMETERS FOR SPECIMENS MANUALY HEALED BY INJECTION OF PU; (A) MACRO-CELL CORROSION CURRENT , (B) CORROSION POTENTIAL, (C) DRIVING POTENTIAL, (D) ANODIC POLARISATION RESISTANCE, (E) CONCRETE RESISTANCE

9.5 Specimens healed with WRA

Four types of healing mechanisms with WRA were tested in this experiment. Similar as with PU, both manual injection of the crack (WRA_MAN) and autonomous healing by encapsulation of the healing agent (WRA_CAPS) are investigated. However, due to the fact that this is done most in practice, spraying the entire crack surface with WRA was also tested. This was done once before crack creation (WRA_SURF_BEFORE) and once after crack creation (WRA_SURF_AFTER). In this section, all these mechanisms are discussed and compared. However, prior to this comparison, it has to be noted that, due to a bad connection with the anode, no parameters could be measured for beam WRA_MAN_3 and consequently, this beam was omitted from this discussion.

9.5.1 Autonomous healing (by encapsulation)

The autonomous healing mechanism by using embedded capsules filled with water repellent agent (WRA) showed very promising results. As can be seen in Figure 9.6, similar (or even better) values were obtained for the different electrochemical parameters than for uncracked beams. First of all, no macro-cell corrosion current occurred during the whole exposure time of 12 weeks. Secondly, an even more consistent value was found for the corrosion potential, ranging from about -250 mV vs. MnO_2, at the start of the experiment, to a value not lower than -220 mV vs. MnO_2 from week 0 until week 12. Similar as for the uncracked beams, the driving potential is also stable between 150 mV and 180 mV, with only a small decrease after week 0, due to crack creation. Healing by encapsulation of WRA resulted in an even higher polarisation resistance of the anode compared to the uncracked beams. For the uncracked beams, an increase of 10 to 15 kΩ was found before the start of the wet/dry-cycles, while in this case this increase amounts to 15 to 25 kΩ. So an even better resistance against corrosion occurred with this healing mechanism. All three beams subsequently showed a slightly increasing anodic polarisation resistance. Finally, after crack creation, the autonomously healed beams showed an even larger increase in corrosion resistance than the cracked beams, reaching values up to 1.7 kΩ. Also, no drop was noticed afterwards, since almost no current flowed through the beams due to the applied healing agent in the crack. Instead, starting from week 0, a linear increase was found due to ongoing hydration, reaching values up to 3 kΩ. In general, it can thus be said that this type of healing mechanism shows very good healing performance through which corrosion initiation can be prevented (at least for an exposure time of 12 weeks).

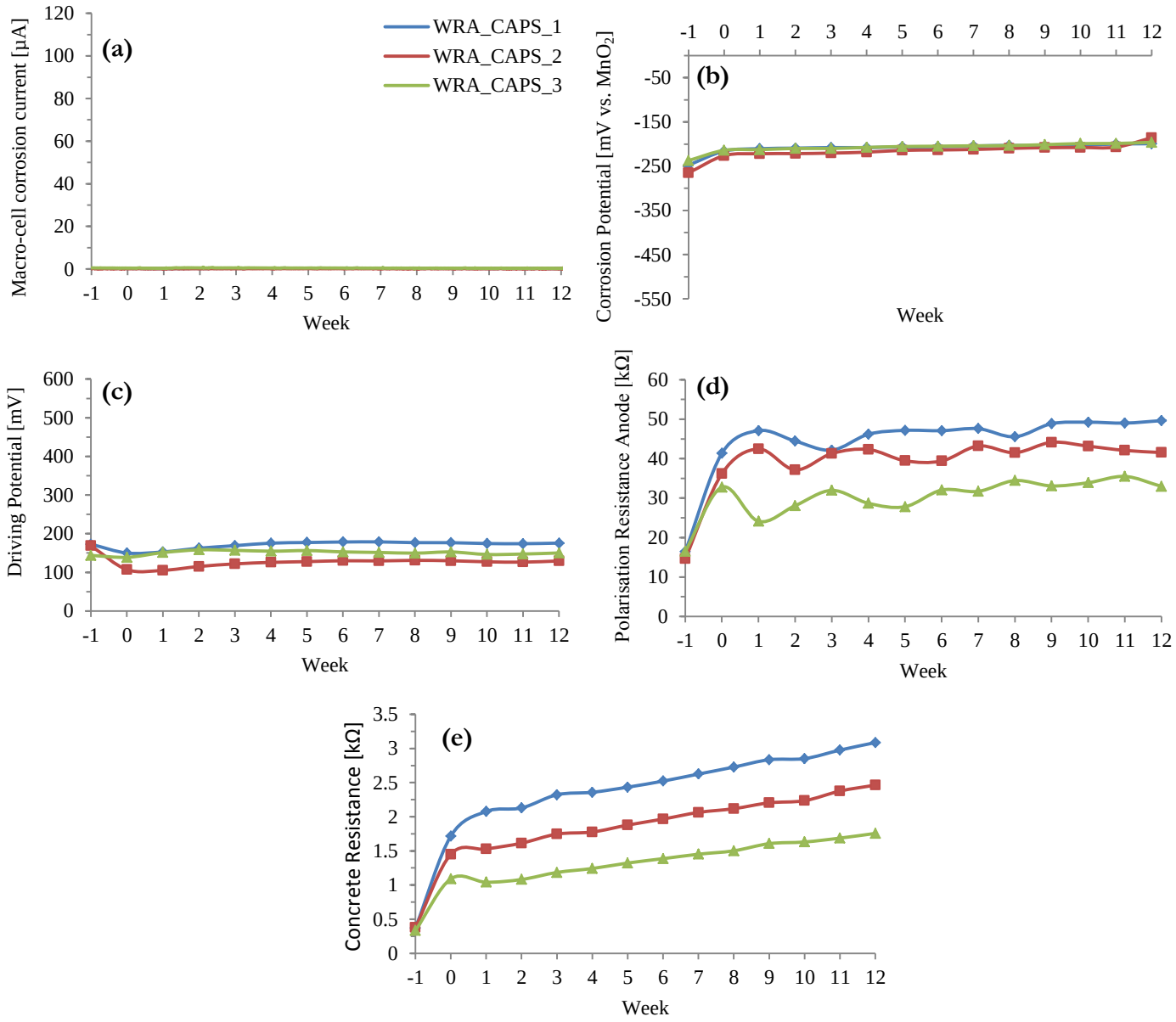

FIGURE 9.6: ELECTROCHEMICAL CORROSION PARAMETERS FOR SPECIMENS AUTONOMOUSLY HEALED BY ENCAPSULATION OF WRA; (A) MACRO-CELL CORROSION CURRENT , (B) CORROSION POTENTIAL, (C) DRIVING POTENTIAL, (D) ANODIC POLARISATION RESISTANCE, (E) CONCRETE RESISTANCE

9.5.2 Manual healing

9.5.2.1 Crack injection

By manually injecting the crack with WRA, almost identical results were obtained as for the autonomous healing using embedded capsules. The obtained values for the different electrochemical parameters can be found in Figure 9.7, however since they are identical as discussed in the previous section, they are not discussed separately. Nevertheless, it can be concluded that this healing mechanism is an at least as good alternative for the aforementioned autonomous healing mechanism and that it thus is very effective in preventing localised corrosion of the rebar.

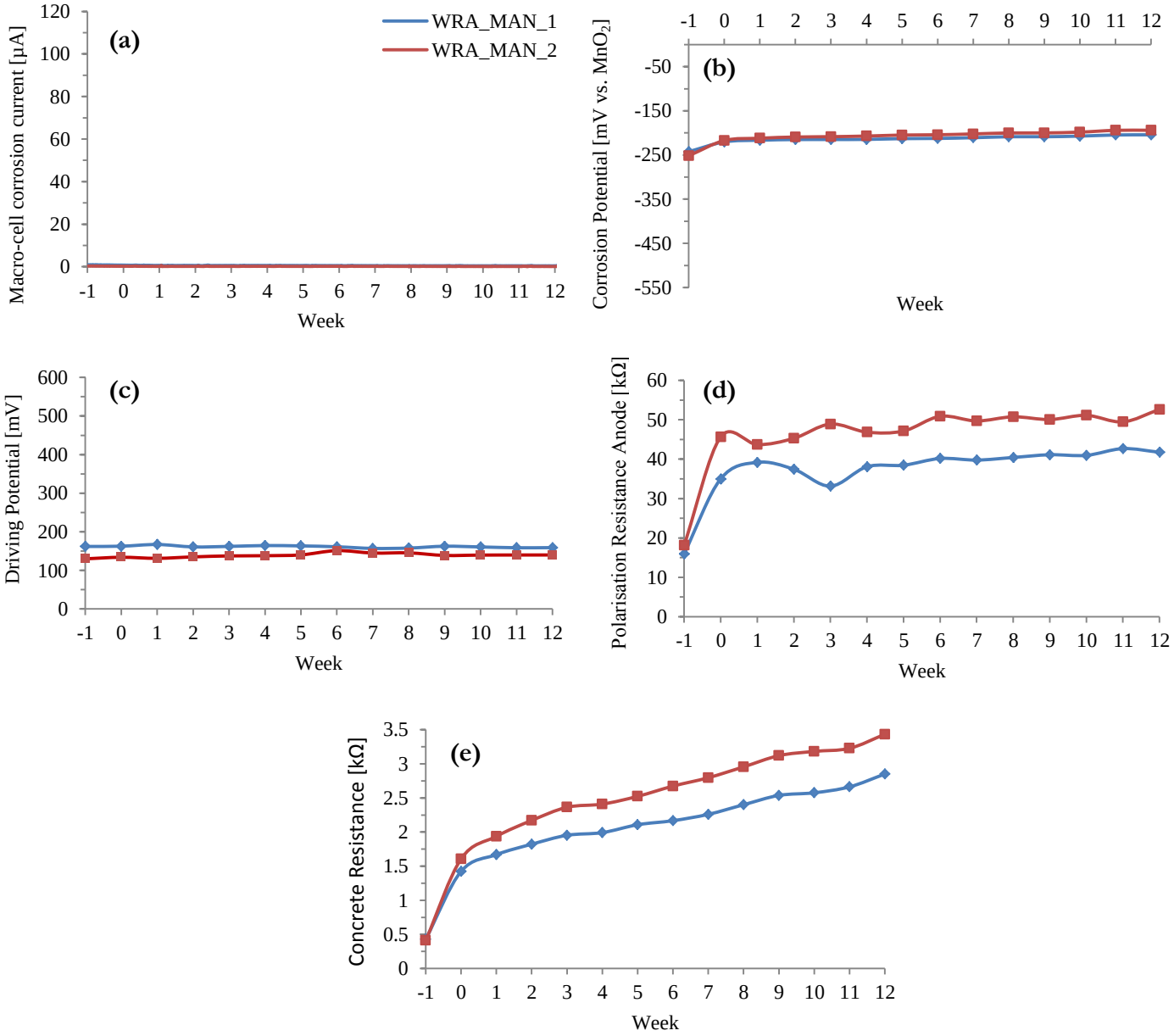

FIGURE 9.7: ELECTROCHEMICAL CORROSION PARAMETERS FOR SPECIMENS AUTONOMOUSLY HEALED BY INJECTION OF WRA; (A) MACRO-CELL CORROSION CURRENT , (B) CORROSION POTENTIAL, (C) DRIVING POTENTIAL, (D) ANODIC POLARISATION RESISTANCE, (E) CONCRETE RESISTANCE

9.5.2.2 Surface impregnation before crack creation

Spraying the water repellent agent on the test surface before the crack was created, showed worse healing performances as the previously discussed healing mechanisms using WRA. After the first wet period, an immediate increase in macro-cell corrosion current (see Figure 9.8) only occurred for one beam, WRA_SURF_BEFORE_2. This increase, reaching values up to 57 μA, was followed by a general slight increase until week 5, reaching a maximum peak value of about 80 μA. After this week, the current gradually decreased again, to finally reach an end value of about 20 μA. Corresponding to these currents, a drop of the corrosion potential could be noticed at week 1 to about -370 mV vs. MnO_2, after which an approximately stable value was obtained ranging between -425 and -450 mV vs. MnO_2. Another indication of bad healing can be derived from the driving potential, which showed an even larger increase after the first wet period than for cracked beams, reaching to a value of about 500 mV. Finally, the concrete resistance was similar as for cracked specimens, showing a drop after crack creation, and from week two, the value of the anodic polarisation resistance already was below 2.7 kΩ, which both confirms this active corrosion state of the rebar.

For WRA_SURF_BEFORE_3, the healing agent was able to prolong the time to corrosion initiation until week 5, when a sudden increase up to 60 μA occurred. From then on, similar results were obtained as for the cracked specimens (slightly decreasing I_{corr}, stable values for E_{corr} (-430 mV vs. MnO_2) and $R_{P,A}$ (3 kΩ) and slightly increasing values for ΔE (from 390 to 550 mV) and R_E (from 0.32 to 0.67 kΩ)). The prolongation could also clearly be noticed for the concrete resistance, since the drop only occurred after four weeks. Finally, beam WRA_SURF_BEFORE_1 also showed delayed corrosion initiation, starting from week 2. Between week 2 and 7, a slightly increasing corrosion current was found with only small peaks after each wet period. This was accompanied with a slight decrease in corrosion potential to a value of -390 mV vs. MnO_2, an increase of the driving potential to 440 mV and a decrease in anodic polarisation resistance to a value not more than 3 kΩ, which stayed constant until the end of the test. In this case, the drop in concrete resistance occurred after seven weeks.

So, just like for manually injection of PU in the crack (see section 9.4.2), no consistency was found in the results when impregnating the test surface with WRA before crack creation. Nevertheless, it can be concluded that this healing mechanism does not lead to good healing performances, since for all three beams, sooner or later, corrosion initiation and a subsequent active state of corrosion occurs. This way, it is not recommended to use this healing technique as such in practice.

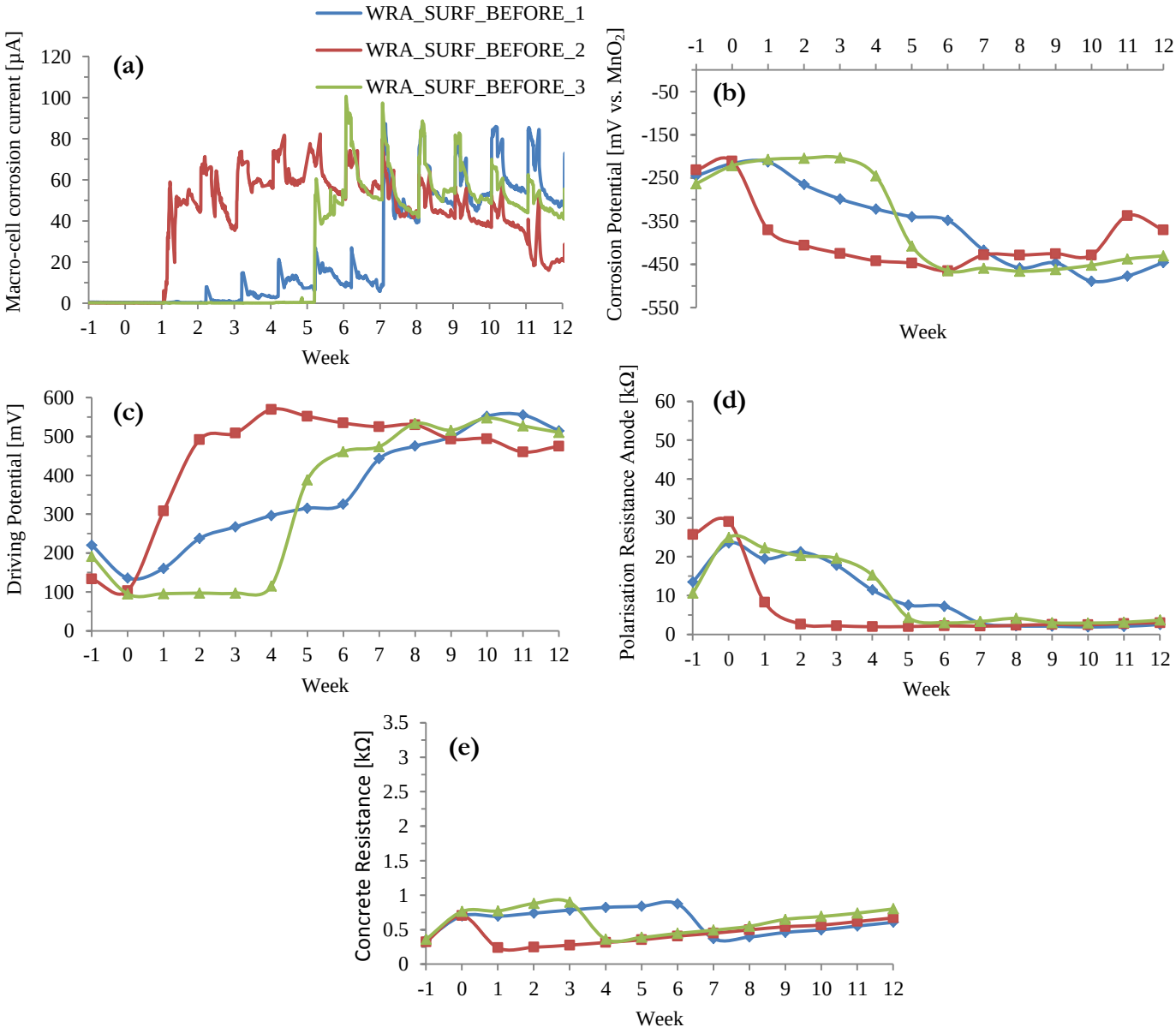

FIGURE 9.8: ELECTROCHEMICAL CORROSION PARAMETERS FOR SPECIMENS MANUALLY HEALED BY SURFACE IMPREGNATION OF WRA BEFORE CRACK CREATION; (A) MACRO-CELL CORROSION CURRENT , (B) CORROSION POTENTIAL, (C) DRIVING POTENTIAL, (D) ANODIC POLARISATION RESISTANCE, (E) CONCRETE RESISTANCE

9.5.2.3 Surface impregnation after crack creation

When the surface was impregnated after the crack was created, good healing performances were obtained for two out of the three specimens (see Figure 9.9). For these two, the results were similar as for uncracked beams, except for the increase in anodic polarisation resistance and concrete resistance. For the third beam, the corrosion current started to gradually increase at week 4 to reach a peak value of 70 µA at week 8. Subsequently, the current decreased again to an end value of about 30 µA. A similar trend was found for the driving potential, reaching a peak value at week 8 of 431 mV. Both the corrosion potential and anodic polarisation resistance showed the opposite trend, with a drop respectively to -450 mV vs. MnO_2 and 3 kΩ at week 8. A

possible cause for these deviating results may be incomplete healing. Finally, the concrete

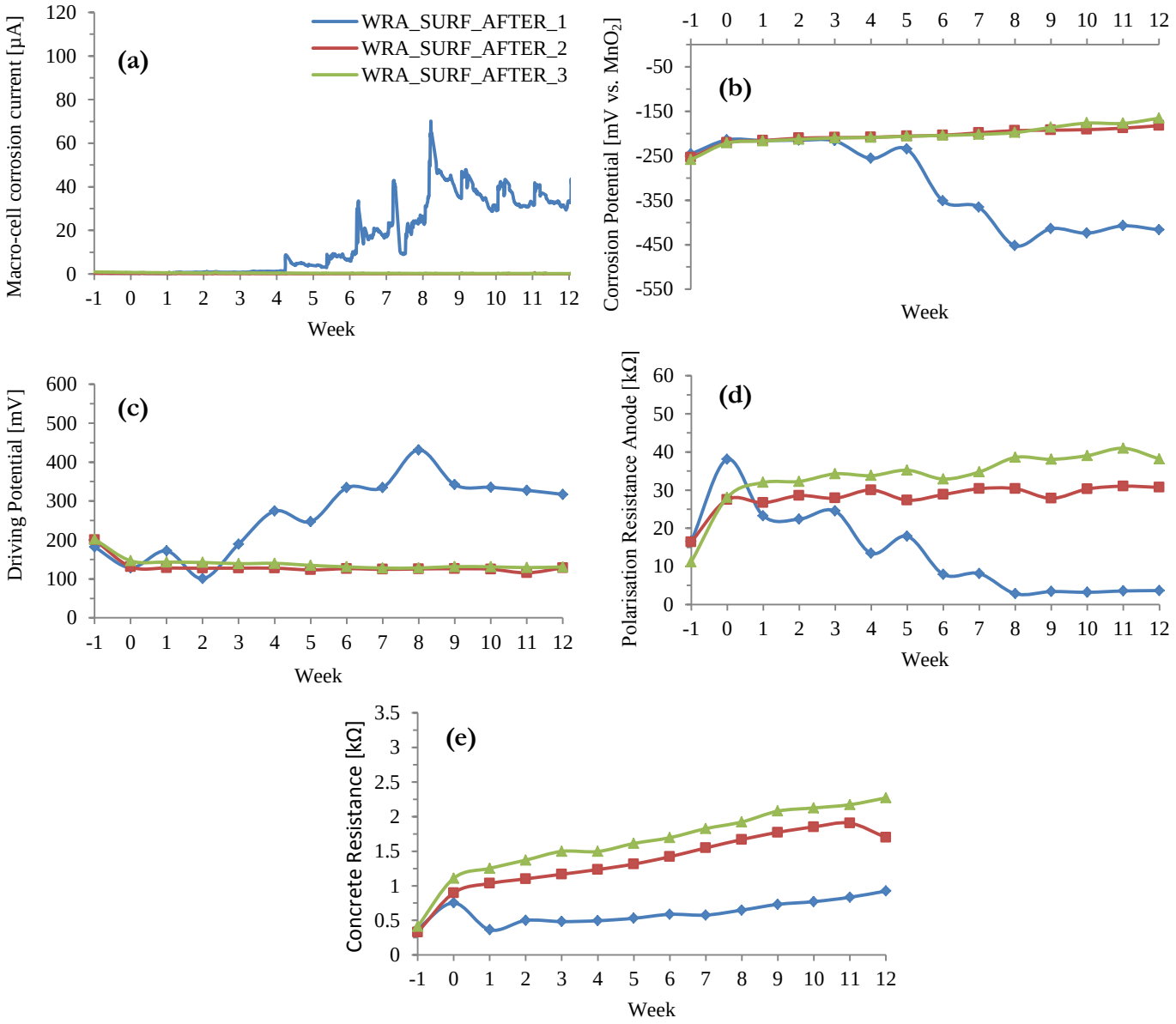

resistance was similar as for cracked beams.

FIGURE 9.9: ELECTROCHEMICAL CORROSION PARAMETERS FOR SPECIMENS MANUALLY HEALED BY SURFACE IMPREGNATION OF WRA AFTER CRACK CREATION; (A) MACRO-CELL CORROSION CURRENT , (B) CORROSION POTENTIAL, (C) DRIVING POTENTIAL, (D) ANODIC POLARISATION RESISTANCE, (E) CONCRETE RESISTANCE

9.6 Cathodic polarisation resistance

In addition to the earlier discussed anodic polarisation resistance ($R_{P,A}$) and concrete resistance (R_E), the cathodic polarisation resistance ($R_{P,C}$) for all test series is discussed in this section. From Figure 9.10, no significant differences were found in the mean cathodic polarization resistance between the different test series. For all series, they showed generally the same increasing trend. Starting from values between 0.5 kΩ and 0.65 kΩ, a small rise could be noticed after week 0 to values ranging from 0.75 kΩ to 0.93 kΩ. This rise was followed by a small drop at week 1, after which a general increasing trend was noticed during the continuation of the experiment, ranging from about 0.675 kΩ at week 1 to end values not higher than 1.75 kΩ.

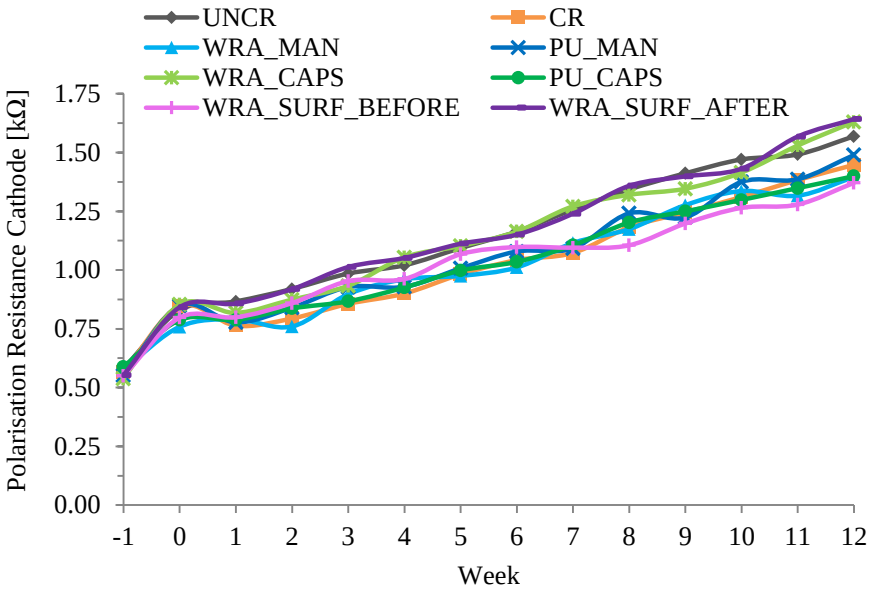

FIGURE 9.10: MEAN CATHODIC POLARISATION RESISTANCE FOR ALL TEST SERIES

9.7 Controlling factors

So, the rate at which the macro-cell corrosion process occurs is also controlled by the three aforementioned resistances. However, in order to determine which is the dominant resistance of the corrosion process, control factors $K_{P,A}$, $K_{P,C}$ and K_E were calculated by dividing the resistances $R_{P,A}$, $R_{P,C}$ and R_E respectively, by the total resistance ($R_{P,A}$ + $R_{P,C}$ + R_E). Figure 9.11 shows the results of the controlling factors for the different test series, calculated from the resistance values recorded at the last electrochemical measurement, i.e. after 12 weeks of exposure. For all test series, the anodic polarisation resistance was clearly the dominant factor. For series UNCR, WRA_MAN, WRA_CAPS and WRA_SURF_AFTER, the control factor even amounted more than 0.8, which means that the corrosion process is for more than 80 % controlled by the anodic partial reaction. For these test series, the other control factors, $K_{P,C}$ and K_E, were almost similar and both equal to about 0.1 or less.

For the other test series, the anodic control factors were a bit smaller, ranging from 0.5 (for CR) to 0.7 (for PU_MAN). In these cases, the other control factors were of course higher and almost

equal to each other. However, in case of CR, $K_{P,C}$ was equal to about 0.3, which was about 15 % higher than K_E.

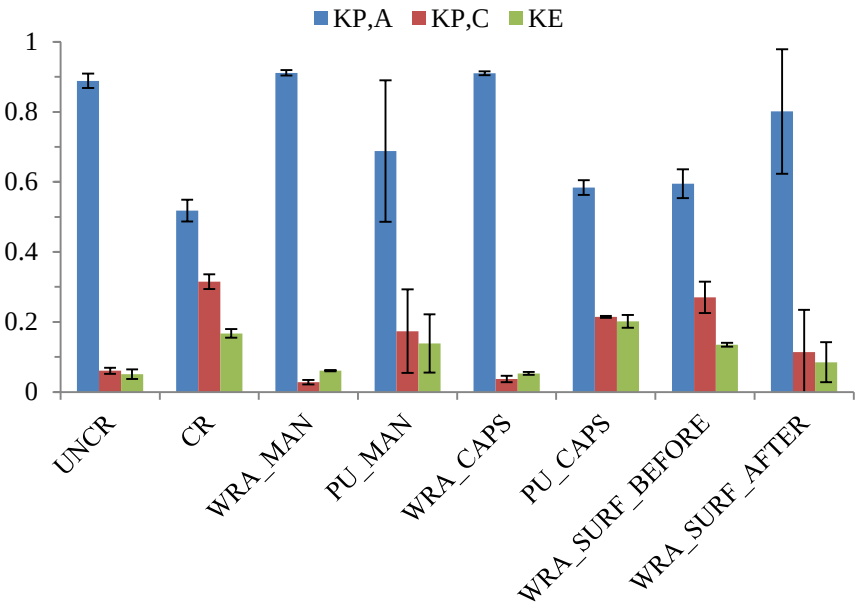

FIGURE 9.11: MEAN VALUES OF THE CONTROLLING FACTORS FOR THE MACRO-CELL CORROSION PROCESS CALCULATED FROM THE ELECTROCHEMICAL PARAMETERS AT WEEK 12. ERROR BARS REPRESENT THE STANDARD DEVIATION ON THE MEAN VALUES

10. Discussion

10.1 Water absorption test

As already known, the presence of cracks in cementitious materials has a detrimental influence on the ingress of aggressive substances. This was confirmed in this study by investigating the capillary water absorption of cracked mortar specimens. It was found that the water absorption for the cracked specimens was almost ten times higher than for uncracked specimens. It is thus clear that repair of cracks is necessary to avoid the fast ingress of aggressive substances into the cementitious matrix.

Although very high healing efficiencies (not lower than 85 %) were obtained for both healing agents, better resistances against water absorption were obtained using the water repellent agent, independent of the used healing mechanism. For each of the healing mechanisms using WRA, the water absorption of the healed specimen was between 1.29 times (22 %) and 1.67 times (40 %) lower than for uncracked specimens, which corresponded to healing efficiencies between 109 % and 115 %. The good healing performances with WRA can probably be attributed to the leakage of the healing agent on the mortar surface. Consequently, a part of the exposed test surface area was covered with water repellent agent.

Crack healing with polyurethane showed a healing efficiency ranging between 85 % and 106 %. Due to the higher viscosity of this polyurethane, for some specimens, the cracks were not completely healed over the whole length of the crack. Nevertheless, manually injecting the crack with PU (PU_MAN) still resulted in a 4 % lower cumulative water absorption than for uncracked specimens (UNCR). It can thus be concluded that PU is certainly not a bad healing agent, however, even better results were obtained using WRA.

When comparing the different types of healing mechanisms, the best healing performance was acquired with manual healing by surface impregnation with water repellent agent (WRA_SURF). Obviously, this can be attributed to the fact that in this case, almost no water could be absorbed by the mortar matrix, except through the crack. Nevertheless, still a significant difference could be seen when applying this layer of WRA before or after crack creation. Here, the latter case gave the best results, as evidenced by 20 % lower cumulative water absorption and the about 5 % higher healing efficiency. Moreover, after seven hours, one specimen from the test series WRA_SURF_BEFORE started to act as if it was unhealed. From that moment, a rapid increase in cumulative water absorption was observed, which can be attributed to incomplete crack healing.

As already mentioned, manually injecting the crack with healing agent also gave very promising results. Both with PU and WRA, this technique resulted in lower cumulative water absorption than for uncracked specimens. Also autonomous self-healing by encapsulated healing agent was very effective in reducing the ingress of water through cracks in cementitious materials, especially when WRA is used as healing agent.

One backside of the crack healing was the fact that for all healed test series, the absorption rate of water started to increase after eight hours of exposure. This can possibly be explained by incomplete crack healing or damage to the bond between the mortar and the reinforcement bars. The largest difference was found for WRA_MAN, which showed an increase of more than 125% higher from the initial sorption coefficient of 0.41 $kg/m^2/h^{0.5}$ and the secondary coefficient equal to 0.92 $kg/m^2/h^{0.5}$. For test series PU_MAN and PU_CAPS, which had a sorption coefficient after these first eight hours of 1.26 $kg/m^2/h^{0.5}$ and 1.22 $kg/m^2/h^{0.5}$ respectively, this absorption rate was even higher than for uncracked specimens (1.21 $kg/m^2/h^{0.5}$). From this, it can be concluded that there is still room for improvement in this research.

10.2 **Chloride penetration test**

The results for the chloride penetration test (with artificial cracks) confirmed that crack repair was definitely necessary, since at a depth of 21 to 24 mm the chloride concentration in cracked samples was more than 25 times higher compared to uncracked samples. However, unlike for the water absorption test (with realistic cracks), the best healing performances were obtained using PU as healing agent, with self-healing efficiencies not lower than 94 % over the entire crack depth. Independent of the used healing mechanism (manual or autonomous) and the penetration depth, lower chloride concentrations were found compared to WRA as healing agent. However, this certainly does not mean that WRA cannot result in good healing performances, which already has been proven by the water absorption test (see previous section). For example, by manually injecting the crack with WRA, self-healing efficiencies were obtained ranging from 56 to even 143 % at certain depths. So, both healing agents show promising results in preventing chloride ingress, but for this test higher efficiencies are obtained with PU.

When comparing the different healing mechanisms, both manually injecting the healing agent (before immersion) and encapsulation of the healing agent, showed medium to excellent healing performances, with healing performances not lower than 37 %. As mentioned earlier, using PU as healing agent result in chloride concentrations equal or even lower than for uncracked specimens, which corresponds to healing efficiencies of 100 % for PU_CAPS over the whole crack depth and of 94 to 143 % for PU_MAN. So, it can be concluded that PU is very effective in blocking chloride ingress in artificial cracks in concrete, no matter which healing mechanism is used. When comparing both mechanisms using WRA, it has to be noted that manually injecting WRA clearly showed better healing performances than using embedded capsules. Not taking into account the rather odd concentrations at the surface, a maximum difference of 70 % was found between both mechanisms.

Finally, it could be concluded that, although lower chloride concentrations were obtained than when leaving the crack unhealed and although this healing mechanism may be successful in blocking the ingress of chlorides from the moment of application, manually injecting a crack after three weeks of exposure to a chloride environment leads to bad healing performances. In other words, this healing mechanism is not recommended and crack should be healed as soon as possible after its formation.

10.3 **Corrosion monitoring**

Finally, a comparison between the different healing mechanisms and healing agents could also be made through corrosion monitoring of concrete beams by measuring different electrochemical parameters during a cyclic exposure to a chloride solution with a concentration of 33 g/l (1 day wet, 6 days dry) for a period of 12 weeks. First of all, the results of these measurements showed no indication of an active state of corrosion in the uncracked concrete specimens over the whole exposure period. This is logical since it takes more time for chlorides to diffuse to the reinforcement. However, the presence of cracks seemed to have a big influence. From the first week, corrosion initiated for all cracked beams and after 12 weeks of exposure, all cracked beams showed major corrosion activity, with measured corrosion currents up to 100 μA. It can thus be confirmed that the presence of a crack in a concrete beam leads to deterioration of the passive layer of the rebar, due to more and easier penetrating chlorides, which subsequently results in corrosion activity.

When looking at the healing mechanisms with PU, corrosion initiation could not be prevented by encapsulation of the healing agent. So, already from the start of the experiment, an active state of corrosion was present for the beams of this test series. However, compared to the cracked specimens with untreated cracks, the effect of the healing agent was visible since less corrosion activity was found in the propagation phase. For example, the corrosion potential for PU_CAPS was about 15 % higher (less negative) than for cracked beams and a difference in macro-cell corrosion current at the end of the experiment was found up to 60 %. Moreover, by manual injection of PU in the crack, no consistent results were obtained. One beam showed no corrosion, one beam does reach an active state of corrosion but only after two weeks of exposure, while the corrosion state of the third beam is situated in between the aforementioned two. Thus, although the effect of the healing agent was clearly visible, two out of the three beams showed corrosion activity. From this, it can be concluded that, in most of the cases, using PU as healing agent cannot (completely) prevent corrosion initiation and propagation.

On the contrary, both autonomous healing (by encapsulation) as well as manual healing (by injection) with WRA seemed to be very effective in preventing localised corrosion at the rebar (at least for an exposure time of 12 weeks). Both mechanisms showed identical results, i.e. no macro-cell corrosion current occurred and stable values were found for the corrosion potential (about -220 mV vs. MnO_2) and the driving potential (± 160 mV). Compared to uncracked beams, even higher anodic polarization resistance (up to 50 kΩ) were obtained, corresponding to a difference up to 20 %.

Finally, manual healing by surface impregnation with WRA was also investigated. When done before crack creation, bad healing performances were found. For example, an even larger increase in driving potential was obtained compared to cracked beams, reaching to a value of about 500 mV. For some beams, corrosion initiation could be prolonged, but corrosion initiation and a subsequent active state of corrosion occurred for all beams after an exposure time of 7 weeks. From this, it can be concluded that this healing mechanism is not successful in preventing localised corrosion. When impregnation of the surface with WRA was done after crack creation, good healing performances were obtained for two out of the three specimens, with similar results

as for uncracked beams. However, one beam experienced corrosion activity from week 4 onwards. This could probably be attributed to incomplete healing.

10.4 Overall conclusion

Based on previous separate conclusions from the different experiments, an overall conclusion can be made. In Table 10-1, an overview is given of the ability of different healing agents and mechanisms in resisting water absorption, chloride ingress and/or corrosion initiation. The following criteria are thereby used:

- Bad = Resistance is less than for cracked specimens
- Good = Resistance is better than for cracked specimens but less than for uncracked specimens
- Excellent = Resistance is better than for uncracked specimens

TABLE 10-1: OVERVIEW OF RESISTANCES OF DIFFERENT HEALING AGENTS AND HEALING MECHANISMS AGAINST WATER ABSORPTION, CHLORIDE INGRESS AND CORROSION INITIATION

Healing agent	**Healing mechanism**	**Resistance against …**		
		Water absorption	**Chloride ingress**	**Corrosion**
PU	PU_CAPS	Good	Excellent	Bad
	PU_MAN	Excellent	Excellent	Bad
	PU_MAN_AFTER	/	Bad	/
WRA	WRA_CAPS	Excellent	Good	Excellent
	WRA_MAN	Excellent	Good	Excellent
	WRA_MAN_AFTER	/	Bad	/
	WRA_SURF_BEFORE	Excellent	/	Bad
	WRA_SURF_ AFTER	Excellent	/	Good

It can be seen that, although the performances of other mechanisms are certainly not bad in most of the cases, only two healing mechanisms perform well for all three tests: autonomous healing mechanism by encapsulation of water repellent agent (WRA_CAPS) and manual healing by injection of the crack with water repellent agent (WRA_MAN). Further, also surface impregnation with water repellent agent after crack creation (WRA_SURF_AFTER) showed good to excellent resistances against water absorption and corrosion. However, since this mechanism was not tested against chloride ingress in the chloride penetration test, further investigation is necessary in order to confirm the good healing performances of this mechanism.

In general, water repellent agent thus seemed to be a more efficient healing agent than polyurethane. When comparing the healing mechanisms, it can be stated that both manually injecting the crack, as well as using embedded capsules can lead to overall good healing performances. Pending further research, it can be provisionally stated that this also counts for impregnating the test surface with a water repellent agent after crack formation. Consequently, it is recommended to use one of these healing mechanisms in practice. Of course, in order to

choose the correct healing agent and healing mechanism, also some other factors have to be taken into account depending on the circumstances, such as labour intensiveness, time consumption, costs, space requirement (for application), etc. However, this is beyond the scope of this research.

Part IV
Conclusions

11. Conclusions

The presence of cracks in reinforced concrete has a big influence on the ingress of aggressive substances such as chlorides in the concrete. The risk of chloride-induced corrosion will thus be much higher when cracks are present. In order to avoid the fast ingress of aggressive substances in the concrete matrix and subsequent chloride-induced corrosion, it is clear that repair of cracks is necessary. However, in order to obtain a good healing performance of the crack, the choice of the right healing agent is crucial. In this master's dissertation, the influence of two healing agents (polyurethane (PU) and water repellent agent (WRA)) on the corrosion behaviour and transport properties of reinforced concrete was investigated, using different healing mechanisms: autonomous healing by encapsulation of the healing agent and manual healing by injection of the healing agent into the crack or by impregnation of the crack surface. This was done through three types of tests: a water absorption test on mortar prisms in order to investigate the capillary water uptake through the (healed) cracks, an accelerated chloride diffusion test on concrete cylinders with artificial cracks in order to investigate the chloride penetration and corrosion monitoring on cracked concrete beams subjected to cyclic exposure to a chloride solution with realistic concentration.

It was concluded that, although the performances of other mechanisms are certainly not bad in most of the cases, only two healing mechanisms performed well for all three tests: autonomous healing mechanism by encapsulation of water repellent agent (WRA_CAPS) and manual healing by injection of the crack with water repellent agent (WRA_MAN). Further, also surface impregnation with water repellent agent after crack creation (WRA_SURF_AFTER) showed good to excellent resistances against water absorption and corrosion.

In case of manual injection or encapsulation of the healing agent in the concrete crack or matrix respectively, the polyurethane showed good to excellent performances against water absorption and chloride ingress, but not against corrosion initiation. In general, water repellent agent thus seemed to be a more efficient healing agent than polyurethane. When comparing the healing mechanisms, it can be stated that both manually injecting the crack, as well as using embedded capsules can lead to overall good healing performances. Pending further research, it can be provisionally stated that this also counts for impregnating the test surface with a water repellent agent after crack creation. Consequently, it is recommended to use one of these healing mechanisms in practice.

Of course, in order to choose the correct healing agent and healing mechanism, other factors such as cost and time consumption also have to be taken into account. However, this is beyond the scope of this master's dissertation.

.

12. Future research

During the water absorption test, it was found that for all healed test series, the absorption rate of water started to increase after eight hours of exposure, probably due to incomplete crack healing. From this, it can be concluded that there is still room for improvement in this research. So, an even more complete healing of the cracks should be found.

Further, the resistance against chloride penetration was not tested for all healing mechanisms in this research. So, to confirm the good healing performances of this healing mechanism and to get a more complete view of the behaviour of this healing mechanism in different circumstances, surface impregnation with water repellent agent applied after crack creation (WRA_SURF_AFTER), which already showed good to excellent resistances against water absorption and corrosion initiation, should also be tested against chloride penetration.

Corrosion monitoring of the cracked concrete beams can be followed up further, in order to investigate the long-term behaviour of the healing agents. After the exposure, the beams can be split and the anodic rebar can be removed and visually examined to see the damage due to corrosion.

Bibliography

Ahmad, S. (2003). Reinforcement corrosion in concrete structures, its monitoring and service life prediction - A review. *Cement and Concrete Composites*, *25*, 459–471.

American Society for Testing and Materials. (2009). ASTM C876-91: Standard test method for half-cell potentials of uncoated reinforcing steel in concrete., *91*(Reapproved).

Andrade, C., Garcés, P., & Martínez, I. (2008). Galvanic currents and corrosion rates of reinforcements measured in cells simulating different pitting areas caused by chloride attack in sodium hydroxide. *Corrosion Science*, *50*(10), 2959–2964.

Angst, U. (2011). *Chloride induced reinforcement corrosion in concrete - Concept of critical chloride content – methods and mechanisms*. *Concept of Critical Chloride Content—Methods and Mechanisms*.

Angst, U., Elsener, B., Larsen, C. K., & Vennesland, Ø. (2009). Critical chloride content in reinforced concrete - A review. *Cement and Concrete Research*, *39*(12), 1122–1138.

Araújo, M., Chatrabhuti, S., Gurdebeke, S., Alderete, N., Van Tittelboom, K., Raquez, J.-M., … Gruyaert, E. (2018). Poly(methyl methacrylate) capsules as an alternative to the proof-of-concept'' glass capsules used in self-healing concrete. *Cement and Concrete Composites*, *89*.

Beck, M., Burkert, A., Harnisch, J., Isecke, B., Osterminski, K., Raupach, M., … Warkus, J. (2012). Deterioration model and input parameters for reinforcement corrosion. *Structural Concrete*, *13*(3), 145–155.

Bertolini, L., Carsana, M., Gastaldi, M., Lollini, F., & Redaelli, E. (2016). Corrosion of Steel in Concrete and Its Prevention in Aggressive Chloride-Bearing Environments. *5th International Conference on Durability of Concrete Structures*, 13–26.

Blagojevic, A., Fennis, S., & Walraven, J. C. (1991). Impact of cracks on chloride-induced corrosion and durability of reinforced concrete structures - a literature review, *25*(c), 847–852.

Cao, C., Cheung, M. M. S., & Chan, B. Y. B. (2013). Modelling of interaction between corrosion-induced concrete cover crack and steel corrosion rate. *Corrosion Science*, *69*(24), 97–109.

Dai, J. G., Akira, Y., Wittmann, F. H., Yokota, H., & Zhang, P. (2010). Water repellent surface impregnation for extension of service life of reinforced concrete structures in marine environments: The role of cracks. *Cement and Concrete Composites*, *32*(2), 101–109.

De Belie, N., Van Tittelboom, K., Maes, M., Van Belleghem, B., & Van den Heede, P. (2017). Self-healing concrete in aggressive environments. *Proceedings of the 1st International Conference on Construction Materials for Sustainable Future*, (April), 42–48.

De Schutter, G. (2014). *Damage to concrete structures*. Ghent.

Elsener, B., Andrade, C., Gulikers, J., Polder, R., & Raupach, M. (2003). Hall-cell potential measurements—Potential mapping on reinforced concrete structures. *Materials and Structures*, *36*(7), 461–471.

Gulikers, J., & Raupach, M. (2006). Modelling of reinforcement corrosion in concrete. *Materials and Corrosion*, *57*(8), 603–604.

Justnes, H., Kim, M. O., Ng, S., & Qian, X. (2016). Methodology of calculating required chloride diffusion coefficient for intended service life as function of concrete cover in reinforced marine structures. *Cement and Concrete Composites*, *73*, 316–323.

Khitab, A., Anwar, W., & Arshad, M. T. (2017). Predictive Models of Chloride Penetration in concrete: An Overview. *MUST Journal of Engineering and Applied Sciences*, *1*(1), 1–14.

Layssi, H., Ghods, P., Alizadeh, A. R., & Salehi, M. (2015). Electrical Resistivity of Concrete, (May).

Maes, M., Van Tittelboom, K., & De Belie, N. (2013). Resistance of cracked concrete healed by means of polyurethane against chloride penetration.

Medeiros M. H. F., R. F. C. M.-J. R. a H. P. (2017). Corrosion potential: influence of moisture, water-cement ratio, chloride content and concrete cover. *Revista IBRACON de Estruturas E Materiais*, *10*(4), 864–885.

Michel, a., Otieno, M., Stang, H., & Geiker, M. R. (2016). Propagation of steel corrosion in concrete: Experimental and numerical investigations. *Cement and Concrete Composites*, *70*, 171–182.

Montemor, M. F., Simões, a. M. P., & Ferreira, M. G. S. (2003). Chloride-induced corrosion on reinforcing steel: From the fundamentals to the monitoring techniques. *Cement and Concrete Composites*, *25*(4-5 SPEC), 491–502.

Nagesh, M., & Bhattacharjee, B. (1998). Modeling of Chloride Diffusion in Concrete and Determination of Diffusion Coefficients. *ACI Materials Journal*, *95*(2).

Orazem, M. E., & Tribollet, B. (2017). Electrochemical Impedance Spectroscopy.

Otieno, M. B., Alexander, M. G., & Beushausen, H.-D. (2010). Corrosion in cracked and uncracked concrete – influence of crack width, concrete quality and crack reopening. *Magazine of Concrete Research*, *62*(6), 393–404.

Otieno, M., Beushausen, H., & Alexander, M. (2016a). Chloride-induced corrosion of steel in cracked concrete - Part I: Experimental studies under accelerated and natural marine environments. *Cement and Concrete Research*, *79*, 373–385.

Otieno, M., Beushausen, H., & Alexander, M. (2016b). Chloride-induced corrosion of steel in cracked concrete - Part II: Corrosion rate prediction models. *Cement and Concrete Research*, *79*, 386–394.

Poursaee, A. (2014). Corrosion sensing for assessing and monitoring civil infrastructures. *Sensor Technologies for Civil Infrastructures*, *Volume 1:* , 357–382.

Qian, S. Z., Zhou, J., & Schlangen, E. (2010). Influence of curing condition and precracking time on the self-healing behavior of Engineered Cementitious Composites. *Cement and Concrete Composites*, *32*(9), 686–693.

Ribeiro, D. V., & Abrantes, J. C. C. (2016). Application of electrochemical impedance spectroscopy (EIS) to monitor the corrosion of reinforced concrete: A new approach. *Construction and Building Materials*, *111*, 98–104.

Sandberg, P. (1999). Factors affecting the chloride thresholds for uncracked reinforced concrete exposed in a marine environment . Part I : Field exposure tests of reinforced concrete THE IDENTIFICATION AND USE OF, *1*(June), 92–98.

Sangoju, B., Gettu, R., & Bharatkumar, B. H. (2017). Study of the parameters governing the chloride induced corrosion of reinforcement steel in cracked concrete. *Indian Concrete Journal*, *91*(3), 37–48.

Schwenk, W. (1972). Korrosionsgefährdung und Schutzmaßnahmen bei Elementbildung zwischen erdverlegten Rohren und Behältern. *Das Gas- Und Wasserfach*, 546–550.

Shi, X., Xie, N., Fortune, K., & Gong, J. (2012). Durability of steel reinforced concrete in chloride environments: An overview. *Construction and Building Materials*, *30*, 125–138.

Snoeck, D., Van Tittelboom, K., Steuperaert, S., Dubruel, P., & De Belie, N. (2014). Self-healing cementitious materials by the combination of microfibres and superabsorbent polymers. *Journal of Intelligent Material Systems and Structures*, *25*(1), 13–24.

Tuutti, K. (1982). Corrosion of steel in concrete. Swedish Cement and Concrete Research Institute.

Van Belleghem, B., Kessler, S., Van den Heede, P., Van Tittelboom, K., & De Belie, N. (2017). *Chloride induced reinforcement corrosion behavior in self-healing concrete with encapsulated polyurethane*.

Van Belleghem, B., Van den Heede, P., & De Belie, N. (2016). Resistance to chloride penetration of self-healing concrete with encapsulated polyurethane. *Proceedings of the 4th International Conference on Sustainable Construction Materials and Technologies*.

Van Belleghem, B., Van den Heede, P., Van Tittelboom, K., & De Belie, N. (2017). Quantification of the service life extension and environmental benefit of Chloride Exposed Self-Healing Concrete. *Materials*, *10*(1).

Van Belleghem, B., Van Tittelboom, K., & De Belie, N. (2017a). *Efficiency of self-healing cementitious materials with encapsulated polyurethane to reduce water ingress through cracks*.

Van Belleghem, B., Van Tittelboom, K., & De Belie, N. (2017b). Use of encapsulated healing agents to limit water uptake through cracks in mortar, 1–10.

Van Den Heede, P. (2014). *Durability and Sustainability of Concrete with High Volumes of Fly Ash*. *University of Ghent*.

Van Tittelboom, K., & De Belie, N. (2013). *Self-healing in cementitious materials-a review*. *Materials* (Vol. 6).

Van Tittelboom, K., Snoeck, D., Gruyaert, E., Debbaut, B., De Belie, N., Wang, J., & De Araújo, A. (2016). Real-scale testing of the efficiency of self-healing concrete. *Concrete Repair, Rehabilitation and Retrofitting IV*, 443–450.

Wang, L., & Ueda, T. (2011). Mesoscale Modelling of the Chloride Diffusion in Cracks and Cracked Concrete. *Journal of Advanced Concrete Technology*, *9*(3), 241–249.

Wang, X. Y., & Zhang, L. N. (2016). Simulation of Chloride Diffusion in Cracked Concrete with Different Crack Patterns. *Advances in Materials Science and Engineering*, *2016*.